CHANGES IN SEASONAL PRECIPITATION OF EAST CENTRAL NORTH AMERICA WITH CONNECTIONS TO GLOBAL CLIMATE

A DISSERTATION

SUBMITTED TO THE FACULTY OF THE GRADUATE SCHOOL

OF THE UNIVERSITY OF MINNESOTA

BY

Benjamin Fulper Hardt

IN PARTIAL FULFILLMENT OF THE REQUIREMENTS

FOR THE DEGREE OF

DOCTOR OF PHILOSOPHY

Dr. R. Lawrence Edwards

October 2010

Acknowledgements

I would like to thank the many people who helped me in my graduate career. In particular, I would like to thank the contributions of Greg Springer and Harry Rowe, without whom this project would not have been undertaken. Thanks to Gene Turner for permission to enter Buckeye Creek Cave and collect samples BCC2, 4, 6, 9, and 10. Thanks also to Cliff and Lois Lindsey for access to Culverson Creek Cave and permission to collect sample CCC1.

Thanks to the members of the isotope lab for all of their help over the years, particularly Hai Cheng for his tireless efforts.

Thanks to my committee: Larry Edwards, Calvin Alexander, Katsumi Matsumoto, Justin Revenaugh, and Bryan Shuman

Thanks also to my advisor: Larry Edwards

Finally, I want to thank my family for their tireless support over the years.

For Margaret Kosmala, my friend, partner, and teammate in life.

Table of Contents

Table of Tables

Table of Figures

Chapter 1: Introduction

The study of pre-historic climate change (paleoclimatology) has made vital contributions to our understanding of the global climate system. Dependable instrumental climate data is only available for the last ~150 years and paleoclimate proxy data have provided useful ways to extend the record beyond the period of anthropogenic influence. Uncertainty about the consequences of CO_2 warming of global temperatures make it imperative to improve understanding of the boundary conditions of global climate. Pleistocene records have shown that the climate is capable of far greater variability than has been observed even over the last 10,000 years, including the gradual buildup of continental ice sheets and the abrupt shifts of millennial events and glacial terminations. These insights into climatic instability, especially abrupt events, require consideration of such behavior in the future.

Climate models are a key tool in developing our understanding of the global climate system and paleoclimate data are a means to validate and improve these models. Paleoclimate records are able to capture frequencies of variability that are longer than the instrumental data can resolve. This has the benefit of removing some of the noise in instrumental records and provides information about responses to extreme climate states.

One of the great challenges of paleoclimate work is the difficulty of dating materials that contain climatic information. As a result, detecting leads and lags within the climate system remains a significant challenge and intercomparison of records from disparate locations often requires assumptions about the mechanisms involved. Lake and ocean cores are restricted by the limitations of carbon-14 dating, which include uncertain

reservoir effects and variable ^{14}C production rates in the atmosphere, which limit ^{14}C age calibration beyond 26 kyr BP (Reimer et al., 2004). Ice core records provide an excellent chronology when annual bands are visible, but are geographically restricted to polar and alpine regions. These challenges make it difficult to compare records across regions and evaluate which factors may be driving changes in the climate system.

Climate records from stalagmites do not suffer from these problems. Trace concentrations of uranium within the crystalline calcite allow stalagmites to be dated precisely and accurately (Edwards et al., 1987; Li et al., 1989; Shen et al., 2002). Furthermore, karst regions, areas of limestone bedrock where caves develop, are found across the globe, irrespective of climate. As layers of calcium carbonate accumulate in the stalagmite over time, they capture details about the temperature and precipitation at the time of deposition (Hendy and Wilson, 1968). Previous work on cave deposits from the Asian summer monsoon region have proved invaluable for deciphering the mysteries of glacial terminations (Cheng et al., 2009), and establish a benchmark for the chronology of other records based on well established climatic teleconnections (Cheng et al., 2006; Dykoski et al., 2005; Kelly et al., 2006; Wang et al., 2004, 2001).

The research presented here is an attempt to establish a new benchmark for climate change in eastern North America. Despite the advances made in understanding polar and tropical climate changes, comparatively less is understood about changes in temperate latitudes. Because a large percentage of the human population lives in the temperate zone, it is crucial to improve our understanding of the potential variability in this region. The continental United States is of particular interest because it could act as a bridge between changes in monsoon regions and the Laurentide ice sheet, creating the potential

for feedbacks within the climate system. The Asian summer monsoon creates downwelling air over the subtropical North Atlantic, producing stronger high pressure and enhancing the semi-permanent anticyclone of the Bermuda High (Rodwell and Hoskins, 2001). The Bermuda High then influences southerly moisture transport from the Gulf of Mexico into the continental interior (Adams and Comrie, 1997; Chang and Smith, 2001; Davis et al., 1997; Henderson and Vega, 1996; Keim, 1997). Ice ages depend on the transfer of water mass from the oceans to the continents, so changes in the strength of that transfer can affect the rate of ice sheet growth. The latent heat flux associated with precipitation may also have an impact on the melting of ice sheets during glacial terminations (Bromwich et al., 2005).

West Virginia is well situated to record changes in moisture flow from the Gulf of Mexico. The Bermuda High, possibly modulated by the El Niño Southern Oscillation (Seager et al., 2005), provides a substantial control on the seasonal distribution of precipitation in the region (Hardt et al., 2010), so speleothems from WV can provide a measure of the connection between monsoon regions and the Laurentide ice sheet.

In monsoon regions, the strong seasonal wet/dry cycle makes it likely that oxygen isotopes ($\delta^{18}O$) in speleothem are determined by the strength of the summer monsoon rains (Wang et al., 2001). The magnitude of the signal (~5-6‰) severely limits the number of processes that could produce such large shifts. Temperature, which has been a frequent interpretation of speleothem $\delta^{18}O$, could only explain a small fraction of this variability and the tropics do not experience the same magnitude of annual temperature variability that is observed in the mid-latitudes.

In mid-latitude sites, it is considerably more difficult to constrain the interpretation of oxygen isotope variability. The range of variability is more limited (~2-3‰), allowing a wider range of factors that could significantly impact $\delta^{18}O$. Mean annual temperatures are expected to show much greater variability on glacial/interglacial cycles in temperate latitudes than they would in the tropics, so temperature effects must be considered.

In order to establish the dominant control on speleothem $\delta^{18}O$, it is advantageous to look at modern climate and periods for which there is ample climatic data. North American lakes have recorded changes in both temperature and precipitation, providing a useful point of comparison with $\delta^{18}O$. Therefore, modern climate and isotopes in precipitation, combined with $\delta^{18}O$ from the the Holocene (Chapter 2, Hardt et al., 2010) can provide a method to calibrate the interpretation speleothem $\delta^{18}O$, which can the be applied to times when fewer records exist for comparison.

Glacial cycles are the most dramatic aspect of the Pleistocene climate. Building upon the climatic interpretation developed with the Holocene samples, it is possible to evaluate the behavior of WV climate over three separate glacial cycles (Chapter 3).

The termination events that mark the end of glacial intervals are particularly compelling intervals of study. Continental ice sheets, which take nearly 100 kyr to develop, collapse in less than 10 kyr with widespread consequences (Cheng et al., 2009). While the timing of these terminations is determined by summer insolation, several aspects remain mysterious (Denton et al., 2006). Therefore, a speleothem record from WV, which is only ~300 km from the maximum extent of the Wisconsinan ice sheet, can provide additional insight into the climatic processes driven by and possibly affecting the continental glaciers (Chapter 4).

Many of the climatic changes that are observed in the paleoclimate record are tied to seasonlity, a critical aspect of climate change. The growth and decay of ice sheets is paced by warm season melting due to changing summer insolation (Hays et al., 1976). Strong insolation also enhances low pressure in monsoon regions and leads to strong changes in atmospheric circulation and tropical precipitation (Wang et al., 2001). In addition to the effects of summer, the abrupt climate transitions associated with millennial scale events are dominated by changes in the winter season (Denton et al., 2005).

The research presented here will hopefully broaden the discussion about changing seasonality to include the potential effects of spring (and autumn). Results between samples and over several time intervals provide a consistent story about the changes in seasonal precipitation and the processes that may control them.

Chapter 2: The seasonality of east central North American precipitation based on three coeval Holocene speleothems from southern West Virginia[1]

We present a replicated record of Holocene climate change from a cave in West Virginia, USA. Based on analysis of stable isotopes in precipitation ($\delta^{18}O_w$) from the closest Global Network of Isotopes in Precipitation (GNIP) station in Coshocton, OH, we interpret enriched oxygen isotopes in calcite ($\delta^{18}O_c$) as representing an increase in the relative contribution of summer precipitation to annual totals. Significant coherence between local summer (July and August) precipitation and the Summer North Atlantic Oscillation (SNAO) index on multi-decadal timescales suggests that summer precipitation in our study area is strongly influenced by changes in the Bermuda High. A strengthened Bermuda High circulation would increase summer precipitation amounts in the region and lead to enriched $\delta^{18}O_c$ of speleothem calcite. Our $\delta^{18}O_c$ record achieves maximum values during the mid-Holocene, consistent with previous studies indicating an intensified Bermuda High circulation at that time. At 4.2 ka, $\delta^{18}O_c$ transitions to lower values at a time when numerous records around the globe document significant changes in the hydrologic budget. Over the last 2000 years, there are intervals of substantially decreased $\delta^{18}O_c$, coincident with aridity in the Yucatan, Alpine glacial advances, and a weakened Asian summer monsoon.

---

[1] This chapter was previously published in Earth and Planetary Science Letters. The full citation for the published version is:

Hardt, B., Rowe, H. D., Springer, G. S., Cheng, H., & Edwards, R. L. (2010). The seasonality of east central North American precipitation based on three coeval Holocene speleothems from southern West Virginia. *Earth and Planetary Science Letters*, *295*(3-4), 342-348. doi:10.1016/j.epsl.2010.04.002

Keywords: speleothem; seasonality; Holocene; Bermuda High; Summer North Atlantic Oscillation; East Central North America

1. INTRODUCTION

1.1. The Bermuda High in the Paleoclimate Record

The mid-Holocene has long been associated with an increased influence of the North Atlantic subtropical high pressure system, also known as the Bermuda High (BH) (Bartlein et al., 1998; COHMAP Members, 1988; Shuman et al., 2002). Changes in lake levels (Shuman and Donnelly, 2006) and forest species composition (Shuman et al., 2004) in the eastern United States during the mid-Holocene are attributed to an intensified BH circulation altering the balance of summer to winter precipitation. Model results support this interpretation as they consistently demonstrate increased summer precipitation during the mid-Holocene (Braconnot et al., 2007; COHMAP Members, 1988; Diffenbaugh et al., 2006; Harrison et al., 2003).

Speleothems have previously been successfully used to determine changes in the seasonality of precipitation (Wang et al., 2001). Therefore, we have produced a replicated, absolutely dated record from three coeval speleothems to test the conclusions of Shuman and Donnelly (2006) that strengthened BH circulation during the mid-Holocene significantly altered the balance of seasonal precipitation in east central North America (ECNA). By working with speleothems we can establish a radiometric timescale using U/Th disequilibrium techniques and provide a high-resolution time series from oxygen isotopes in calcite ($\delta^{18}O_c$). Our $\delta^{18}O_c$ record can significantly advance understanding of Holocene climate in ECNA by supplementing regional lake records that

document species change, fire history, and aridity (Kneller and Peteet, 1993, 1999; Watts, 1979).

1.2. Role of the Bermuda High circulation in modern climate

The BH provides a major control on the advection of summer moisture from the Gulf of Mexico to ECNA (Davis et al., 1997). However, the impacts of the BH extend beyond ECNA, affecting precipitation in the Great Plains (Chang and Smith, 2001), as well as the southwestern (Adams and Comrie, 1997) and southeastern United States (Keim, 1997). In the southeastern US (immediately south of our study site), the relative impact of the BH on the seasonality of precipitation is stronger than the effect of the North Atlantic Oscillation, Southern Oscillation Index, or Pacific North America mode (Henderson and Vega, 1996). A stronger BH circulation would likely expand its influence northward and more strongly affect our study site, resulting in greater advection of moisture from the Gulf of Mexico.

The BH is also closely linked to global monsoon systems (Rodwell and Hoskins, 2001). The North American summer monsoon (NASM) significantly influences the western edge of the BH, inducing stronger southerly flow (Rodwell and Hoskins, 2001) and enhancing moisture transport from the Gulf of Mexico to ECNA. For this reason, precipitation in ECNA increases in response to activation of the NASM system in the summer (Higgins et al., 1997). A Rossby wave response to the heating of the Tibetan plateau further strengthens the BH by inducing descent over the subtropical North Atlantic in response to changes in the Asian summer monsoon (ASM) (Rodwell and Hoskins, 2001).

The summer North Atlantic Oscillation (SNAO) provides an effective measure of modern summer sea-level pressure (SLP) anomalies in the extratropical North Atlantic (Folland et al., 2009). The positive phase of the SNAO is characterized by higher SLP in the subtropical North Atlantic, consistent with an enhanced BH. While there are larger anomalies from mean SLP in northwest Europe, it appears that the positive SNAO captures a stronger BH signature. This relationship allows comparison between summer precipitation data from our study area and the BH as represented by the SNAO index, thereby demonstrating a connection between the modern BH circulation and summer precipitation in ECNA.

2. METHODS

2.1. Site Description

The cave site (37°58' N, 80°24'W, 600 masl) is located in Mississippian limestone of the Greenbrier Group in the Allegheny Mountains of West Virginia (Cardwell et al., 1968; Dasher and Balfour, 1994) (Figure 1). Buckeye Creek Cave (BCC) contains 7.14 km of mapped passages, and samples were collected from chambers approximately 35m below the surface. Oxygen isotopes of drip waters (-8.5‰) approximate local mean annual values from precipitation (-8.37‰, JM Welker et al. 2002). Cave temperatures (10.7°C) are stable throughout the year and are similar to local mean annual temperature (10.2°C).

2.2. Sample collection and analysis

All stalagmite samples were collected >1 km from the cave entrance, minimizing surface effects on cave temperature or humidity (White, 2004). The recovered stalagmites were cut in half along the growth axis, polished, and drilled for stable isotope

and dating analyses. Samples were excluded if they contained excessive detrital material, vugs, or if the crystal structure was not coarse calcite. As a result, one section of sample BCC-4 (from 25 to 85 mm depth) is excluded from analysis (See Figure S1). This conservative methodology is applied in order to provide the clearest climate record possible.

Stable isotope samples were milled at 1-mm intervals along the vertical growth axis and analyzed using a GasBench II coupled to a ThermoFinnigan DeltaPlusXP IRMS. Samples were standardized to V-PDB using NBS-19, with standard and unknown precisions for $\delta^{18}O$ and $\delta^{13}C$ averaging 0.10‰. Methods are the same as used in Springer et al. (2008). By milling along the growth axis instead of taking discrete samples at regular intervals, we aimed to minimize potential aliasing of the isotope record (Fairchild et al., 2006).

Radiometric age constraints were provided by U/Th dating techniques developed for carbonates (Broecker, 1963) and adapted for measurement on an inductively coupled plasma mass spectrometer (Edwards et al., 1987; Shen et al., 2002) at the University of Minnesota. Calcite powder was sampled using a dental drill with a 0.9-mm diameter tungsten-carbide drill bit. Age errors are generally small and on the same order as the growth rate over the sampled interval (~1 mm). An age model was constructed by linear interpolation between U/Th ages to create a radiometric timescale for $\delta^{18}O_c$ and $\delta^{13}C_c$ measurements (See Tables S1 and S2). Analyses were performed on a Finnigan-MAT Element with a single MasCom multiplier using the decay constants reported by Cheng et al. (2000). The top (depth=0) of sample BCC-6 was assigned an age of -53 years BP (0 BP = 1950) as it was actively growing at the time of collection.

Comparison of oxygen and carbon isotopes yields no significant correlation during the period of study, indicating that crystallization most likely occurred under equilibrium conditions (Hendy, 1971). The replication between samples and our process of averaging the records further strengthens the argument that observed variability represents a true climate signal (Baker et al., 1997).

The range of isotopic variability in our record over the Holocene is less than 1.5‰, making noise a significant concern in the interpretation of our record. To address this problem we produced a composite record to increase confidence at the expense of resolution. A composite record of $\delta^{18}O_c$ was constructed using Analyseries (Paillard et al., 1996). The time series from each stalagmite was re-sampled at annual resolution by linear interpolation between data points. Once the records were on the same timescale, they were averaged, smoothed using a 121-year symmetric filter and re-sampled at a 60 year interval using a cubic spline. These values were chosen to limit the effects of frequencies above the Nyquist. By producing an averaged composite record, we can focus on aspects of the record that are robustly captured by multiple samples, increasing the likelihood of isolating a climate signal.

2.3.Spectral analysis of modern precipitation

Analyseries was also used to compare local July and August precipitation to the SNAO index using Blackman-Tukey cross-correlation (Blackman and Tukey, 1959). July and August precipitation was chosen to best match the SNAO index, which is defined based on July and August loading factors. Summer precipitation data for Lewisburg, WV (37°51'N, 80°24'W) were obtained from the National Climate Data Center. Gaps in the years 1931, 1932, 1935, 1936, 1945, and 1946 were filled by substituting rainfall data

from nearby White Sulphur Springs (37°47'N, 80°18'W). Because neither meteorological station will provide an exact record of precipitation at the cave site, we view this as a reasonable solution to the missing data given the close proximity of both Lewisburg and White Sulphur Springs to BCC (Figure 1 inset). Comparison between the two sites for the sum of July and August rainfall since 1933 (the period of available data) reveals significant correlation (slope= 0.66±0.09, r^2=0.43, p=2.5 x 10^{-8}). Cross-correlation analysis was performed with available data from 1902 through 2007using a Tukey window with 30 lags ($p \leq 0.01$).

3. RESULTS

3.1. Speleothem results

The most striking feature of our record is a pronounced decline in $\delta^{18}O_c$ values between 4.3 and 4.1 ka BP. This shift marks the end of a ~2 kyr interval of enriched $\delta^{18}O_c$ values during the mid-Holocene. Each sample shows a transition to higher values occurring between 6.4 and 6.2 ka, with a return to lower values around 4.2 ka (Figure 2).

In the most recent section of the record, values of $\delta^{18}O_c$ exhibit short-term decreases coincident with significant climatic events in other regions (Figure 3). The record during the Medieval Climate Anomaly (MCA) contains generally more enriched values, with decreases in $\delta^{18}O_c$ beginning around the time of the transition to the Little Ice Age (LIA).

3.2.Results of spectral analysis of modern precipitation

Comparison of summer (July and August) precipitation data from Lewisburg, WV to the SNAO (Folland et al., 2009) reveals significant coherence at multi-decadal timescales ($p \leq 0.01$) with no apparent phase lag (Figure S2). After filtering both records

at a frequency of 0.04 year^{-1} with a bandwidth of 0.015 year^{-1} to isolate this multi-decadal component, the two records display clear similarities (Figure 4). These values were chosen in order to isolate the coherent variability demonstrated by the Blackman-Tukey analysis. While significant coherence occurs at higher frequencies, these are less likely to contribute to the $\delta^{18}O_c$ speleothem record, which is sampled at multi-decadal scales.

4. DISCUSSION

4.1 Interpretation of $\delta^{18}O$

The principles of using isotopic data as a climate proxy in speleothems were first set out by Hendy and Wilson (1968). The empirical basis for interpretation of $\delta^{18}O$ has been the relationship in meteoric water between isotopic composition and temperature or the amount of precipitation (Dansgaard, 1964; Rozanski et al., 1993). While these principles have frequently been applied to paleoclimate studies, they are not always determinative. The slope of the relationship between $\delta^{18}O_w$ and temperature decreases noticeably at mean annual temperatures above ~10°C (Jouzel et al., 1987, 1994). Even in Greenland ice, where isotopes have successfully been used to determine paleotemperatures, seasonal precipitation patterns likely influence annualized signals (Werner et al., 2000) and calibration of the local temperature relationship based on borehole data yields a slope of only 0.33‰/°C (Cuffey et al., 1995), far less than those reported by Dansgaard (1964) (0.69‰/°C) or Rozanski et al. (1993) (0.58‰/°C). Bowen & Wilkinson (2002) cite a growing body of evidence suggesting that $\delta^{18}O$ in paleoclimate records attributed to temperature may be due to circulation or seasonal changes. Schmidt et al. (2007) further argue that the substitution of space for time in establishing the relationship between temperature and $\delta^{18}O_w$ does not appear valid when applied to

glacial-interglacial cycles at a single location. As a result, speleothem studies, particularly since Wang et al. (2001), have moved away from relying on annual temperature as the primary explanation for $\delta^{18}O_c$ variability (Lachniet, 2009).

Available IAEA data from the GNIP station in Coshocton, OH (~300 km from our study site) indicate a correlation between amount weighted monthly mean oxygen isotopes in precipitation ($\delta^{18}O_w$) and temperature (Figure 5a) of 0.27±0.03‰/°C (r^2=0.587, p=6x10^{-12}), notably less than the monthly value determined by Yurtsever (1975) (0.52‰/°C) in a multiple station analysis. This indicates that $\delta^{18}O_w$ is not a strong function of temperature in the region of our study site. The available data from Coshocton, which only includes four complete annual cycles, prevent a similar analysis between annual temperatures and $\delta^{18}O_w$. However, the similarity between the slopes derived by Rozanski et al. (1993) (0.58‰/°C) and Yurtsever (1975) (0.52‰/°C) using annual and monthly data, respectively, suggests that monthly values can be used to approximate the annual relationship. As described in section 2.1, cave temperatures approximate mean annual values for the region. As calcite precipitates from solution, there is an additional temperature-based fractionation of approximately -0.24‰/°C (Kim and O'Neil, 1997). The atmospheric and calcite precipitation effects are additive, yielding a net fractionation of ~0.03‰/°C. Applying such a standard to our composite record (range=0.86‰) would reflect an unreasonable temperature change over the Holocene (~28.7°C). Correlations between $\delta^{18}O_w$ and the amount of precipitation are weak and positive (see Figure 5b).

However, as an indirect effect of the temperature dependence, we may be able to infer changes in seasonal variability from $\delta^{18}O$ values. Summer months are characterized

by relatively enriched $\delta^{18}O_w$ values with more depleted values associated with winter precipitation (IAEA/WMO, 2006) (Figure 5c). Studies of modern isotopes in precipitation indicate that seasonality provides an effective mechanism to explain changes in mean annual isotopic values (Vachon et al., 2007). An increase (decrease) in summer rainfall relative to the rest of the year would result in higher (lower) $\delta^{18}O_c$ values. Based on the data from Coschocton, a +0.4‰ shift in mean $\delta^{18}O_w$ can be achieved by increasing summer (JJA) precipitation by 66% (leaving all other seasons unchanged). The same effect can be achieved by increasing summer precipitation by 28% while decreasing winter (DJF) precipitation by 28% (Table 1). Similar effects have been shown in other studies of North American paleoclimate (Amundson et al., 1996; Edwards et al., 1996). Therefore, a strengthened BH circulation carrying more Gulf moisture would result in a greater contribution of summer precipitation to annual totals, resulting in relatively enriched $\delta^{18}O_w$. Because of the dependence of $\delta^{18}O_w$ values on the seasonal temperature cycle, warmer summers (and/or colder winters) may contribute to or amplify changes in $\delta^{18}O_w$.

In presenting a record of replicated $\delta^{18}O_c$ variability in three coeval speleothems, we find variation that is consistent with changes in the relative contribution of summer rainfall in the region. As summer months are also associated with higher levels of evaporation, such a change in seasonality will have significant effects on lake levels, groundwater recharge, streamflow, and plant communities (Shuman et al., 2004). It is important to note that our $\delta^{18}O_c$ record does not provide direct information about evaporation or the total annual amount of precipitation. Because $\delta^{18}O_c$ and $\delta^{13}C$ are independent of each other, evaporation is not likely to directly control variability in the

oxygen isotope record. However, $\delta^{13}C$ and trace-metal data from sample BCC-2 have previously been linked to long-term droughts during the Holocene (Springer et al., 2008). A decrease in annual precipitation that was equally distributed across all seasons would be recorded as a drought by $\delta^{13}C$ and trace-metals, yet $\delta^{18}O_c$ would remain unchanged. As seen in Figure 2, some arid intervals determined by Springer et al., 2008 correspond to depleted $\delta^{18}O_c$, suggesting a stronger decrease in summer precipitation associated with these events.

4.2. Climatic implications of the isotopic record

The abrupt isotopic shift in the BCC record at ~4.2 ka is coincident with widespread climatic changes in North America and worldwide. In the Rocky Mountains, upland tree vegetation experienced a significant die off, attributed to a decrease in summer temperature (Benedict et al., 2008) and the upper Midwest experienced several prolonged droughts during this transition interval (Booth et al., 2005). Evidence of aridity in the Red Sea basin (Arz et al., 2006) and Mesopotamia (Staubwasser et al., 2003), as well as widespread ecological and hydrologic changes in Africa and South America (Marchant and Hooghiemstra, 2004) point to the global nature of this event.

As monsoon systems have a large impact on subtropical circulation (Rodwell and Hoskins, 2001), the long-term trend in our record may be explained by reduced adiabatic descent over the sub-tropical North Atlantic due to a weakening Asian summer monsoon over the Holocene (Dykoski et al., 2005). If that is the case, then the transition at 4.2 ka may be a non-linear response to the gradual decline of summer insolation, possibly relating to the activation of ENSO in the late Holocene (Conroy et al., 2008). El Niño events are associated with an increase in regional winter precipitation (Wang et al.,

2006), which, combined with the weakened influence of the ASM, would result in more negative $\delta^{18}O_c$. Alternatively the observed transition in our record may be a time-transgressive feature across eastern North America, as Kirby et al. (2001) noted a similar shift at ~5 ka in northern New York state (43°03'N, 78°58'W).

Our stalagmite record also provides some interesting results over the past 2000 years. Beginning at ~800 A.D., there is a small, but noticeable decline in $\delta^{18}O_c$ values that is temporally coincident with the Late Tang weak monsoon period (LTWMP) observed in Chinese speleothems (Zhang et al., 2008) and first identified as an aridity event in the Yucatan (Curtis et al., 1996; Hodell et al., 2001). As detailed by Zhang et al. (2008), the timing of the LTWMP is coincident with several notable climatic events in the Northern Hemisphere, consistent with a southerly shift in the Intertropical Convergence Zone. Similarly, there is a noted decrease in $\delta^{18}O_c$ during the Late Ming weak monsoon period (LMWMP) defined by Zhang et al. (2008). The expression of this variability appears best captured by sample BCC-4, but it is also apparent to a lesser degree in the composite record (Figure 3). These results are consistent with the link between the Asian summer Monsoon and the BH circulation as noted by Rodwell & Hoskins (2001), and further validate our interpretation.

Our results are also consistent with previous work arguing that the seasonality of precipitation in ECNA has changed over the Holocene (Shuman and Donnelly, 2006), most likely due to changes in the intensity of the BH. Summer precipitation constituted a greater proportion of annual totals during the mid-Holocene, with a transition to more seasonally distributed precipitation at around 4.2 ka. The most positive values in our record occur from 4 to 6 ka and roughly correspond to an interval of lower lake levels at

Crooked Pond (Shuman et al., 2001), consistent with the argument of Shuman and Donnelly (2006) about the effects of a seasonal shift in precipitation toward summer months.

A possible driving factor for the observed variability in $\delta^{18}O_c$ is the divergent trends of summer and winter insolation over the Holocene (Figure 2). BH intensity is influenced by summer temperatures, and its relative importance for precipitation in ECNA appears to have declined over the Holocene along with summer insolation. In contrast, winter insolation increased over the same period, as have January temperatures (Willard et al., 2005). In modern climate, the warmer winters of recent decades correspond to a decrease in the formation of continental anticyclones (Rohli and Henderson, 1998), which form preferentially during winter months and normally block meridional moisture transport (Davis et al., 1997). A diminished blocking pattern due to winter warming would allow increased winter precipitation in ECNA and drive $\delta^{18}O_w$ toward more negative values. El Niño events are also associated with increased winter precipitation in the region (Wang et al., 2006). An increase in winter storms, such as nor'easters, would result in more depleted $\delta^{18}O_c$, and could explain some of the variability seen in more recent parts of the record. As ENSO variability has increased in the late Holocene, this could further enhance the changing seasonal precipitation observed in our record.

5. CONCLUSION

Our replicated record of changing seasonality of precipitation provides new insight into the climate of ECNA during the Holocene. One of the strengths of our methodology is the production of a composite record, helping to filter out noise in

individual samples and focus on more robust aspects of the record. The inherent heterogeneity of karst systems makes a replication test especially important when working with speleothems (Baker et al., 1997), and it has been used in many previous studies to validate the detection of climate signals. .

Our results, consistent with other Holocene records, support the conclusions of Shuman & Donnelly (2006) and provide a high resolution record of changes in the seasonality of precipitation over the last 8,000 years. These changes in the relative contribution of summer precipitation during the Holocene are most likely controlled by variability in BH intensity. The timing of shifts in the BCC record further suggests broader links with northern hemisphere hydroclimate. A sharp reduction in seasonality at ~4.2 ka occurred coincident with aridity events in the upper Midwest, Red Sea, and Mesopotamia. Similarly, short term reductions in seasonality over the last 2,000 years correspond to aridity in the Yucatan and weak monsoon periods in China.

ACKNOWLEDGEMENTS

The authors would like to thank Justin Revenaugh for help with constructing the composite record, Chris Folland for providing data on the SNAO Index, Xianfeng Wang and two anonymous reviewers for comments on the manuscript, and Gene Turner for permission to enter Buckeye Creek Cave and collect the stalagmites used in this project. The research was supported by NSF grants EAR 0903071 to HDR and EAR 0902867 to RLE.

Figures and Tables

Figure 2-1 Study site and modern $\delta^{18}O$ of July Precipitation.

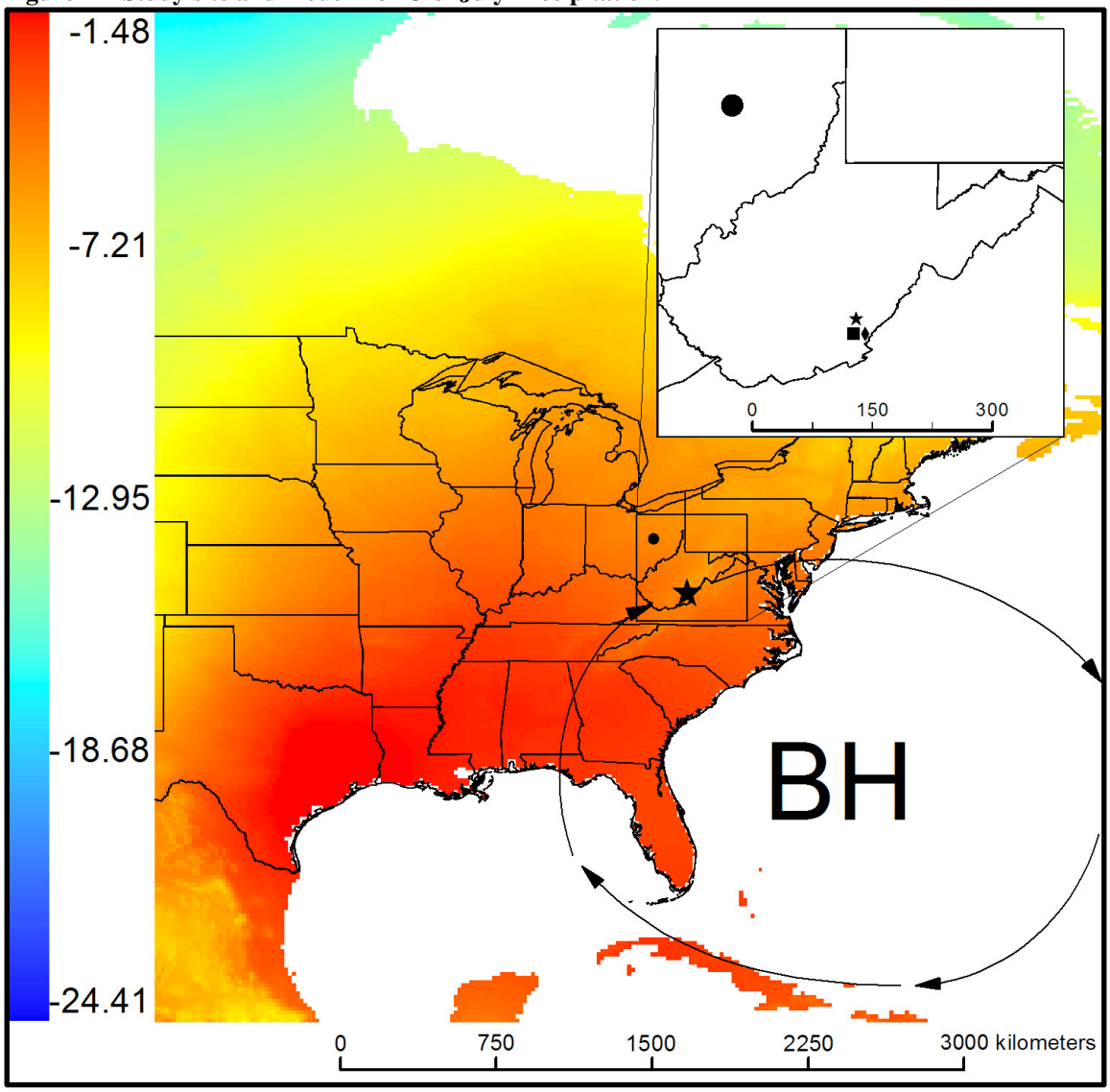

Figure 1. Map of study area in relation to the Bermuda High. Colors indicate mean oxygen isotopic values of precipitation (‰ $\delta^{18}O_w$) for July based on the calculations of Bowen et al. (2005) (Bowen 2009). The cave site is marked with a star.

Figure 2-2 $\delta^{18}O$ record of samples BCC2, 4, and 6.

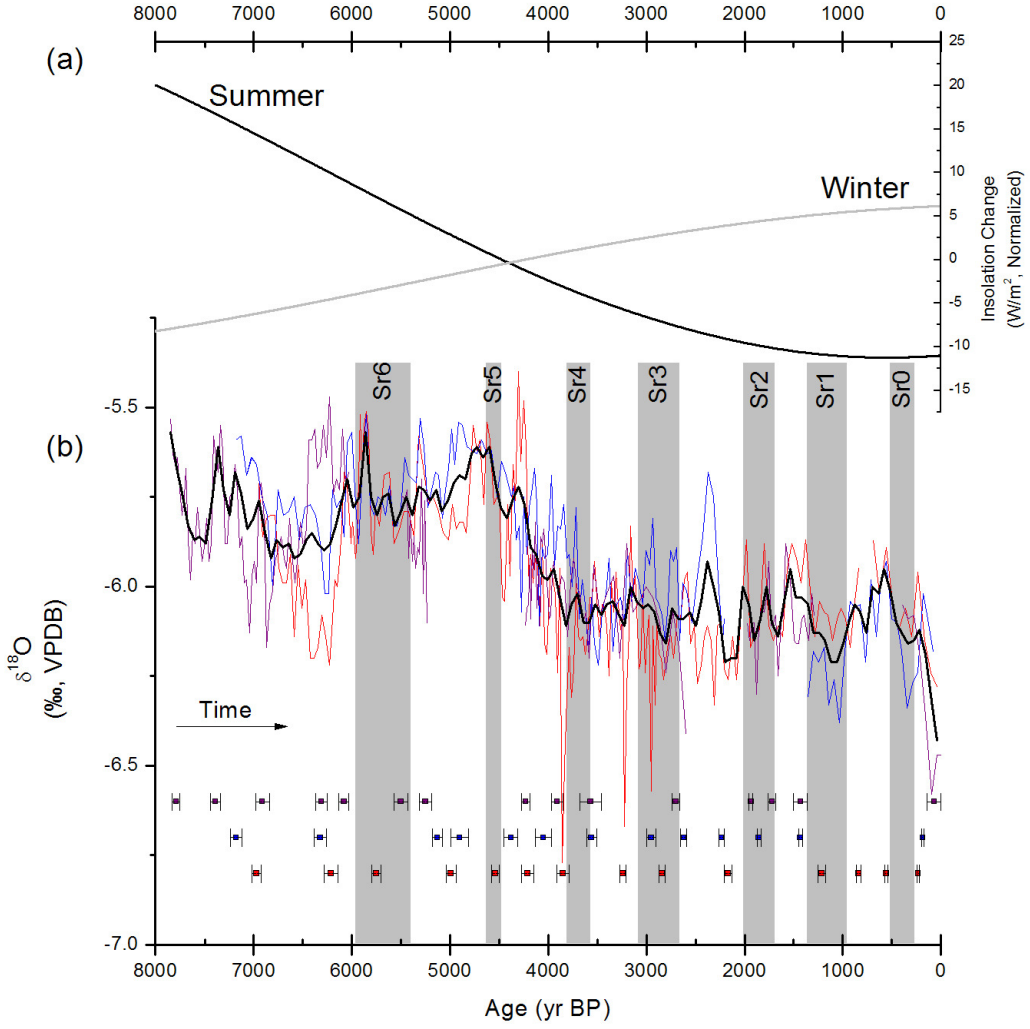

Figure 2. (a) Normalized summer (June 21) and winter (December 21) insolation changes at 38°N over the past 8000 years (Laskar et al., 2004). Insolation values are normalized by removing the mean to allow easier comparison. (b) $\delta^{18}O_c$ from samples BCC-2 (red), BCC-4 (blue), BCC-6 (purple) and the composite time series (black). U/Th dates (with error) used to construct the age models are included below.

Figure 2-3 $\delta^{18}O$ variability over the last 2000 years.

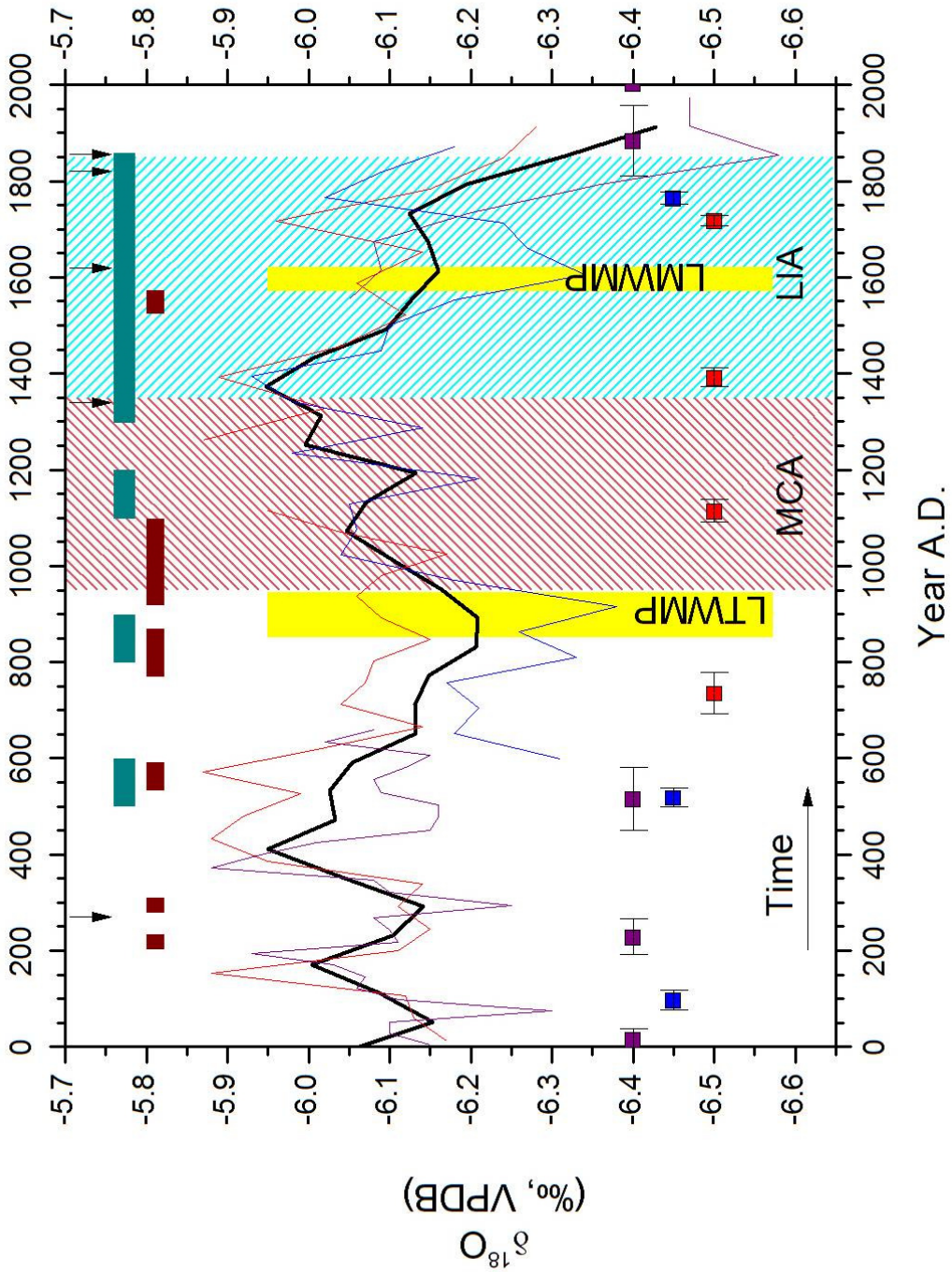

Figure 3. $\delta^{18}O_c$ plotted v. Year AD. Colors are the same as in Figure 2b. The approximate times of the Medieval Climate Anomaly (MCA) and Little Ice Age (LIA) are indicated. The Late Tang and Late Ming weak monsoon periods (LTWMP and LMWMP, respectively) are indicated with yellow bars based on the timing determined by Zhang et al. (2008). Dark cyan bars indicate extension intervals of the Alpine glacier record of Holzhauser et al. (2005). Intervals that come from a single glacier are marked with arrows. Dark red bars denote Yucatan drought events (Haug et al., 2003; Hodell et al., 2005a, 2005b, 2007)

Figure 2-4 Modern summer (JA) precipitation compared to the SNAO.

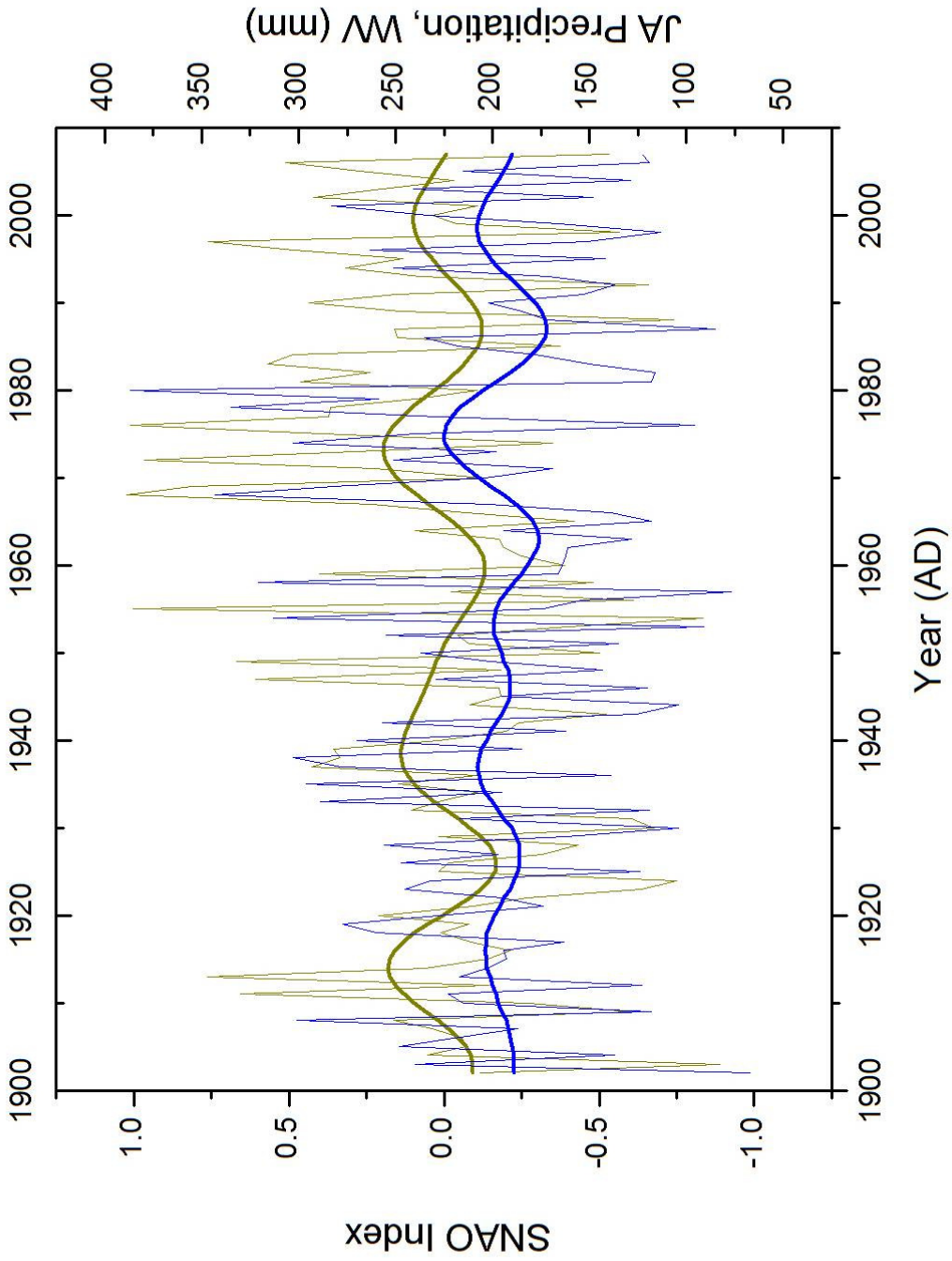

Figure 4. Summer North Atlantic Oscillation (SNAO) Index (dark yellow) compared with July and August (JA) precipitation from southern WV (blue) from 1900 to 2007. Thicker lines are used for the smoothed results produced by filtering at a frequency of 0.04 $year^{-1}$ (25 year period) and a bandwidth of 0.015 $year^{-1}$.

Figure 2-5 Modern isotopes in precipitation and comparison to temperature and amount.

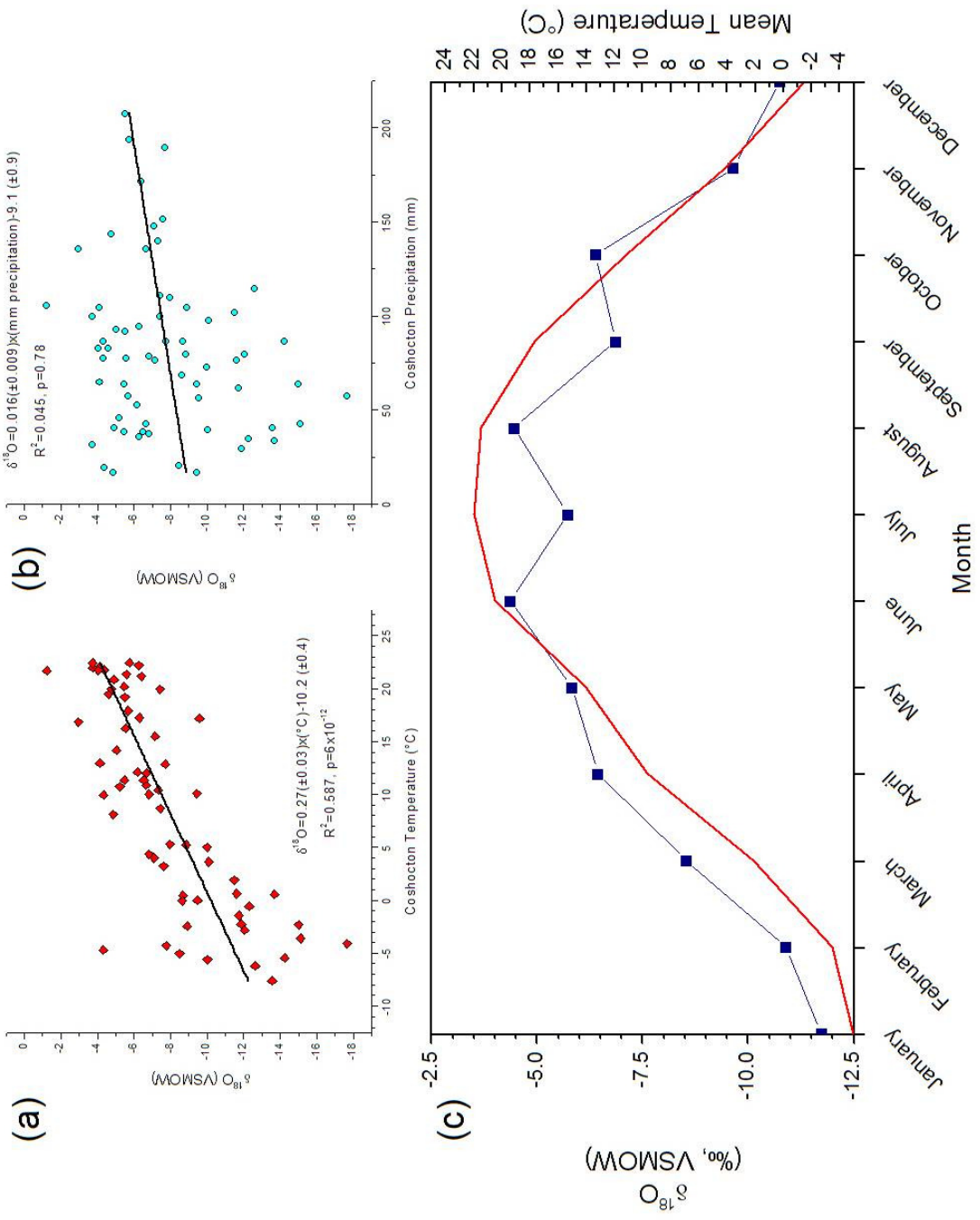

Figure 5. (a) Regression of temperature against $\delta^{18}O_w$ at the GNIP station in Coshocton, OH. Regression equation, R^2 and p-value as indicated with standard errors in parentheses. (b) Regression of precipitation against $\delta^{18}O_w$ at the GNIP station in Coshocton, OH. Regression equation, R^2 and p-value as indicated with standard errors in parentheses. (c) Monthly average $\delta^{18}O_w$ from Coshocton, OH (blue) based on weighted monthly $\delta^{18}O_w$ values plotted with monthly mean temperatures (red) during the sampling interval (1966-1971).

Table 2-1 Modern isotopic composition of seasonal rainfall

Table 1. Modern seasonal distribution of rainfall and isotopic composition compared with two scenarios that would increase mean annual $\delta^{18}O_w$ by 0.4‰, as observed during the mid-Holocene. All data are from the GNIP station in Coshocton, OH.

Season	**$\delta^{18}O$**	**mm modern**	**Summer Alone**	**%change**	**Summer and Winter**	**%change**
DJF	-11.14	195	195	0%	140	-28%
MAM	-6.83	283	283	0%	283	0%
JJA	-5.02	308	513	66%	395	28%
SON	-8.03	204	204	0%	204	0%
Precipitation total (mm)		991	1195		1022	
Annual Mean $\delta^{18}O_w$		-7.36	-6.96		-6.96	

Chapter 3: Precession-scale variability in eastern North American seasonal precipitation and potential links to Atlantic ITCZ migration and thermohaline circulation

Evidence from speleothems in Buckeye Creek Cave (BCC) in east central North America demonstrate clear variability at precessional scales. While monsoon and polar regions respond to changes in summer insolation, BCC $\delta^{18}O$ varies anti-phased (in-phase) with spring (autumn). Millennial-scale events that are coincident with China and Brazil are also recorded by BCC $\delta^{18}O$, although the response is of limited amplitude, suggesting that our record responds more strongly to summer forcing than to winter changes associated with the Younger Dryas, stadials, or Heinrich events, similar to observed changes in Gulf of Mexico sea surface temperatures (SSTs). Based on analysis of modern precipitation, $\delta^{18}O$ most likely represents changes in the balance of seasonal precipitation, suggesting a relative increase in summer precipitation during spring (autumn) insolation minima (maxima). The observed variability in our record could be a response to: variation in the Atlantic Warm Pool (AWP); changes in state of the El Niño Southern Oscillation (ENSO); or a seasonally lagged SST response that enhances the North Atlantic subtropical anticyclone. Glacial meltwater draining into the Gulf of Mexico could also impact seasonal precipitation by depressing SSTs and creating a high pressure anomaly in the northern Gulf. In addition to the effects on seasonal precipitation in east central North America, these scenarios could also alter moisture advection from the Atlantic basin, with consequences for

thermohaline circulation on precessional-scales with a phase lag relative to summer insolation.

Introduction

Seasonality is a major characteristic of global climate. Variability in summer insolation was a major driver of polar and tropical Pleistocene climate, providing a major control on the growth and decay of continental ice sheets, and variability in summer monsoon intensity (Wang et al., 2001). In addition, millennial events are believed to represent a strong response to changes during the winter season (Denton et al., 2005). Because they do not represent the climate extremes of winter or summer, spring and autumn seasons have recently comparatively less attention, with a few observed records showing variability in phase with these transitional seasons. However, model results suggest a potential role of seasonally-lagged sea surface temperature response in affecting winter climate in Europe (Hall et al., 2005), providing a basis for further study.

Materials & Methods

Site Description

The cave site (37°58' N, 80°24'W, 600 masl) is located in Mississippian limestone of the Greenbrier Group in the Allegheny Mountains of West Virginia (Cardwell et al., 1968; Dasher and Balfour, 1994) (Figure 1). Buckeye Creek Cave (BCC) contains 7.14 km of mapped passages, and samples were collected from chambers approximately 35m below the surface. Oxygen isotopes of drip waters (-8.5‰) approximate local mean annual values from precipitation (-8.37‰, Welker et al., 2002). Modern summer precipitation is associated with enriched $\delta^{18}O$, while winter values are

more depleted, and spring and autumn are close to mean annual values (Hardt et al., 2010).Cave temperatures (10.7°C) are stable throughout the year and are similar to local mean annual temperature (10.2°C).

Sample Collection and Analytical Methods

All stalagmite samples were collected in situ from BCC in late 2004, >1 km from the cave entrance. Samples were cut along the growth axis with a tile saw, polished, and drilled for stable isotope and U-series measurements.

Stable isotope samples were milled at 1-mm (BCC9) and 0.5-mm (BCC10) intervals along the vertical growth axis and analyzed using a GasBench II coupled to a ThermoFinnigan DeltaPlusXP IRMS. Samples were standardized to V-PDB using NBS-19, with standard and unknown precisions for $\delta^{18}O$ and $\delta^{13}C$ averaging 0.10‰.

Radiometric age constraints were provided by U/Th dating techniques developed for carbonates (Broecker, 1963) and adapted for measurement on an inductively coupled plasma mass spectrometer (Edwards et al., 1987; Shen et al., 2002) at the University of Minnesota using the decay constants of Cheng et al., 2009 (Cheng et al., 2009). Calcite powder was sampled using a dental drill with a 0.9-mm diameter tungsten-carbide drill bit. Age errors are generally small and on the same order as the growth rate over the sampled interval. Age models were constructed based on U/Th age constraints using cubic splines in *clam* (Blaauw, n.d.) (See Supplemental Tables 1 and 2). Analyses were performed on a Finnigan-MAT Neptune with a single MasCom multiplier, or Faraday cups.

Ice volume correction

The true pattern of variability is actually larger than that recorded by the speleothems. This is because the speleothem record is a function of changes in the $\delta^{18}O_{sw}$, which is enriched during periods of ice sheet expansion. Therefore, the true signal in our record would be approximately 1‰ larger than what is recorded by the speleothem. Removing this effect from records more than ~30ka years old is extremely difficult due to the limitations of ocean core records both in resolution and age control. Over the last glacial cycle, benthic $\delta^{18}O$ records constrained by direct measurements of sea level from corals provides a reasonable means for removing the effect of changes in source water (Cutler et al., 2003).

Spectral analysis and phasing

Power spectra and phase angles between BCC $\delta^{18}O$ and insolation were determined by a cross Blackman-Tukey analysis (Blackman and Tukey, 1959) using AnalySeries (Paillard et al., 1996). Cross-spectral analyses were preformed for each segment of the BCC record – two from BCC9 (which has a hiatus at ~220ka) and one from BCC10. Phase angles quoted in the text are for a periodicity of 23 ka (1 ka ≈ 15.5°).

Results

Evidence from two speleothems collected in Buckeye Creek Cave (BCC) in east central North America show variability in calcite $\delta^{18}O$ ($\delta^{18}O_c$) on a precessional-scale over the last three glacial cycles, consistent with insolation forcing (Figure 1). In contrast to the behavior of speleothems in monsoon regions, $\delta^{18}O_c$ lags summer insolation changes and is generally anti-phased (in-phase) with spring (autumn) insolation (Figure 1), and the apparent lag cannot be explained by dating error, which ranges from 100-400

years (1.6-6.5° in the 23 kyr band). From 330 ka to 226 ka, $\delta^{18}O$ has a phase angle of 107°±7° relative to June 21 (in phase with October 7), similar to the observed phasing during Marine Isotope Stages (MIS) 3-5 (117°±7°, October 17). The period from 220 to 143 ka is shifted younger with a phase angle of only 60°±6° (August 20).

$\delta^{13}C$ shows secular trends towards more enriched values from 290-245 ka, 168-141 ka, and 97-41 ka (Figure 2). Several abrupt shifts punctuate the record, most notably in MIS 3, 4, and 5. Shifts to enriched values occur at 315, 233, 198, 157, 121, 96, 68, 56, and 47 ka. Of these, the event at 96 ka appears the most pronounced. Comparison with $\delta^{18}O$ does not yield any significant correlation, as $\delta^{18}O$ often becomes more depleted as $\delta^{13}C$ becomes more enriched. The range of $\delta^{13}C$ values is ~5.5‰ in BCC9 and ~7‰ in BCC10, much greater than that observed in $\delta^{18}O$ (~2‰ and 1.8‰ respectively).

Discussion

Interpretation of $\delta^{13}C$

In many ways, interpretation of $\delta^{13}C$ is more challenging than $\delta^{18}O$ due to the smaller mass of carbon in the precipitating solution. Several processes are known to influence $\delta^{13}C$ in speleothems. Changes in vegetation structure between C_3 and C_4 plants in the overlying landscape can alter $\delta^{13}C$ by changing the isotopic composition of soil CO_2 (Dorale et al., 1998). Alternatively, increased rock-water interaction time or precipitation of calcite in the vadose zone could also impact $\delta^{13}C$ (Fairchild et al., 2000, 2006a, 2006b). All three of these processes will tend towards enriched values during dry conditions. However, because there is no evidence that C_4 vegetation typical of prairie ecosystems extended as far east as our site, and the magnitude of change that can be accomplished by rock-water interaction alone is limited by the isotopic composition of

the bedrock (and unlikely to explain values as high as 1.55‰), prior precipitation appears the most likely explanation for our record.

When calcite is precipitated in the vadose zone above the cave, $\delta^{13}C$ values increase in the residual solution. This is due to the relative enrichment of values of CO_2 and $CaCO_3$ from dissolved HCO_3^- (Hendy, 1971). Since carbon atoms are partitioned equally into calcite and CO_2, the net result is an increase in the isotopic value of the residual solution.

Coincident with the increase in $\delta^{13}C$ are changes in the solution's Mg/Ca and Sr/Ca ratios. As calcite precipitates, only trace concentrations of Mg and Sr are incorporated in the new crystal. The solution thus becomes enriched in Mg and Sr. Speleothems records of Mg/Ca more reliably measure prior precipitation than Sr/Ca as Sr inclusions in calcite are correlated with growth rate (Huang and Fairchild, 2001). Holocene samples from BCC show good correlation of $\delta^{13}C$ with Mg/Ca and Sr/Ca (Springer et al., 2008), consistent with a prior precipitation mechanism.

The driver behind this process requires the loss of CO_2 from the system. If the CO_2 produced by calcite precipitation remains in contact with the solution, it will re-equilibrate and re-dissolve the calcite. When the CO_2 is allowed to vent from the vadose zone, isotopically light carbon is removed from the system. The vadose zone is defined as unsaturated, meaning that some fraction of available pore space is air-filled (f_{air}). As the system dries out and f_{air} increases, there is increasing likelihood that air-filled passages will be connected to each other and to the surface, allowing CO_2 to escape. In order for the vadose zone to dry out, aridity must persist over a period of time.

Sea Level change and millennial events recorded in $\delta^{13}C$

Carbon isotopes appear to broadly track changes in sea level (Figure 3), particularly over MIS 3-5. As ice volume increases and temperatures cool, the atmosphere has less energy to evaporate moisture, leading to generally drier conditions. In addition to the more gradual changes associated with ice volume, several high frequency shifts to more enriched values occur during Heinrich events (Figure 4). The timing is coincident (within error) to similar changes in the Asian summer monsoon, and in Greenland temperature. The likely cause for this is a southward shift of the jet stream caused by fluctuations in the spatial extent of the Laurentide ice sheet (Calov et al., 2002), which also led to a southward displacement of the intertropical convergence zone (ITCZ) (Chiang et al., 2003; Wang et al., 2004).

Interpretation of $\delta^{18}O$

Previous work on samples from Buckeye Creek cave indicate that $\delta^{18}O_c$ varies in response to the composition of meteoric water, which is locally determined by season and moisture source as summer precipitation from the Gulf of Mexico exhibits more positive values than during other times of the year (Hardt et al., 2010). Based on analysis of modern isotopes in precipitation at the nearest station of the Global Network of Isotopes in Precipitation at Coshocton, OH (IAEA/WMO, 2006), temperature and the total amount of precipitation are unlikely to provide a strong control on $\delta^{18}O_c$ (Hardt et al., 2010). $\delta^{18}O$ and temperature at Coshocton do exhibit a significant correlation ($p<0.001$) based on monthly measurements, but with a slope of only +0.27‰/°C, far less than what has been observed in multi-station analyses (Rozanski et al., 1993; Yurtsever, 1975). Because oxygen isotope fractionation between water and calcite is of similar magnitude

and opposite sign (~-0.24‰/°C) (Kim and O'Neil, 1997), it is unlikely that temperature provides a substantial role in determining $\delta^{18}O_c$. Precipitation actually exhibits a non-significant positive correlation (p=0.78) with $\delta^{18}O$, the opposite relationship predicted by an amount effect (Hardt et al., 2010). Therefore, we interpret $\delta^{18}O_c$ as reflecting changes in the annual balance of precipitation between summer and winter. Because annual precipitation totals in the region do not depend on a single season, $\delta^{18}O_c$ does not provide a determination of wet or dry conditions, which appear to be best explained by $\delta^{13}C$ (Springer et al., 2008).

Controls on Seasonality of Precipitation

The North Atlantic subtropical anticyclone provides a significant control on seasonal precipitation in the continental United States (Davis et al., 1997). When the subtropical anticyclone, one component of the North Atlantic Oscillation (NAO), is strong, our site experiences an increase in summer rainfall (Hardt et al., 2010), with a corresponding decrease in winter precipitation (Davis, 1976). Previously studied samples from BCC showed enriched $\delta^{18}O_c$ during the mid-Holocene (Hardt et al., 2010), consistent with model results showing a stronger subtropical anticyclone and greater summer precipitation in the region. Several processes can produce a stronger anticyclone, including: warmer continents or cooler sea surface temperatures (SSTs) in the subtropical north Atlantic (Parrish and Peterson, 1988); a stronger ASM (Rodwell and Hoskins, 2001); a stronger North American Summer Monsoon (NASM) (Rodwell and Hoskins, 2001).

Relative v. Absolute Summer Precipitation

$\delta^{18}O$ likely reflects mean annual values of precipitation and varies in response to changes in the seasonal balance between summer and winter. Based on the relatively weak response to winter-season forced climatic shifts associated with millennial scale events, we argued that $\delta^{18}O_c$ is more strongly controlled by summer precipitation. Model results from the middle Holocene support this interpretation as they show elevated summer precipitation without any real change during winter. In addition, the modern precipitation data from nearby Lewisburg, WV supports this view as absolute JJA precipitation is a strong predictor of relative summer precipitation to annual totals (adjusted- $R^2 = 0.66$, $p<0.001$). In contrast, DJF precipitation does not show a significant relationship with a slope of essentially zero. See Figure 5

Links to ENSO

In addition to the relationship between JA precipitation and the Summer North Atlantic Oscillation demonstrated by Hardt et al., 2010, ENSO also influences the seasonal distribution of precipitation in the BCC region (Mo and Schemm, 2008). Figure 6 shows the correspondence between annual average SST anomalies in the NINO3.4 region of the tropical Pacific and the percentage of annual precipitation that falls during the summer months (JJA). La Niña (El Niño) conditions are associated with an increase (decrease) in relative summer precipitiation.

Anti-correlation with spring insolation

Anti-correlations with spring insolation changes have previously been observed in other climate proxies, although none have yet recorded multiple precessional cycles with precise age control. The Lake Baikal record is tuned to autumn insolation based on an

empirically derived relationship in the dated portion of the sediment core (Prokopenko et al., 2006). Stalagmites in Borneo also show variability antiphased with spring insolation (Partin et al., 2007). Furthermore, while $\delta^{18}O$ in Brazilian speleothems generally varies with summer insolation (Wang et al., 2007; Cruz et al., 2005), several wet periods in northeastern Brazil appear centered on local spring insolation minima (Wang et al., 2004).

Millennial events

When comparing BCC to southern Brazil, several millennial scale events (Wang et al., 2007, 2004; Cruz et al., 2005), corresponding to a southward shift in the mean position of the Atlantic ITCZ, appear to be coincident between the records. Despite a clear phase difference at precession scales, millennial-scale events appear coincident between the records with decreases (increases) in summer precipitation in Brazil corresponding to increases (decreases) in West Virginia $\delta^{18}O_c$ (Figure 7). The response in the Asian Summer Monsoon (ASM) to these events is also coincident and opposite to the observed changes in Brazil. While the timing is within the dating error, the relationship between BCC and the tropics appears damped or non-linear as the amplitude of these events in BCC is much smaller than that observed in Brazil or China. Looking over the full record from BCC reveals a number of other abrupt events that appear to be coincident between the two records (Figure 8).

Relationship with SSTs in the Gulf of Mexico

While Brazilian speleothems follow changes in the southern extent of the Atlantic ITCZ, SSTs in the Gulf of Mexico (Ziegler et al., 2008) determine the northernmost position. Because the Gulf is the source region for precipitable moisture for much of

North America (Peixóto and Oort, 1983), SSTs exert significant influence on moisture transport into the continental interior (Oglesby et al., 1989). Mg/Ca derived SSTs in the Gulf of Mexico also show clear precessional-scale variability, but lack the abrupt shifts associated with stadials, Heinrich events, or the Younger Dryas (Ziegler et al., 2008). Because many abrupt climate shifts in the late Pleistocene are strongly controlled by changes in the winter season (Denton et al., 2005), this suggests a coherence of Gulf SST with summer forcing and at most a weak connection to the winter season. This relationship may be partially explained by the effects of the partitioning of glacial meltwater between the Gulf of Mexico and the North Atlantic (Hill et al., 2006), as the Gulf of Mexico responded more strongly to melting events that drained through the Mississippi. Similar to SSTs in the Gulf of Mexico, our record appears largely insensitive to millennial-scale events, and differences between the timing of our record and that of Gulf SSTs are within the error of the age models (Figure 9). Our record also shows a brief (~2kyr) depletion event coincident with glacial flooding in the Gulf of Mexico (Hill et al., 2006). Lack of overlap between the records precludes further comparison.

Potential explanations for the observed phasing

While BCC is clearly out of phase with the ASM on orbital scales, several millennial-scale events appear to be coincident, despite weaker amplitude in West Virginia (Figure 8). This suggests that the connection between the ASM and is instantaneous within dating uncertainty. Because of the damped response of BCC to millennial events, it is likely that our record is more sensitive to summer forcing, and what response there is

could be explained by the connection between the ASM and the North Atlantic subtropical anticyclone (Rodwell and Hoskins, 2001).

In addition to the phase difference between BCC and the ASM, BCC also does not show the sharp boundaries between periods of increased relative summer precipitation that are seen in ASM records. Instead, BCC shows greater similarity to the more gradual changes observed in southern Brazil (Wang et al., 2007; Cruz et al., 2005), where precipitation is controlled by the seasonal migration of the Atlantic ITCZ. While the ASM is essentially an extension of the ITCZ, the abrupt transitions may be due to the low thermal inertia of continents, which allows stronger penetration of monsoonal rains. In contrast, the oceanic ITCZ responds more linearly to insolation forcing. It is therefore likely that the processes governing $\delta^{18}O_c$ at our site are linked to ocean SSTs.

Given the resemblance between BCC $\delta^{18}O_c$ and Gulf of Mexico SSTs, links between summer precipitation in the eastern US and Gulf SSTs (Wang et al., 2010), and the fact that a +NAO state corresponds to warmer Gulf SSTs (Wang, 2005), we suggest that our record may provide an indirect measure of the northern extent of the Atlantic ITCZ during boreal summer. This would imply a greater range for the seasonal migration of the Atlantic ITCZ during some intervals when the mean ITCZ position is displaced to the south (Wang et al., 2004; Chiang et al., 2003; Haug et al., 2001). Because the ITCZ position in boreal v. austral summer is generally 180° out of phase, this would suggest unique behavior of the Atlantic ITCZ, possibly due to the geometry of the Atlantic basin.

Therefore, our record could simply be a response to variations in the Atlantic Warm Pool (AWP) associated with the ITCZ. The AWP reaches its maximum during September and enhances moistures transport in the continental US by strengthening the

NASM and increasing specific humidity (Wang et al., 2007). However, regional September precipitation is intermediate in $\delta^{18}O$ (-6.86‰, VSMOW) and would not provide very much leverage in changing mean annual values (-7.36‰, VSMOW) (Hardt et al., 2010). In addition, the AWP begins its expanding to the north during the boreal spring, suggesting it would respond more strongly to an increase in the duration of the warm season. Were the AWP the primary forcing of BCC $\delta^{18}O_c$, we would expect a stronger obliquity signal (Huybers, 2006), both in BCC and Gulf SSTs. Precession-scale variability remains the most prominent feature of our record and so the forcing process must similarly vary on a precessional-scale.

Alternatively, changes in the El Niño-Southern Oscillation (ENSO) may be a factor. Modeled ENSO response to orbital forcing produced a result with similar phasing to our record (Timmermann et al., 2007), although transitions between states is more abrupt and the phasing may be a consequence of chosen model parameters. Modeled La Niña (El Niño) -like states occur during positive (negative) $\delta^{18}O_c$ anomalies, consistent with modern climate (Mo and Schemm, 2008; Wang et al., 2006), possibly due to ENSO's influence on the position of the North Atlantic subtropical anticyclone (Seager et al., 2005). While ENSO may contribute to the observed phasing in our record, the correspondence between decreased summer precipitation in West Virginia and wet conditions in both northeast (Wang et al., 2004) and southern Brazil (Wang et al., 2007; Cruz et al., 2005) on millennial scales suggests that ENSO cannot fully explain the observed variability (Wang et al., 2007) in our record. Instead, the link to northeast Brazil is more likely due to an independent connection between a strong North Atlantic subtropical anticyclone and droughts in northeast Brazil (Namias, 1972).

Changes in the strength of the North Atlantic subtropical anticyclone may provide an alternate explanation for the observed phasing in our record. Spring insolation minima producing cooler summer SSTs in the subtropical gyre could enhance circulation and result in stronger seasonal moisture advection from the Gulf of Mexico. Several studies have previously shown a seasonally-lagged response in SSTs (Davis, 1976; Czaja and Frankignoul, 1999; Hall et al., 2005), and summer SSTs show strong autocorrelation with the preceding spring (Kushnir et al., 2002). This mechanism would explain the phasing, gradual rate of change in our record, and a potential connection to millennial events in China and Brazil. An additional factor to consider is the effect of melting ice on GOM SSTs. When summer insolation is high, melting approaches a maximum, leading to a greater flux of cold, fresh, water into the northern GOM via the Mississippi (Nürnberg et al., 2008). Cold meltwater would produce a high pressure anomaly over the northern Gulf and reduce southerly moisture flow into the continental US (Oglesby et al., 1989; Henderson and Vega, 1996), potentially offsetting any enhancement of the subtropical anticyclone by the ASM. This would especially impact our record as warmer Gulf SSTs specifically correspond to wet summers in the eastern US (Wang et al., 2010). During MIS 6-7, our record is slightly younger in phase than during MIS 3-5 or MIS 8, which may be due to a more limited influence of Mississippi river flow during the penultimate glacial period (Nürnberg et al., 2008) (Figure 9).

Links to Thermohaline circulation

A more northerly position of the boreal summer ITCZ could have implications for thermohaline circulation (Dong and Sutton, 2005; Schmidt et al., 2004) by maintaining moisture export from the Atlantic even during periods when the mean ITCZ position is

shifted to the south. When the ITCZ is regionally shifted to the north, warmer SSTs in the northeastern tropical Pacific produce stronger convection and enhanced moisture export from the Atlantic to the Pacific (Xie et al., 2005; Benway et al., 2006). Holocene samples from BCC showed short-term minima in $\delta^{18}O_c$ during periods of drought in the Yucatan (Hardt et al., 2010; Hodell et al., 2001), consistent with a link between BCC $\delta^{18}O_c$ and moisture flow across central America. Cross-isthmus transport, however, depends on conditions both in the Gulf of Mexico and the Pacific, and BCC is more likely to respond only to changes in the Gulf and the AWP, which may account for differences between BCC and measures of salinity in the East Pacific Warm Pool (Benway et al., 2006; Leduc et al., 2007). Significant uncertainty remains about the controls on moisture export from the Atlantic to the Pacific. While paleoclimate studies suggest a link to the ITCZ position (Benway et al., 2006; Leduc et al., 2007), model results suggest that export could be enhanced during Heinrich events (Pahnke et al., 2007). Other studies have suggested a role for cool Atlantic and warm Pacific SSTs (Weaver et al., 2009), El Niño events (Schmittner et al., 2000), and a stronger Caribbean low level jet (Muñoz et al., 2008).

Figures

Figure 3-1 $\delta^{18}O$ of samples BCC9 and 10 compared to Insolation.

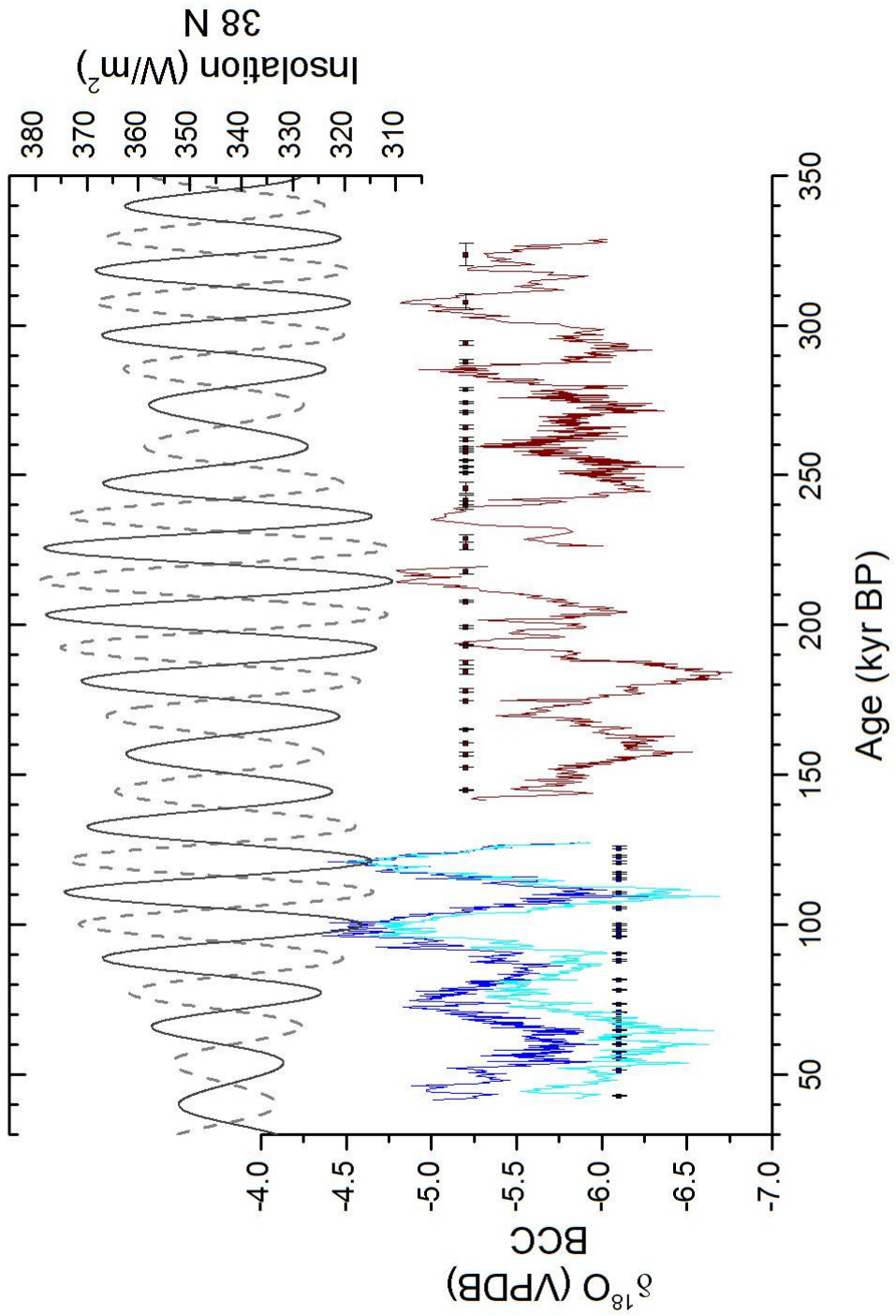

Figure 1. Calcite $\delta^{18}O_c$ of samples BCC10 in dark blue (raw) and light blue (ice volume corrected) and BCC9 in dark red with ages and error bars plotted against spring (March 21, solid grey) and autumn (September 21, dashed) insolation at 38°N latitude (Laskar et al., 2004). $\delta^{18}O_c$ in both samples shows clear precession-scale variability that is anti-phased (in-phase) with spring (autumn) insolation changes. 38°N was chosen as it is the approximate latitude both for our study site and for the Azores, a common center of action for the North Atlantic subtropical anticyclone. As the phasing is the key aspect of the record, the choice of latitude is not a critical factor.

Figure 3-2 $\delta^{13}C$ and $\delta^{18}O$ from samples BCC9 and 10.

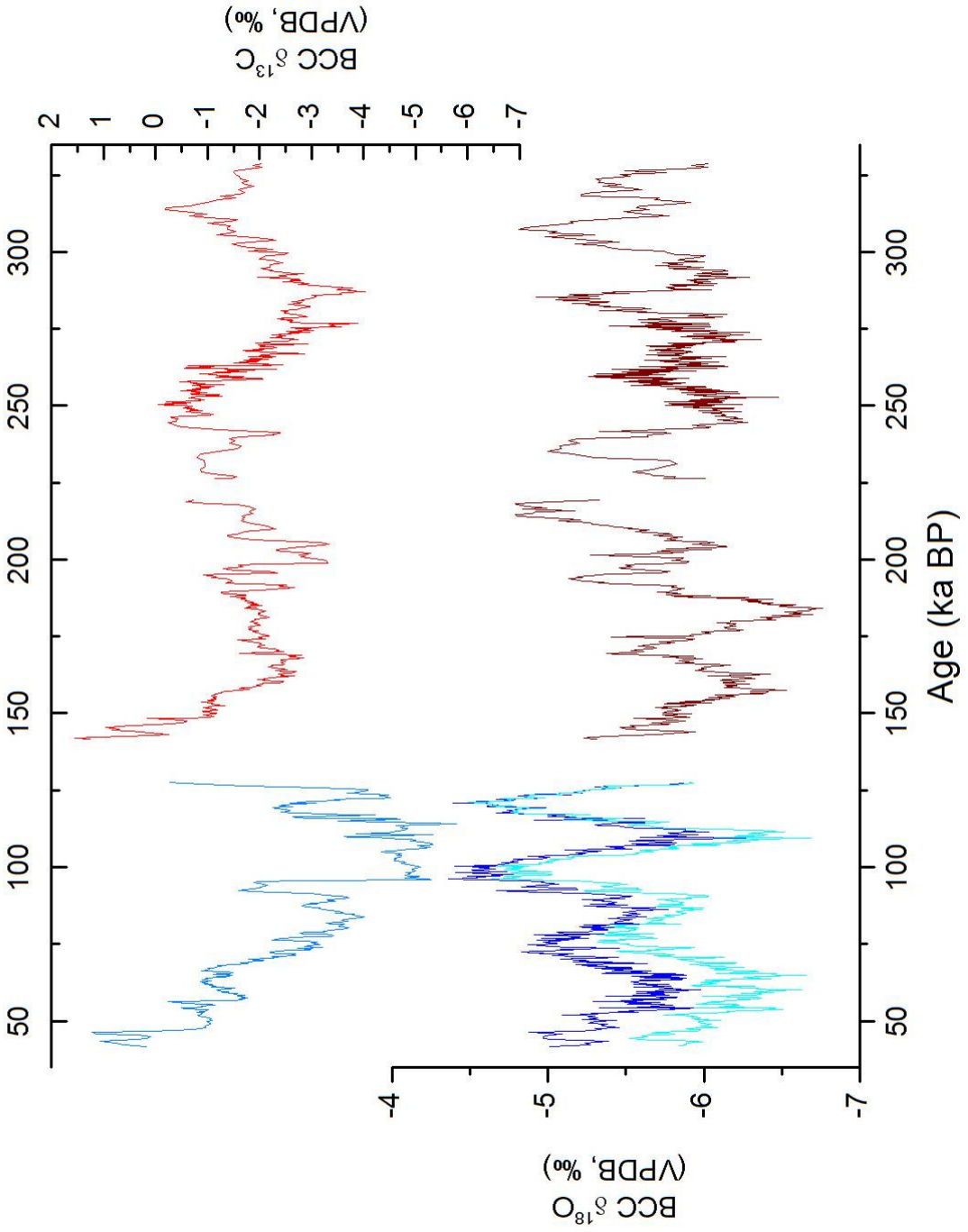

Figure 2. Carbon (top) and Oxygen (bottom) isotopic variability for samples BCC9 and BCC10. Colors for the $\delta^{18}O$ are as shown in Figure 1. BCC9 $\delta^{13}C$ is shown in red and BCC10 in teal.

Figure 3-3 $\delta^{13}C$ compared to sea level.

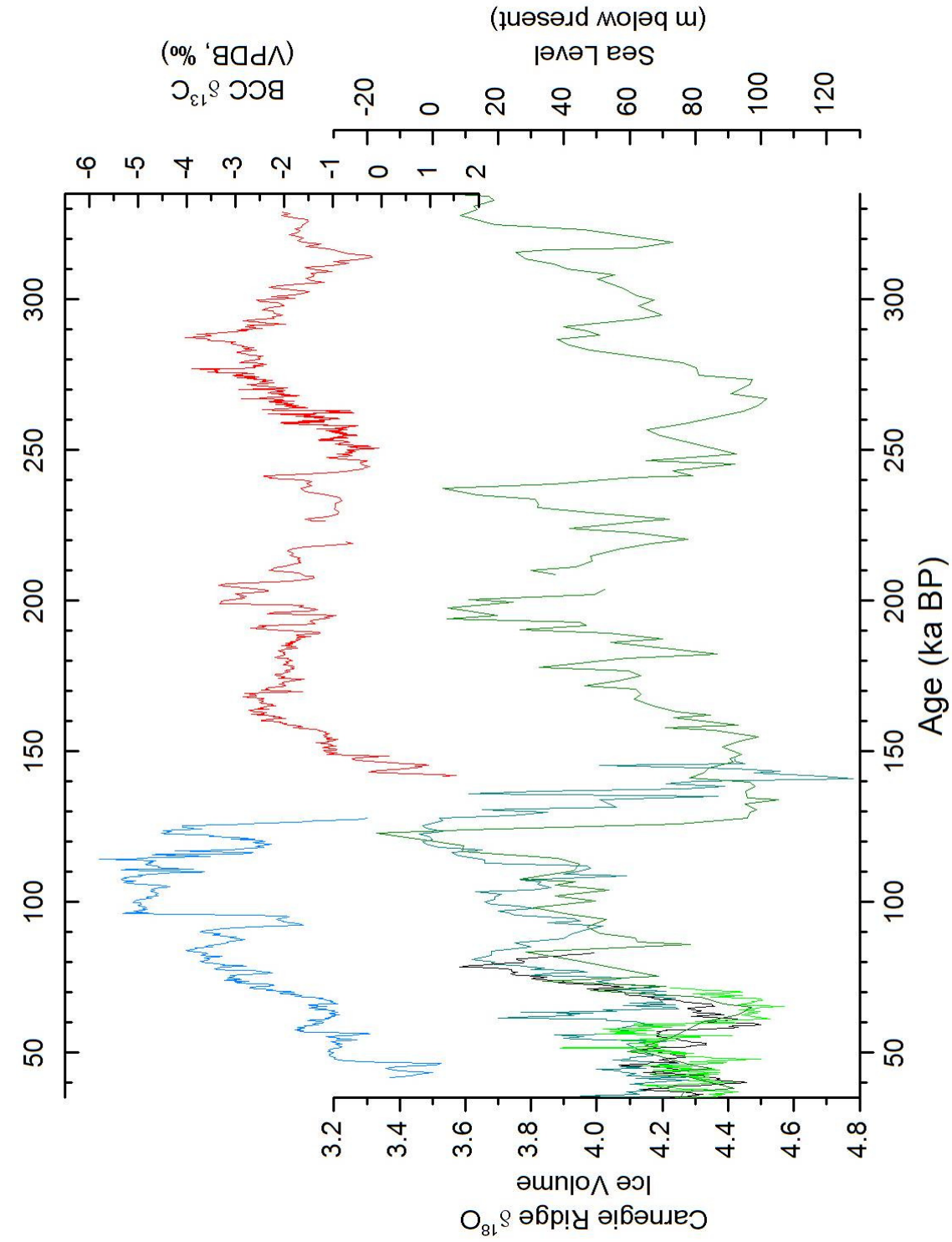

Figure 3. $\delta^{13}C$ from BCC (top, colors as in Figure 2) and records of sea level change (bottom) from the Red Sea (Arz et al., 2007 (black); Siddall et al., 2003 (light and dark green)), and the coral-adjusted ages of core V19-30 in dark cyan (Cutler et al., 2003; Shackleton et al., 1983).

Figure 3-4 Millennial events in $\delta^{13}C$ of sample BCC10.

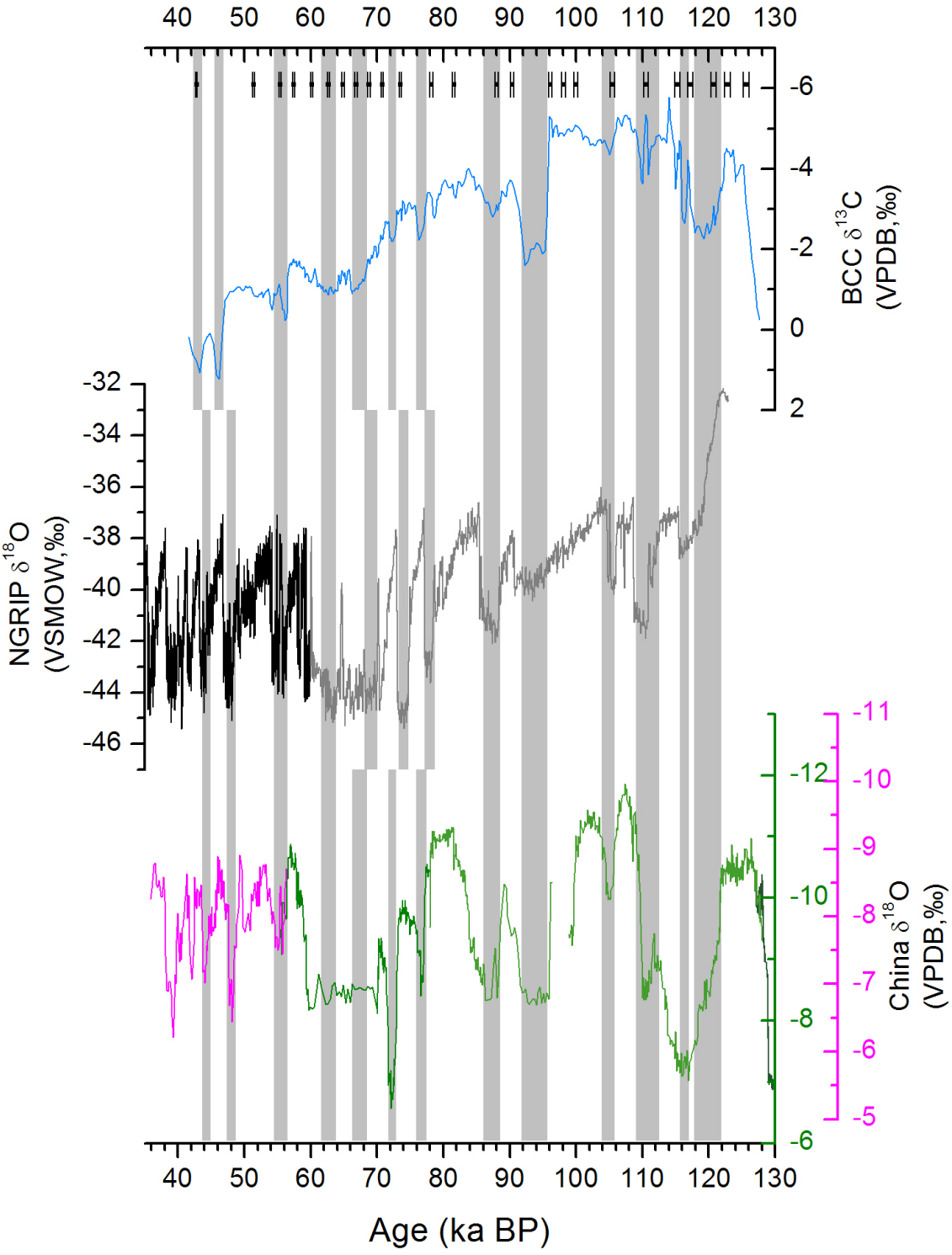

Figure 4. Millennial scale events recorded in BCC 10 $\delta^{13}C$, top compared to NGRIP, middle (Andersen et al., 2004; Svensson et al., 2008) and changes in the Asian summer monsoon recorded at Hulu cave (pink) and Sanbao cave (green), bottom (Cheng et al., 2009; Wang et al., 2008, 2001). Grey bars indicate shifts to enriched values in $\delta^{13}C$ and potential points of correlation with the other records (within dating error).

Figure 3-5 DJF and JJA precipitation amount as predictors of relative summer precipitation.

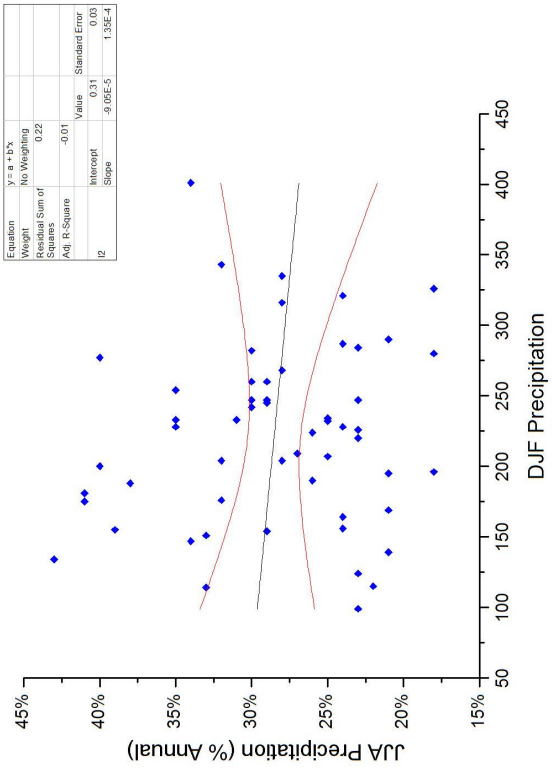

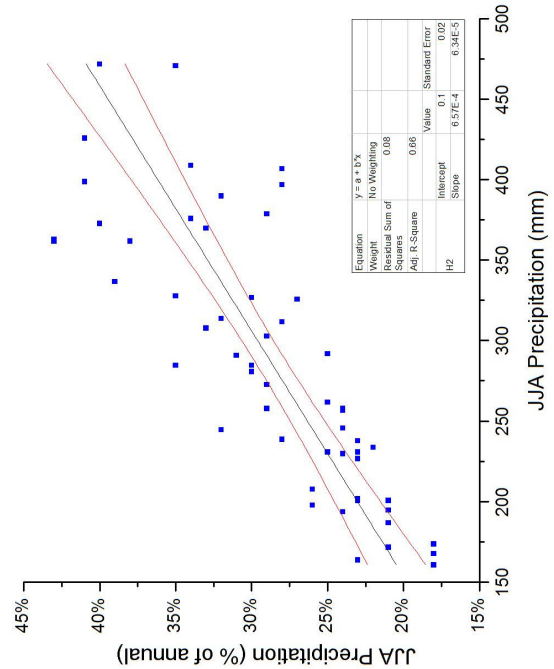

Figure 5. Regression of JJA precipitation as a percentage of annual totals against JJA precipitation (left) and DJF precipitation (right) in mm based on data from Lewisburg, WV from 1950-2009. Red lines indicate the 95% confidence envelope about the slope of the line.

Figure 3-6 Modern relative summer (%JJA) precipitation compared to ENSO.

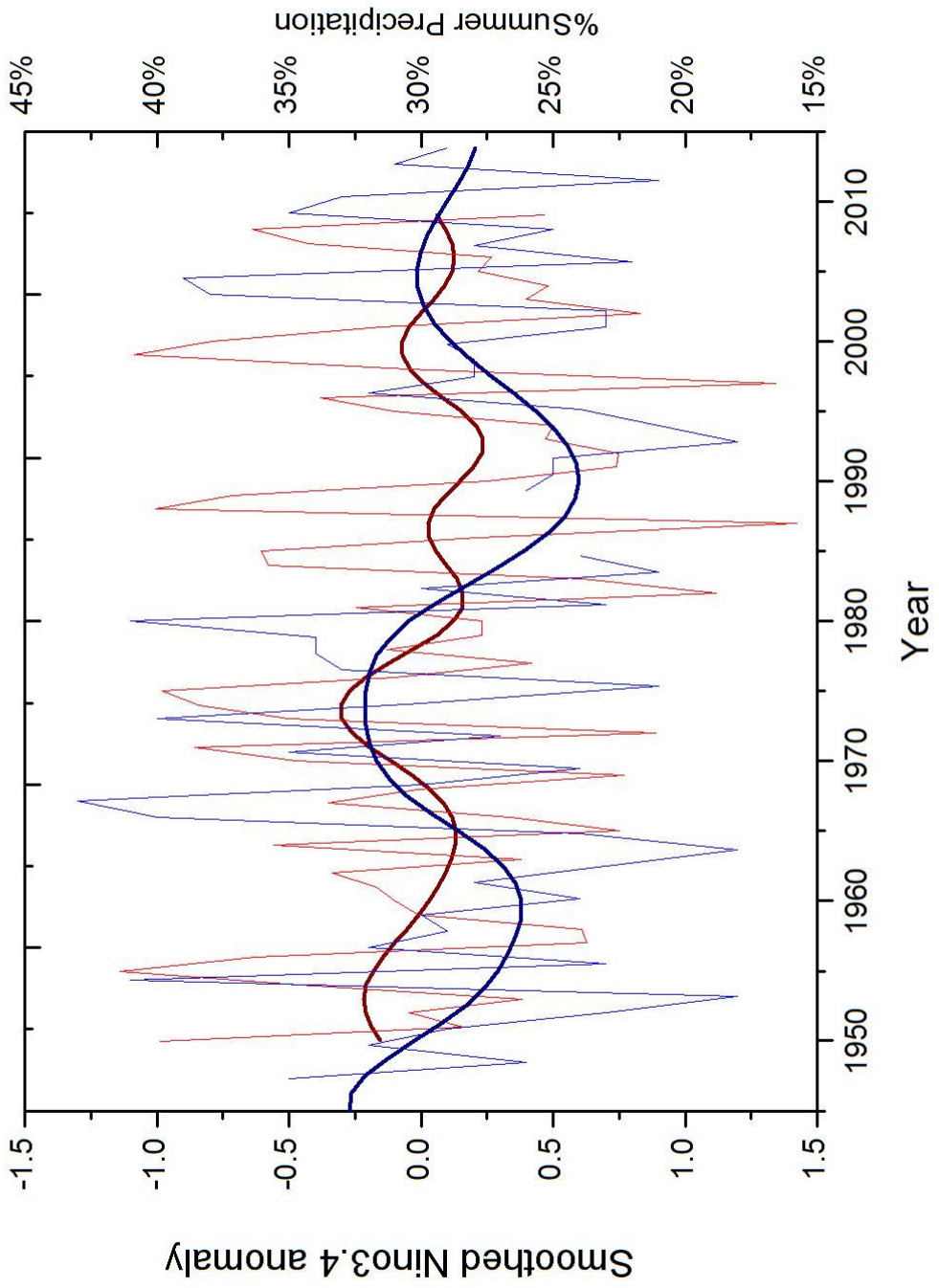

Figure 6. Raw (red) and smoothed (dark red) ENSO state plotted against the % of annual precipitation during JJA at Lewisburg, WV (blue, smoothed-dark blue). Smoothing was performed to isolate multi-decadal variability using a Gaussian filter at a frequency of 0.04 $year^{-1}$ and a bandwidth of 0.04 $year^{-1}$.

Figure 3-7 Orbital and millennial variability in BCC samples compared to Brazil and China.

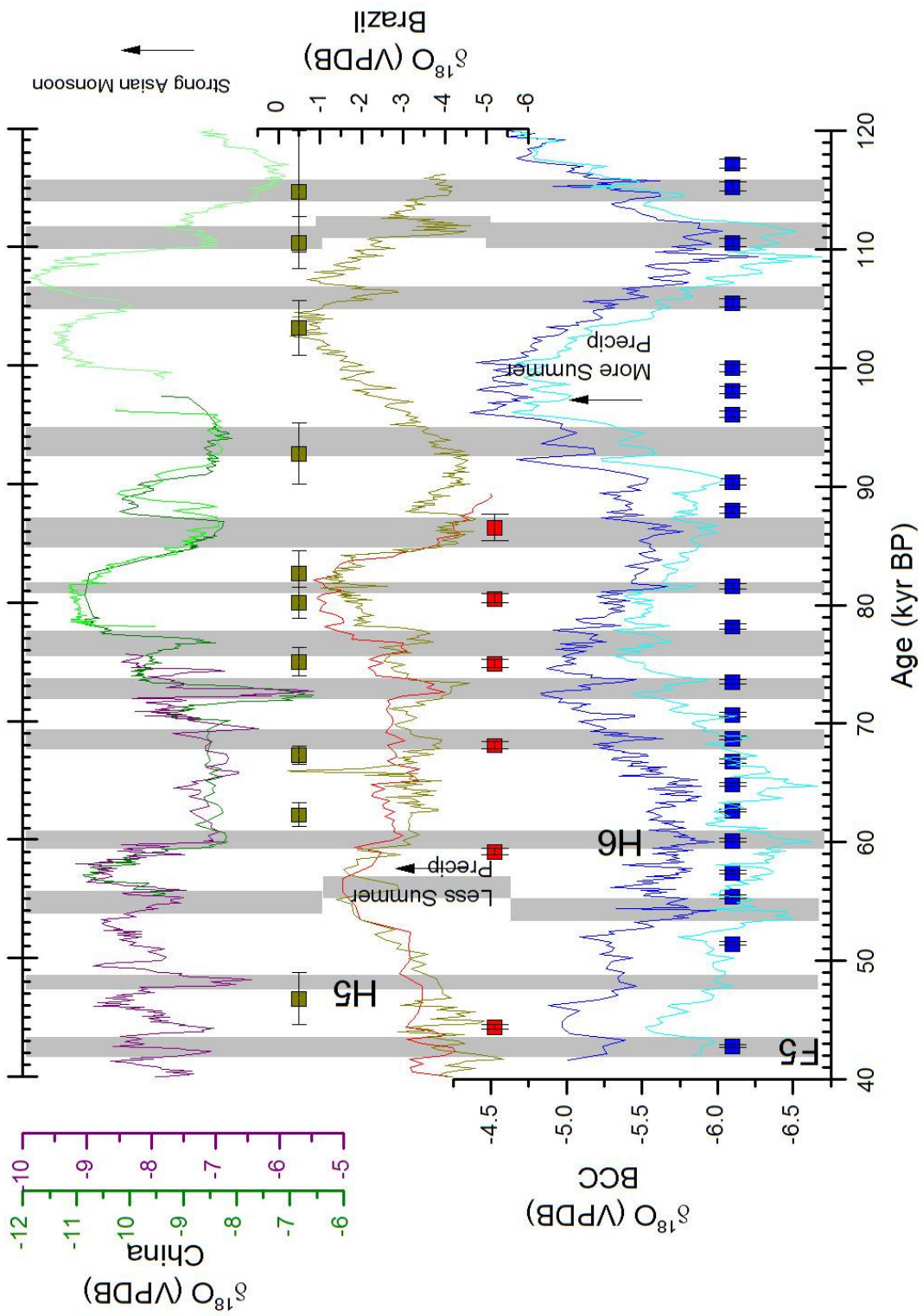

Figure 7. Comparison between BCC10 in dark blue (raw) and light blue (ice volume corrected) and speleothem records from southern Brazil (Wang et al., 2007; Cruz et al., 2005) with ages and errors. ASM records from Hulu (purple)(Wang et al., 2001) and Sanbao (Green) (Wang et al., 2008) are also included for comparison. Brazilian samples are plotted in red (Wang et al., 2007) and gold (Cruz et al., 2005). H5 and H6 refer to Heinrich events 5 and 6 respectively, and F5 refers to flooding event 5 in the Gulf of Mexico (Hill et al., 2006). Grey bars indicate apparent intervals of coincident variability. Records are plotted so that millennial scale events will appear unidirectional.

Figure 3-8 Abrupt events in BCC $\delta^{18}O$ and comparison to the Asian Summer Monsoon.

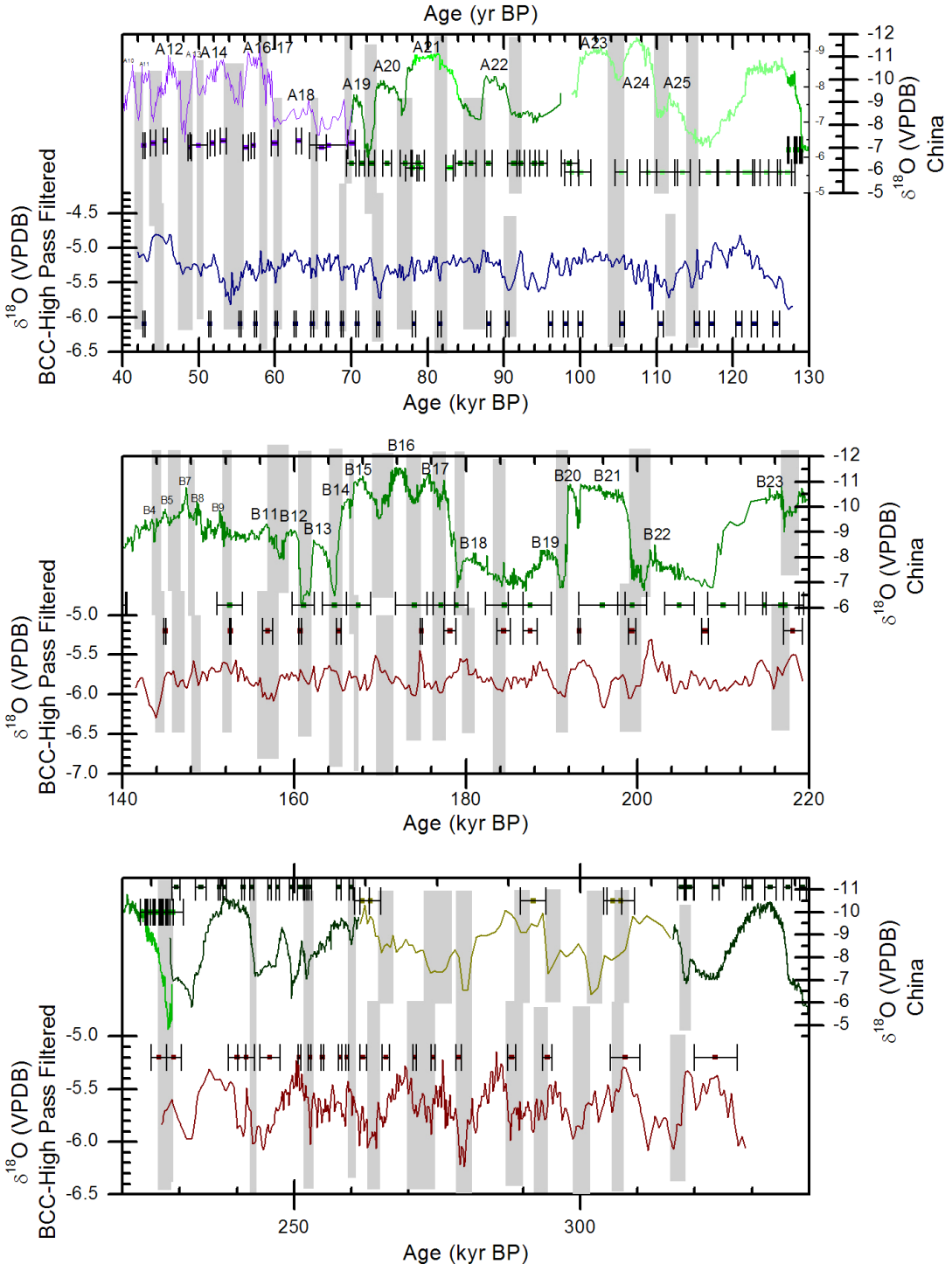

Figure 8. Comparison of high-frequency millennial scale events between BCC and the Asian monsoon. The BCC record was filtered to remove orbital scale variability (periods >15,000 years). Grey bars indicate potential points of correlation between the two records. The Asian monsoon is based on published records from Hulu cave (Wang et al., 2001) (in purple), Sanbao cave (Wang et al., 2008; Cheng et al., 2009) (in shades of green) and Linzhu cave (Cheng et al., 2009) (yellow). Ages and errors used to construct the records are included for comparison. BCC samples are colored as in Figure 3. Chinese interstadial events are labeled following the conventions of supplemental refs 9-11.

Figure 3-9 Correspondence between BCC $\delta^{18}O$ and the Gulf of Mexico.

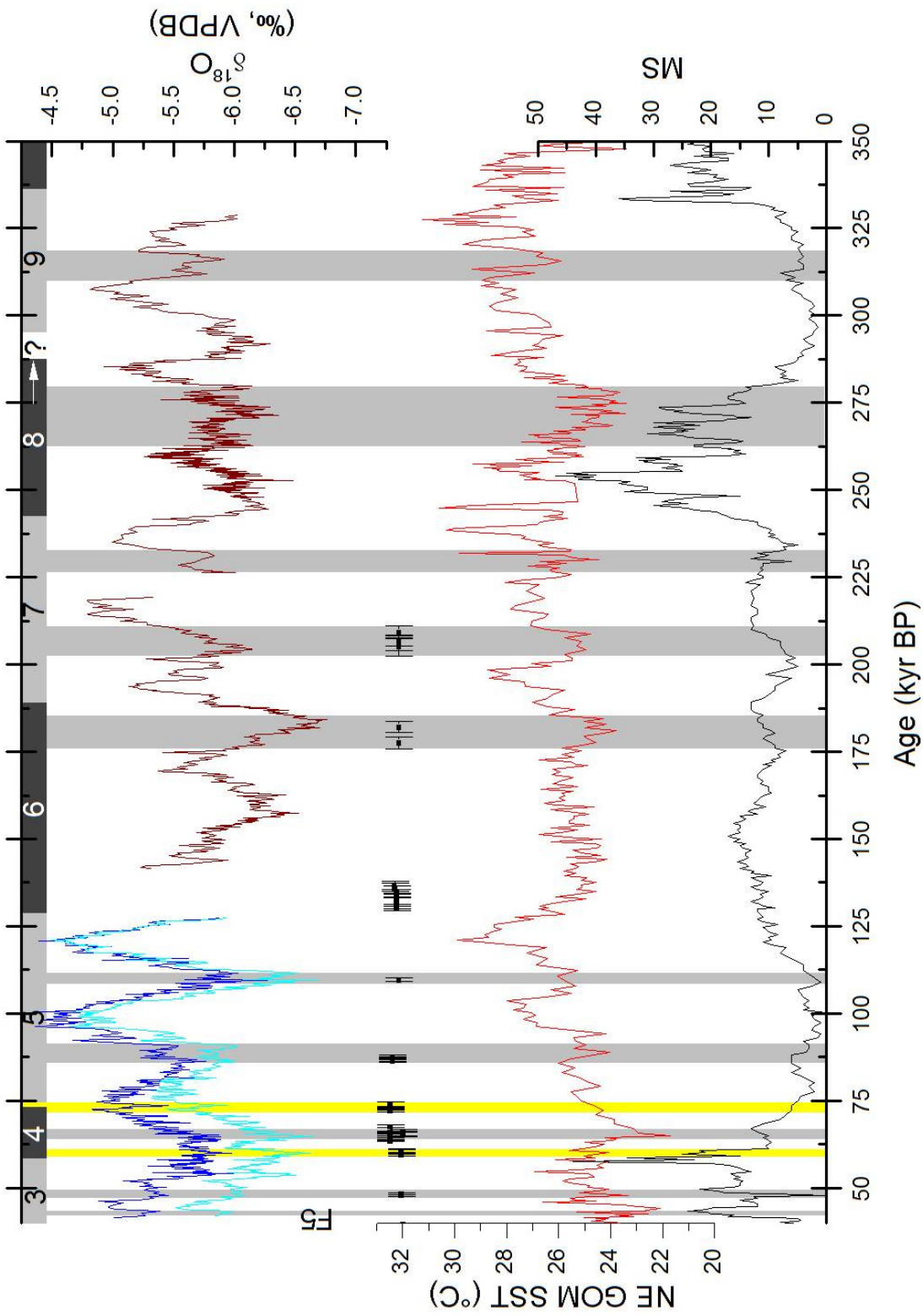

Figure 9. Comparison between Mg/Ca derived SSTs and Magnetic Susceptibility from the Gulf of Mexico (Nürnberg et al., 2008), and samples BCC10 in dark blue (raw) and light blue (ice volume corrected) and BCC9 in dark red. Magnetic Susceptibility (MS) is a proxy for the influx of terrigenous sediment by the Mississippi river. An ice volume correction was applied to BCC10 (light blue) by subtracting the coral-constrained sea level curve from core V19-30 (Cutler et al., 2003). Dated intervals (with error bars) represent wet periods in northeastern Brazil (Wang et al., 2004) associated with a southward shifted ITCZ. Grey bars indicate apparent points of correlation between the records. MIS (Martinson et al., 1987) are labeled at the top, with the timings of Terminations adjusted based on evidence from Chinese speleothems (Cheng et al., 2009).Yellow bars indicate northeastern Brazil wet periods that appear coincident with changes in BCC $\delta^{18}O_c$ but do not have an obvious connection with SSTs in the Gulf of Mexico. These events appear to mark the beginning and end of MIS 4.

Chapter 4: Atmospheric and Oceanic Controls on seasonal precipitation in the Atlantic Basin

Changes in seasonal precipitation recorded by a speleothem from Culverson Creek Cave in West Virginia show strong ties to conditions in the Gulf of Mexico. As meltwater from the Laurentide ice sheet drained through the Mississippi basin, sea surface temperatures were depressed and $\delta^{18}O_{sw}$ was depleted over a large section of the Gulf of Mexico. This continued until the ice sheet retreated beyond the northern borders of the Mississippi watershed, shortly before the Younger Dryas. The overall behavior of speleothem $\delta^{18}O$ is consistent with changes in the strength and position of the North Atlantic subtropical anticyclone, also known as the Bermuda High (BH). Enriched $\delta^{18}O$ occurs during periods of reduced summer precipitation in Florida, consistent with a westward expansion of the BH over the Florida peninsula. Some of the inferred variability in the BH appears to be modulated by the El Niño Southern Oscillation (ENSO) as the middle Holocene shows elevated $\delta^{18}O$ values during a time when northeast Brazil is wet, a situation that would arise from a change in the mean state of the tropical Pacific to La Niña like conditions.

Introduction

Seasonality, Terminations, and Glacial Climate

Glacial terminations are the most prominent climatic events of the Pleistocene. Continental ice sheets, which take nearly 100 kyr to develop, collapse in less than 10 kyr. Changes in the summer insolation are the primary driver of these termination events as

seasonal melting exceeds accumulation (Cheng et al., 2009; Hays et al., 1976). While several aspects of terminations are not yet fully understood, this first order prediction by Milankovitch has held true.

Changes in seasonality have several other impacts on glacial climate. Precipitation in monsoon regions varies in response to summer insolation changes and ITCZ migration (Cheng et al., 2009; Wang et al., 2001), with clear ties to abrupt climate changes recorded in Greenland. These millennial scale events correspond to large changes in winter temperatures (Denton et al., 2005), although on orbital scales, winter insolation minima during glacial terminations are not sufficient to offset warm season melting. Therefore, changes in the strength of the annual cycle represent a significant aspect of global climate variability.

Speleothem Climate Records from West Virginia

Previous work at Buckeye Creek Cave (BCC) in West Virginia has demonstrated that the isotopic composition of speleothem calcite varies in response to the weighted mean annual $\delta^{18}O$ of precipitation, which is determined by the balance of precipitation between summer and winter (Hardt et al., 2010). In the mid-Holocene, enriched $\delta^{18}O$ values correspond to a period when summer precipitation is believed to have been higher than present (Braconnot et al., 2007; COHMAP Members, 1988; Diffenbaugh et al., 2006; Harrison et al., 2003), suggesting that summer is the more important season in controlling $\delta^{18}O$ variability. While winter seasons could also be a contributing factor, Pleistocene samples from BCC (Chapter 3) appear largely insensitive to millennial events, which are believed to represent changes dominated by the winter season (Denton et al., 2005).

Potential role of the Gulf of Mexico

Changes in seasonal precipitation in West Virginia can provide useful information about latent heat transport from the Gulf of Mexico (GOM) into the continental interior (Chapter 3). The GOM is the primary moisture source for most of the precipitation on the North American continent (Peixóto and Oort, 1983), suggesting that changes in southerly moisture flow from the GOM, particularly during the summer, could augment melting driven by sensible heat. The cave site is only ~300 km from the maximum extent of the Laurentide ice sheet during the Wisconsinan glaciation (Lowell et al., 1999), so would be well positioned to record such changes.

Prior to the termination, meltwater began to flow down the Mississippi river into the GOM, affecting both sea surface temperatures (SSTs) and the isotopic composition of surface waters (Flower et al., 2004). Cooler SSTs produce a high pressure anomaly over the northern GOM, acting as a block on southerly moisture flow (Oglesby et al., 1989), which particularly impacts the eastern US (Wang et al., 2010). As the GOM is the moisture source for most of the North American continent, changes in $\delta^{18}O_{sw}$ will directly impact $\delta^{18}O$ of speleothem calcite.

Links to Thermohaline Circulation

While GOM sea surface temperatures partially regulate moisture advection into the continental United States (Oglesby et al., 1989), they also correspond to enhanced freshwater flux from the Atlantic to the Pacific over Central America (Pahnke et al., 2007). Increased export of water vapor increases the salinity of the Atlantic basin and strengthens North Atlantic deep water formation (Dong and Sutton, 2005; Schmidt et al., 2004) (NADW). Warmer SSTs in the western hemisphere warm pool (spanning the

Atlantic and the Pacific) maintain a northern position of the intertropical convergence zone (ITCZ), enhancing convection over the Central American isthmus, which acts as an atmospheric bridge between the Atlantic and Pacific basins (Xie et al., 2005). Heinrich events and stadials that shift the mean ITCZ position to the south may produce a positive feedback due to the resulting decrease in NADW (Leduc et al., 2007).

The subtropical anticyclone can influence moisture export by strengthening the northeast trade winds and enhancing evaporation over the Caribbean (Muñoz et al., 2008). The strength of the North Atlantic subtropical anticyclone is controlled by downwelling air driven by the Asian Summer Monsoon (ASM), southerly flow induced by the North American Summer monsoon and GOM SSTs (Oglesby et al., 1989; Rodwell and Hoskins, 2001; Weaver et al., 2009), and changes in the land-sea temperature contrast. The position of the subtropical anticyclone, another factor influencing seasonal precipitation in the eastern US, is also influenced by the El Niño Southern Oscillation (ENSO) (Seager et al., 2005).

By analyzing $\delta^{18}O$ in a West Virginia speleothem that grew over the last glacial termination, we can investigate several aspects of climate that affect the Atlantic basin. Seasonal precipitation changes in WV correspond to changes in moisture availability in North, Central, and South America across this critical climatic transition.

Methods

Site Description

Culverson Creek Cave (CCC) (37°56' N, 80°26'W, ~650 masl) is located in Mississippian limestone of the Greenbrier Group in the Allegheny Mountains of West Virginia (Cardwell et al., 1968; Dasher and Balfour, 1994).

Sample collection and analysis

Sample CCC1 was collected >300m from the cave entrance, minimizing surface effects on cave temperature or humidity (White, 2004). The recovered stalagmite was cut in half along the growth axis, polished, and drilled for stable isotope and dating analyses.

Stable isotope samples were milled at 0.5-mm intervals along the vertical growth axis, using the midpoint as the assigned depth for the age model. Stable isotope analyses were performed using a GasBench II coupled to a ThermoFinnigan DeltaPlusXP IRMS. Samples were standardized to V-PDB using NBS-19, with standard and unknown precisions for $\delta^{18}O$ and $\delta^{13}C$ averaging 0.10‰. Milling along the growth axis instead of taking discrete samples at regular intervals minimizes potential aliasing of the isotope record (Fairchild et al., 2006).

Radiometric age constraints were provided by U/Th dating techniques developed for carbonates (Broecker, 1963) and adapted for measurement on an inductively coupled plasma mass spectrometer (Edwards et al., 1987; Shen et al., 2002) at the University of Minnesota. Calcite powder was sampled using a dental drill with a 0.9-mm diameter tungsten-carbide drill bit. Powdered samples at 189 mm and 468.5 mm were homogenized and split for replicate analysis. Chemical procedures for isolation of uranium and thorium were run along with a chemical blank. Age determinations were made using U/Th measurements conducted on a Finnigan Neptune inductively coupled plasma mass spectrometer with a single MasCom multiplier using the decay constants of Cheng et al., 2009. All ages are in stratigraphic order, consistent with closed system behavior. Relative age errors vary from 2.4‰-6.1‰ with an average error of 3.4‰ (see Supplemental Table 1). The age model was constructed by linear interpolation between

28 dated layers over the length of the sample (496 mm) (Supplemental Table 2). Error weighted means were used for the ages of dated horizons with replicate samples. For most of the record, the method used to construct the age model did not significantly alter the timing of events, with the exception of intervals when growth rate changed substantially. As a result, the precise behavior of $\delta^{18}O$ at Termination I and the 8.2 ka event is not well constrained. However, that does not preclude analysis of the isotopic composition immediately prior to and after these events. Additional uncertainty exists between ~8.3 and ~10.7 ka as there are no ages over this relatively small depth interval.

Ice Volume Correction

An ice volume correction was applied to $\delta^{18}O$ using the sea level curve shown in Figure 8 of Edwards et al., 2003 and references therein. Direct measurements of sea level beginning at 22 ka were connected with a series of linear segments. Sea level was converted to isotopic space by assuming a maximum enrichment of 1‰. This correction does not take into account the unique isotopic characteristics of the GOM due to the direct inflow of glacial meltwater. Uncertainties about the age scale of marine sediments, even within the limits of radiocarbon dating, preclude a precise analysis. In addition, the mean $\delta^{18}O$ depletion of GOM seawater is poorly constrained.

Correction for Gulf of Mexico $\delta^{18}O_{sw}$

Because of the potential effect on precipitation in the much of North America, the isotopic composition of the Gulf of Mexico will subsequently impact the mean annual $\delta^{18}O$ of precipitation, including at our site in West Virginia. Therefore it is worthwhile to attempt to correct the δ18Oc record from CCC for changes in δ18Osw of the Gulf. Two main uncertainties make this task difficult. First, the magnitude of the shift over the

entire Gulf is poorly constrained. Second, the age uncertainty of the Gulf record is nearly 10 times the uncertainty in CCC1, with the additional complication of applying a reservoir correction. If we assume that the ages of the Orca record are essentially correct and make some reasonable guesses as to the mean isotopic effect on the Gulf, it is possible to remove the source water effect and isolate the impacts of changing seasonality.

The observed change at Orca Basin (~3‰), near the Mississippi river delta is larger than the average effect due to its proximity to the outflow of glacial meltwater. However, observations from as far away as the Yucatan show a 1‰ shift (Williams, 1984). Therefore we assume that the mean Gulf isotopic response is 1/3 of that observed in the Orca Basin, with estimated error of ±50%. To isolate the response in the Gulf alone, the ocean-wide ice volume response is subtracted from the Orca observations prior to dividing by 3, then added back in.

Results

Oxygen and carbon isotopes do not show a clear relationship (r^2= 0.076), suggesting that kinetic effects are unlikely to be significant. Intervals within the record that show apparent correlation generally occur when both $\delta^{18}O$ and $\delta^{13}C$ shift toward depleted values (Figure 1), the opposite one would expect were kinetics determinative (Hendy, 1971).

Replication with BCC

CCC1 overlaps with samples from BCC during the mid-Holocene and variations in $\delta^{18}O$ and $\delta^{13}C$ appear well replicated between the records (Figure 2). Some minor allowances must be given for the use of different half-lives in age determinations as those

from BCC rely on the decay constants of Cheng et al., 2000 while CCC1 is based on those used in Cheng et al., 2009. In addition, growth rates in CCC1 are much faster, so the two records do not have the same temporal resolution.

CCC1 $\delta^{18}O$ is about 1‰ heavier than concurrent samples from BCC even though the two caves are only ~5 km apart. This may be due to the orientation of the ridges overlying the cave sites. The terrain above BCC is south facing, so any snow pack will melt sooner from this site, likely prior to leaf out by vegetation. Because CCC is not south-facing, snowpack would melt later in the season and a greater percentage would be taken up by vegetation, resulting in a greater contribution of summer precipitation to dripwaters and therefore more enriched $\delta^{18}O_c$. In addition, BCC is ~35 m below the surface, allowing greater homogenization of dripwaters between the soil horizon and the cave while CCC has only 10-15m of bedrock above the chamber where CCC1 was collected.

Characterization of $\delta^{18}O$

CCC1 began growth at ~20.66 ka BP (Figure 3), around the time of the formation of the terminal moraine of the Erie lobe of the Wisconsinan ice sheet (20.71±0.27) (Lowell et al., 1999). A depletion event also occurs at ~19.5ka, prior to a likely hiatus at ~19 ka, about the time of the first rise in sea level after the LGM (Clark and Mix, 2002). $\delta^{18}O$ values during this interval are elevated relative to the Holocene, but once a correction has been made for the effects of ice volume on $\delta^{18}O_{sw}$, LGM $\delta^{18}O$ appears more in line with Holocene values (Figure 4). The depletion that begins around Heinrich Event 1 (H1) largely mirrors changes in $\delta^{18}O_{sw}$ in the GOM (Flower et al., 2004) (Figure 3).

No significant response is observed across Termination I, although growth rates do achieve a local minimum. After the termination, $\delta^{18}O$ values are generally anti-phased with spring insolation changes, in line with observations of Pleistocene samples from nearby BCC (Chapter 3).

The Younger Dryas (YD) is characterized by two brief depletion events within an overall trend of increasing values. Similar to observations of the ASM in China (Dykoski et al., 2005; Wang et al., 2001), the initial shift towards negative values occurs at ~13 ka and reaches a minimum at ~12.5 ka (Figure 4). At this point, the two records diverge, with the ASM remaining weak until ~11.6 ka, while CCC1 becomes more enriched, with an additional depletion event at ~11.9 ka that does not have an analog in China.

Following the YD, $\delta^{18}O$ oscillates between enriched and depleted values, prior to a shift of ~1‰ between 8.4 and 8.2 ka. After this point, $\delta^{18}O$ remains relatively stable until growth stops at ~5.3 ka.

Growth Rates

Fast growth rates occur during the Mystery interval (Denton et al., 2006), beginning at ~16.9 ka and continuing until ~15.1 ka. After a brief interval of slow growth around Termination I, rates increase again between ~14.5 and 10.7 ka. Growth rates pick up again at ~8.26 ka and remain high until deposition ceased at ~5.3 ka.

Characterization of $\delta^{13}C$

CCC1 $\delta^{13}C$ values are between -0.5‰ and -2‰ during the LGM, substantially enriched relative to the rest of the record. Once growth begins again at 16.9 ka, values become more depleted and generally remain between -3‰ and -6.5‰. Shifts to enriched values occur at 15.9 ka, 15.2 ka, 13.3 ka, 13.0 ka, 9.7 ka, and 8.3 ka.

Discussion

Climate during the LGM

Previous work on regional samples has invoked seasonality of precipitation as the dominant control on $\delta^{18}O$, although temperature effects could not be entirely ruled out (Hardt et al., 2010, *in prep*). The enriched values observed in CCC1 during the LGM support this argument as it is not reasonable for temperatures within ~300 km of the Laurentide ice sheet at the LGM to be similar to the mid-Holocene. Furthermore, model results have suggested that the region near the southern margin of the ice sheet experienced wetter summers during the LGM (Bromwich et al., 2005). We therefore interpret $\delta^{18}O$ in terms of changes in seasonal precipitation, with the summer season likely to be dominant. Temperature could still be a factor, but only to the extent that it influences atmospheric circulation or by enhancing the seasonal contrast in $\delta^{18}O$.

Carbon values are also enriched during the LGM. Previous work on regional samples has indicated that $\delta^{13}C$ is likely an aridity proxy, with enriched values during times of low precipitation relative to evaporation (Springer et al., 2008). This suggests that drought conditions may have existed despite increased summer precipitation. Such a pattern has been proposed for the mid-Holocene, where lake levels decreased despite an increase in summer rainfall (Shuman and Donnelly, 2006).

Because summer is the key season for ablation of the ice sheet, the increased moisture flux during warm months may be more important. In addition to the sensible heating of the ice sheet due to solar insolation, it is possible that latent heat flux could provide an additional lever that pushes the ice sheet toward a glacial termination.

Relationship between CCC1 $\delta^{18}O$ and the Gulf of Mexico

During the summer, precipitable moisture in East Central North America (ECNA) is primarily sourced from the GOM (Davis et al., 1997). In fact, the GOM is the primary moisture source for precipitation in much of North America (Peixóto and Oort, 1983), so changes in the GOM will likely be expressed in $\delta^{18}O$ of CCC1. There are two primary means by which this could occur. First, cool SSTs associated with glacial meltwater draining via the Mississippi would suppress moisture transport by reducing the amount of water vapor the air could hold. Second, isotopically light glacial meltwater (approximately -35‰, (Vetter et al., 2009)) could deplete surface waters in the GOM enough to impact our record. Estimates from Orca Basin have shown a strong impact of isotopically light meltwaters from the Laurentide ice sheet on local $\delta^{18}O_{sw}$ (Flower et al., 2004) (Figure 3). Flow of glacial meltwater to the GOM via the Mississippi continued until shortly before the YD, when the ice sheet had retreated beyond the continental divide and was no longer in the Mississippi watershed (Tarasov and Peltier, 2005). The magnitude of the shift observed at Orca Basin is due to its proximity to the Mississippi river delta and such a large shift (~3‰) is not reasonable for the entire GOM. However, other work has shown $\delta^{18}O_{sw}$ to be depleted by 1‰ in the southern GOM just west of the Yucatan (Williams, 1984), suggesting a significant impact of glacial meltwater $\delta^{18}O_{sw}$ for most of the GOM.

The primary difference between the Gulf corrected record and the correction for ice volume alone is observed during the Bølling-Allerød, which now appears to be enriched relative to the periods before and after (Figure 5). This result is consistent with drier Florida summers observed at this time and during other warm intervals, such as the

middle Holocene. An additional consequence of this correction is a larger shift observed during the transition to the YD.

Evaluating the relative roles of the Bermuda High and ENSO

During the LGM, enriched $\delta^{18}O$ is consistent with a strengthened North Atlantic subtropical anticyclone. This interpretation is consistent with evidence of dry conditions in northeast Brazil over the same period (Figure 6) (Cruz et al., 2009) as a strengthened Bermuda high promotes drought conditions in that region (Namias, 1972). During the early Holocene, this relationship flips, with generally wet conditions in NE Brazil during a period of enriched $\delta^{18}O$ in CCC1 and samples from BCC. This suggests that the subtropical anticyclone alone is not strictly determinative across the entire record, but that ENSO may also be involved. La Niña-like conditions, believed to exist during the early to mid-Holocene would result in both wetter conditions in NE Brazil (Lau and Zhou, 2003) and an increase in summer precipitation in ECNA (Mo and Schemm, 2008; Wang et al., 2006). NE Brazil also switches to drier conditions in the late Holocene, as CCC1 ceases growth and samples from nearby BCC indicate a decrease in summer precipitation. This behavior is consistent with El Niño-like conditions, which are believed to have developed around this time. While clear similarities exist between precipitation in NE and southern Brazil on millennial timescales that are inconsistent with a super ENSO mechanism (Wang et al., 2007), ENSO may provide a more significant control on orbital scales. This is consistent with observations in CCC1 where enhanced summer precipitation in ECNA is associated with dry intervals in NE Brazil on shorter timescales.

Comparison between CCC1 and Florida lakes (Donders & de Boer et al., 2009) reveals patterns consistent with changes in the position or extent of the BH. CCC1 $\delta^{18}O$ appears to be anticorrelated with %Pinus in Florida lakes (Figure 6), a proxy for changes in summer precipitation (Donders & de Boer et al., 2009). When the BH expands westward over the Florida peninsula, summer precipitation decreases. Therefore the anticorrelation between these two sites is consistent with changes in the BH. Because WV and Florida maintain this relationship throughout the record, even as WV and northeast Brazil switch between in-phase and anti-phased behavior, this suggests that the BH is CCC1 is responding to ENSO-driven shifts in the position of the BH (Seager et al., 2005). Northeast Brazil precipitation is related to the strength of the BH (Namias, 1972), so changes in the mean position may not have the same impact.

The Younger Dryas, pre-Boreal, and potential links to thermohaline circulation

During the YD, the response in $\delta^{18}O$ of CCC1 appears anomalous compared to observations in China, southern Brazil, and other locations. SSTs in the subtropical North Atlantic are steadily decreasing during this time (Bard et al., 2000), which would strengthen the anticyclone (Wan et al., 2009) and produce greater relative summer precipitation in ECNA (Figure 7). Stronger subtropical high pressure will enhance the NE trade winds, advecting warm water into the GOM via Ekman transport, enhancing the Gulf Stream, and thus North Atlantic deep water circulation (Bjerknes, 1964). While NADW formation was likely shifted to the south during the YD, estimates of the intensity of circulation from grain size measurements indicate that circulation was increasing over the YD after a minimum at the beginning of the event (Praetorius et al., 2008). Carbon isotopes, a measure of ocean ventilation, show a similar structure, as do

SSTs and salinity measurements from the Caribbean (Schmidt et al., 2004), suggesting a potential low-latitude influence on late Pleistocene thermohaline circulation.

Following the YD, the Laurentide ice sheet decreased in spatial area, with rapid retreat between 9 and 8 ka. Previous work has suggested that the collapse of the Hudson Bay ice dome at ~8.2 ka led to a wetter climate in the eastern US (Shuman et al., 2002). In addition to the faster growth rates at this time, $\delta^{18}O$ indicate a greater proportion of summer precipitation. This suggests that the removal of the high pressure anomaly created by the ice sheet allowed greater moisture advection from the GOM. This behavior is opposite to that observed during stadial events, when $\delta^{18}O$ decreased (Chapter 3) and $\delta^{13}C$ indicated drier conditions (Springer et al., *in prep*). The difference is likely due to the fact that the ice area expanded during stadials (and Heinrich events) (Marshall and Koutnik, 2006), while the Wisconsinan ice sheet rapidly contracted at ~8.2 kyr BP.

Increased precipitation over Central America reflects changes in the export of moisture from the Atlantic basin, producing more saline waters, and strengthening NADW and thermohaline circulation. Lakes in Guatemala indicate aridity over the period from 18-11 ka, a time when spring (fall) insolation was at a maximum (minimum) (Bush et al., 2009), similar to CCC1 $\delta^{18}O$ and the phasing in Pleistocene speleothems from BCC. This is also consistent with observations during the Holocene when depleted $\delta^{18}O$ was observed in BCC samples during known periods of drought in the Yucatan (Curtis et al., 1996; Hardt et al., 2010; Hodell et al., 2001).

Glacial Terminations

Comparison of the record from CCC across Termination I to samples from BCC that grew around the times of Terminations II and III (Figure 8) indicates that a greater

proportion of the Laurentide ice sheet may have been in GOM watershed during MIS 2 and 6 than MIS 8. Following T-II, growth in sample BCC10 did not begin until ~1300 years after the event. $\delta^{18}O$ then begins at low values and becomes more enriched over time similar to the behavior of CCC1 at an equivalent time after T-I. Sample BCC9, however, more enriched shortly after T-III. One potential explanation for the different response at T-III is that the Laurentide ice sheet extended farther south during the ultimate and penultimate glaciations.

Terminal moraines indicate that the Huron, Erie, and Ontario lobes extended farther south during the LGM than they had during previous glacial cycles (Lowell et al., 1999). This would indicate that the Wisconsinan ice sheet was more likely to affect atmospheric circulation in WV. In addition, a greater mass of ice within the Mississippi watershed would have a greater impact on conditions in the Gulf of Mexico, both in temperature and $\delta^{18}O_{sw}$ (Flower et al., 2004). Such an increase in mass south of the continental divide could be a simple reflection of the greater reach of the eastern lobes of the ice sheet. However, western lobes (Des Moines, Green Bay, etc…) were not as extensive at the LGM as they had been during previous glaciations, so the overall mass balance is somewhat uncertain and changes in ice sheet thickness could be as important as spatial extent. Erosional effects of the Laurentide ice sheets could also have shifted the location of the continental divide to a more northerly position, greatly increasing the mass of ice within the Mississippi watershed.

Conclusion

The behavior of $\delta^{18}O$ over the last Termination largely confirms the interpretation of Hardt et al., 2010 and Chapter 3 of this thesis. Previous work on samples from West

Virginia caves has argued that $\delta^{18}O$ reflects changes in the seasonality of precipitation. That interpretation is supported by sample CCC1, which does not appear to be responsive to temperature changes and corresponds with paleoclimate records in both North and South America consistent with seasonal precipitation variability driven by changes in the BH. Over some portions of the record, ENSO may have altered the influence of the BH by changing its longitudinal position.

Over glacial cycles, three potential mechanisms were described as controlling precipitation seasonality in WV: changes in the Atlantic Warm Pool; the strength or position of the Bermuda High; and the El-Niño Southern Oscillation (Chapter 3). These climate modes are not exclusive and likely interact in several ways. A stronger BH will strengthen the northeasterly trades, enhancing Ekman transport through the Yucatan strait and help expand the AWP into the northern GOM (Bjerknes, 1964). Warmer SSTs in the GOM will also induce a low pressure anomaly that would allow increased moisture advection by strengthening southerly flow (Oglesby et al., 1989) leading to increased summer precipitation in the eastern US (Wang et al., 2010). ENSO has previously been shown to influence the westward position of the BH (Seager et al., 2005).

The correspondence with northeast Brazil over the Holocene suggests that ENSO could be a significant factor, as northeast Brazil is wet (dry) during La Niña (El Niño) phases, just as WV is more likely to experience an increase in summer (winter) precipitation. However, at the LGM, CCC1 indicates summer precipitation comparable to the mid-Holocene while NE Brazil is relatively dry, which can be explained by changes in the strength of the BH circulation. The consistent relationship between CCC1 and

%Pinus in Florida lakes strongly suggests that the BH serves as an intermediary between ENSO and seasonal precipitation at our site.

Figures

Figure 4-1 $\delta^{13}C$ and $\delta^{18}O$ from sample CCC1.

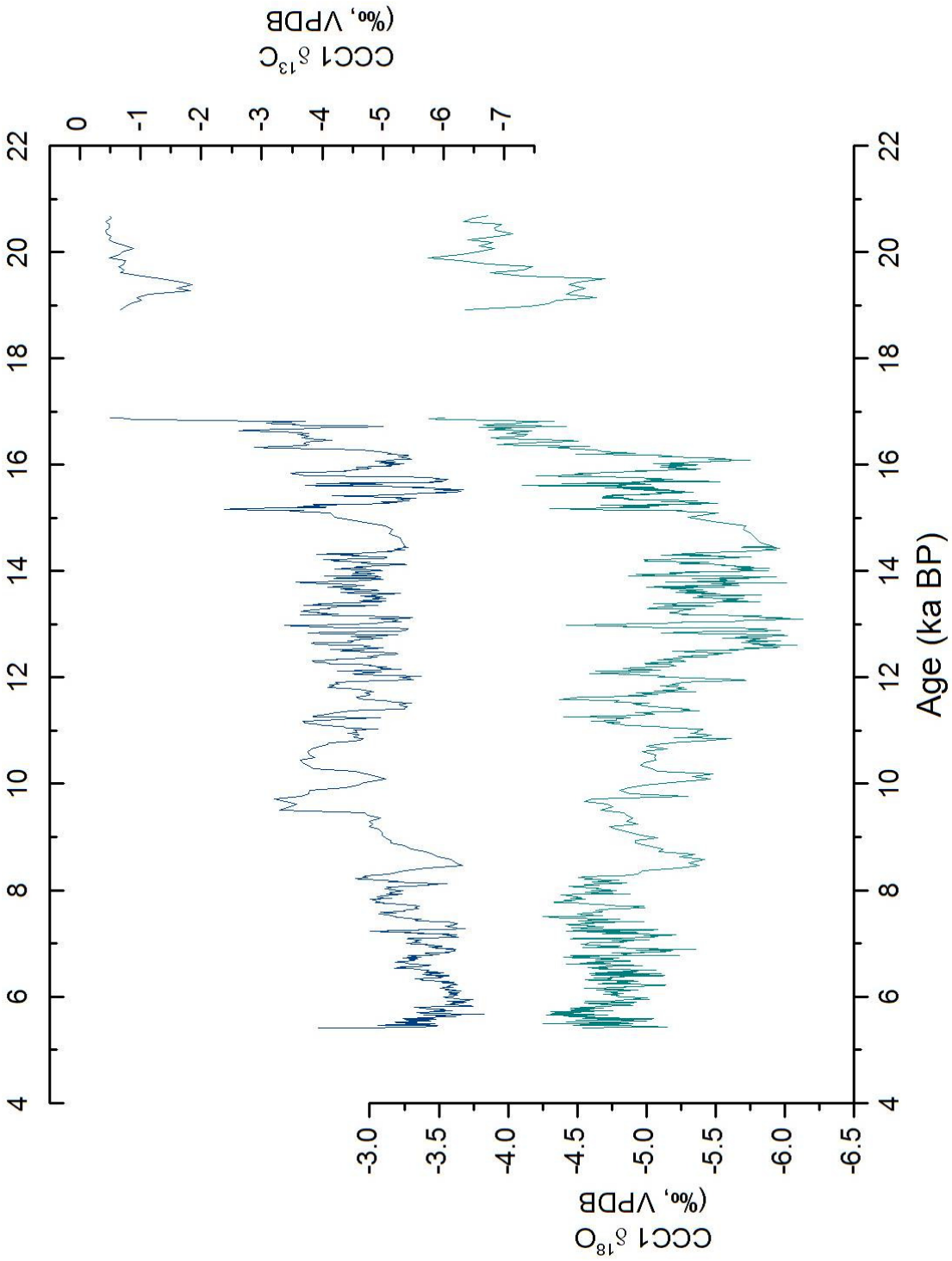

Figure 1. $\delta^{13}C$ (top) and $\delta^{18}O$ (bottom) from CCC1.

Figure 4-2 Replication of CCC1 isotopes with BCC Holocene samples.

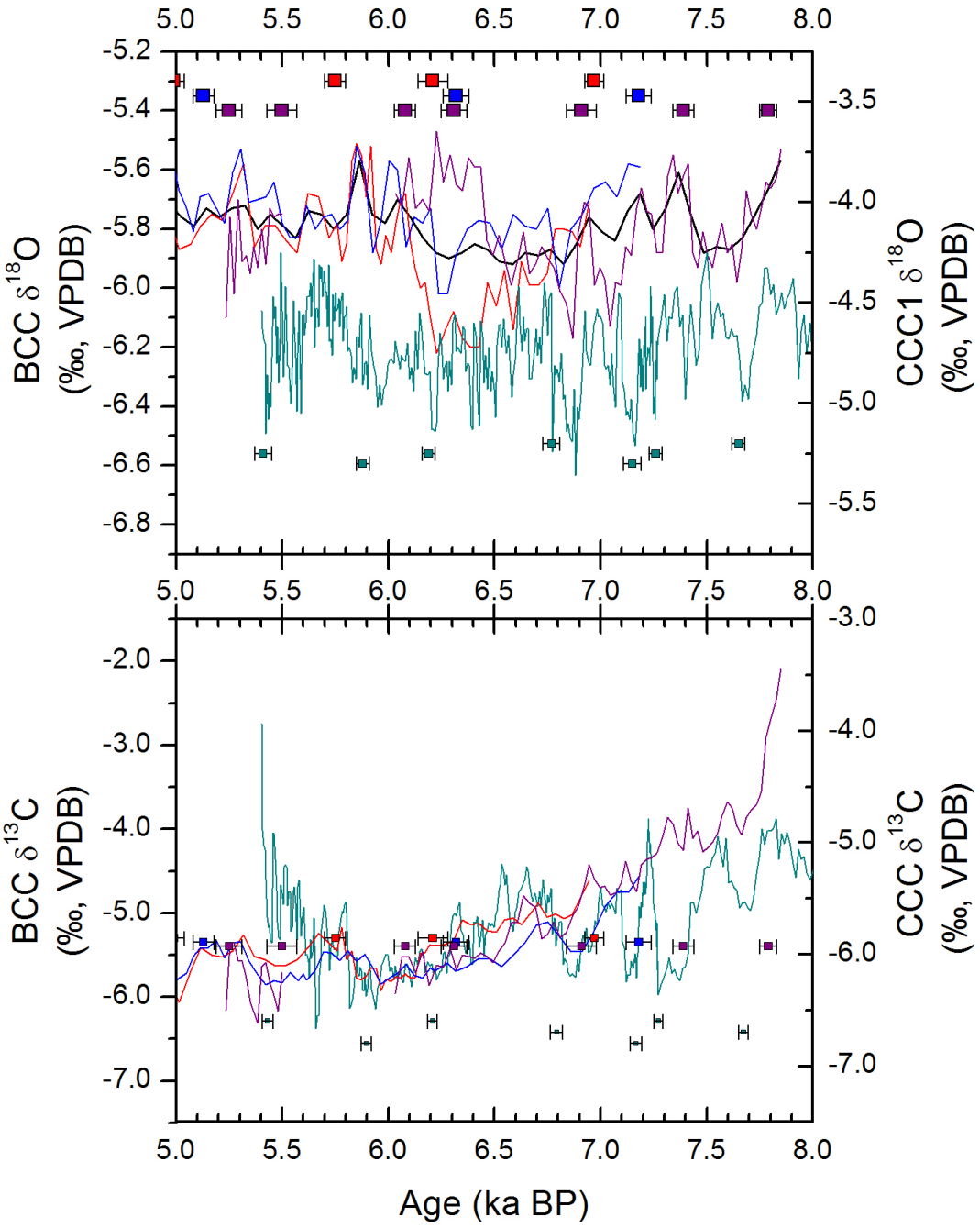

Figure 2. Evaluation of the degree of replication of $\delta^{18}O$ (top) and $\delta^{13}C$ (bottom) between CCC1 and samples from BCC. CCC1 (right axis) is plotted in teal, along with age constraints. BCC samples 2 (red), 4 (blue), and 6 (purple), along with the composite record (black) are plotted on the left axis. See text for explanation for the 1‰ offset between the two caves.

Figure 4-3 Comparison of CCC1 raw $\delta^{18}O$ with the Gulf of Mexico

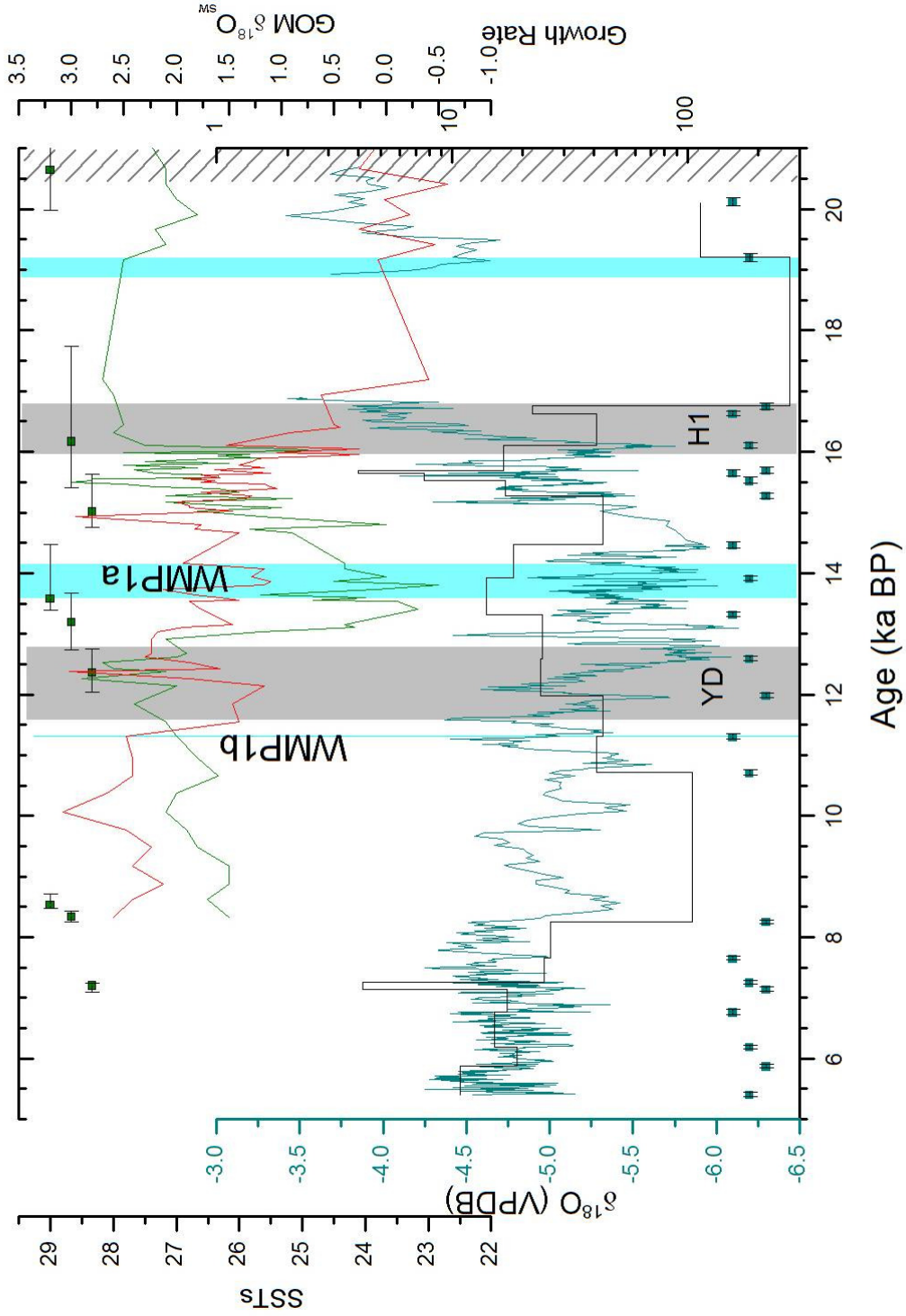

Figure 3. Gulf of Mexico $\delta^{18}O_{sw}$ (green) and SST (red) (Flower et al., 2004) plotted with calibrated radiocarbon dates used for the age model of the core. CCC1 raw $\delta^{18}O_c$ (not corrected for ice volume) in teal, plotted along with changes in growth rate (plotted as yrs/mm). Blue bars indicate meltwater events. The Younger Dryas and Heinrich event 1 are shown in Grey. The hatched interval shows the timing of a glacial advance of the Erie Lobe (Lowell et al., 1999).

Figure 4-4 Ice Volume Corrected $\delta^{18}O$ compared to the Gulf of Mexico, the North Atlantic, and the Asian summer monsoon.

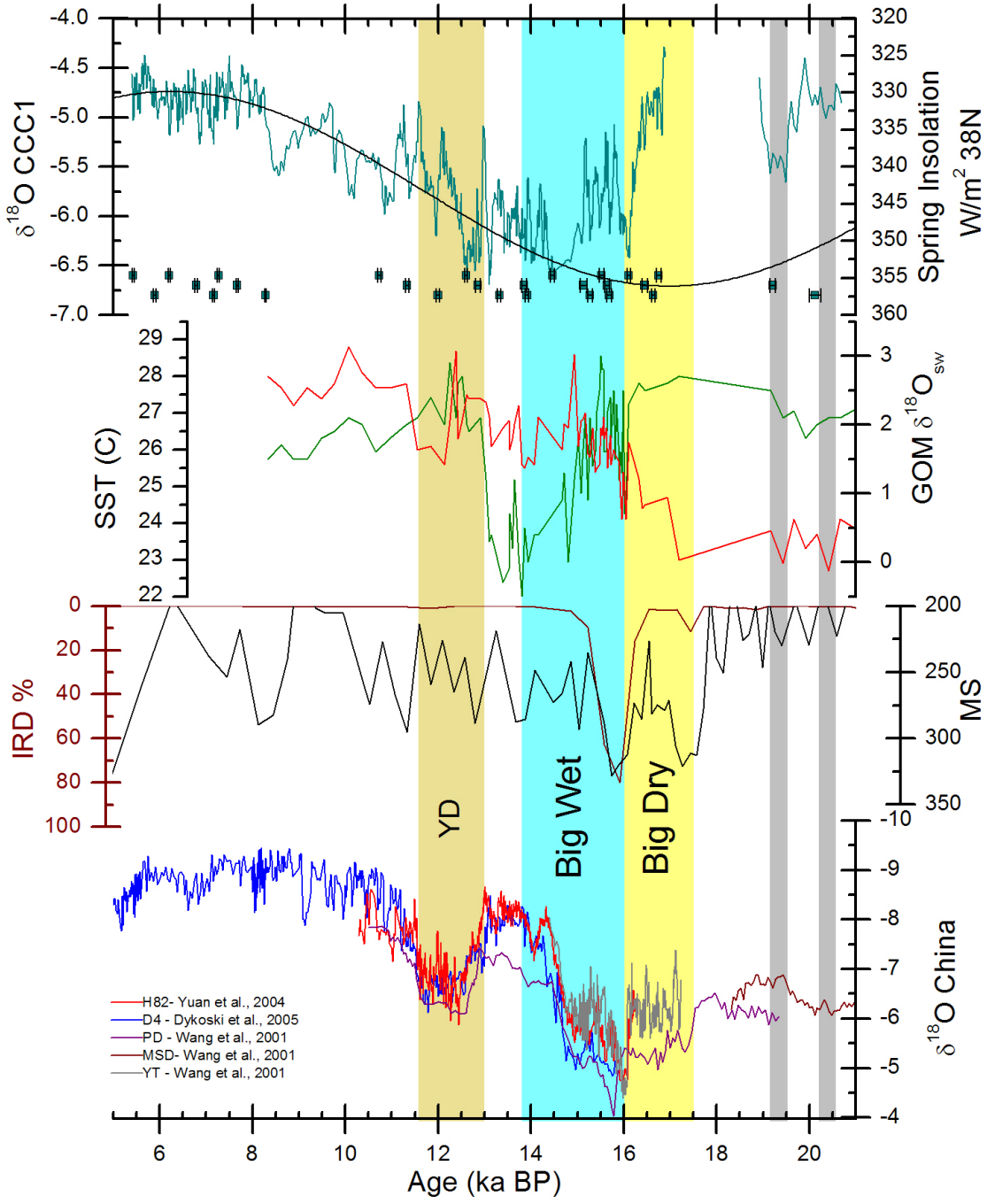

Figure 4. CCC1 (top) plotted against $\delta^{18}O_{sw}$ from the Orca Basin along with IRD% and Magnetic susceptibility from core SU81-18 (Bard et al., 2000). Speleothem records from Hulu (Wang et al., 2001) and Dongge (Dykoski et al., 2005) caves are also included for comparison. The Younger Dryas, and the "Big Wet" and "Big Dry" portions of the Mystery interval (Broecker et al., 2009) are labeled. Additional grey bars indicate potential points of comparison between CCC and the Gulf of Mexico SSTs.

Figure 4-5 Estimate of correction for Gulf of Mexico $\delta^{18}O_{sw}$.

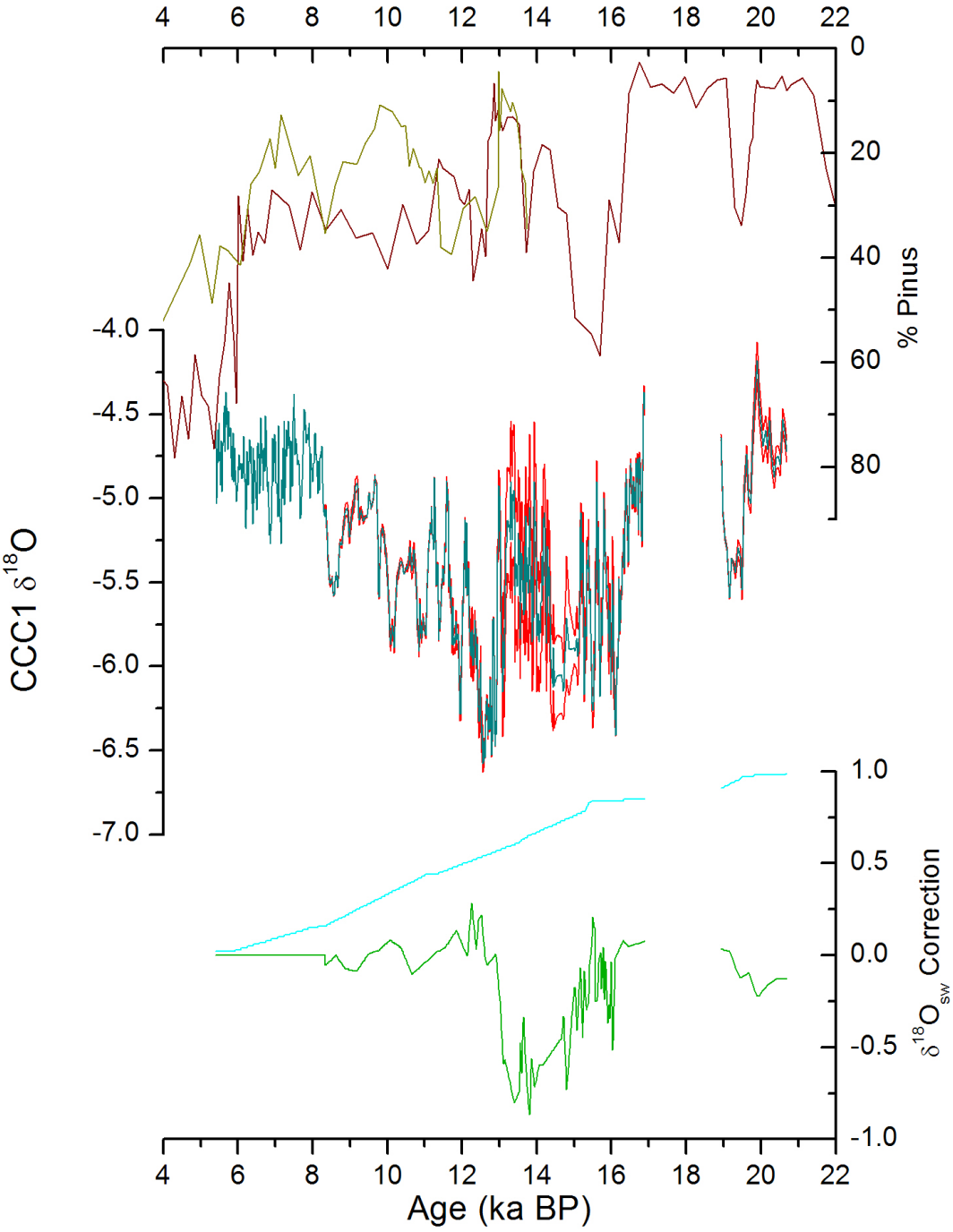

Figure 5. Top: %Pinus record from Florida lakes, colors as in Figure 3. Middle: CCC1 record after applying a correction for changes in the isotopic composition of the GOM (see Supplemental text for details). Red lines indicate the upper and lower bound after assuming a 50% error in the correction for GOM conditions. Bottom: Seawater corrections applied to CCC1, with assumed GOM effect in green and ice volume in light blue.

Figure 4-6 Comparison of CCC1 $\delta^{18}O$ with records from Brazil and Florida.

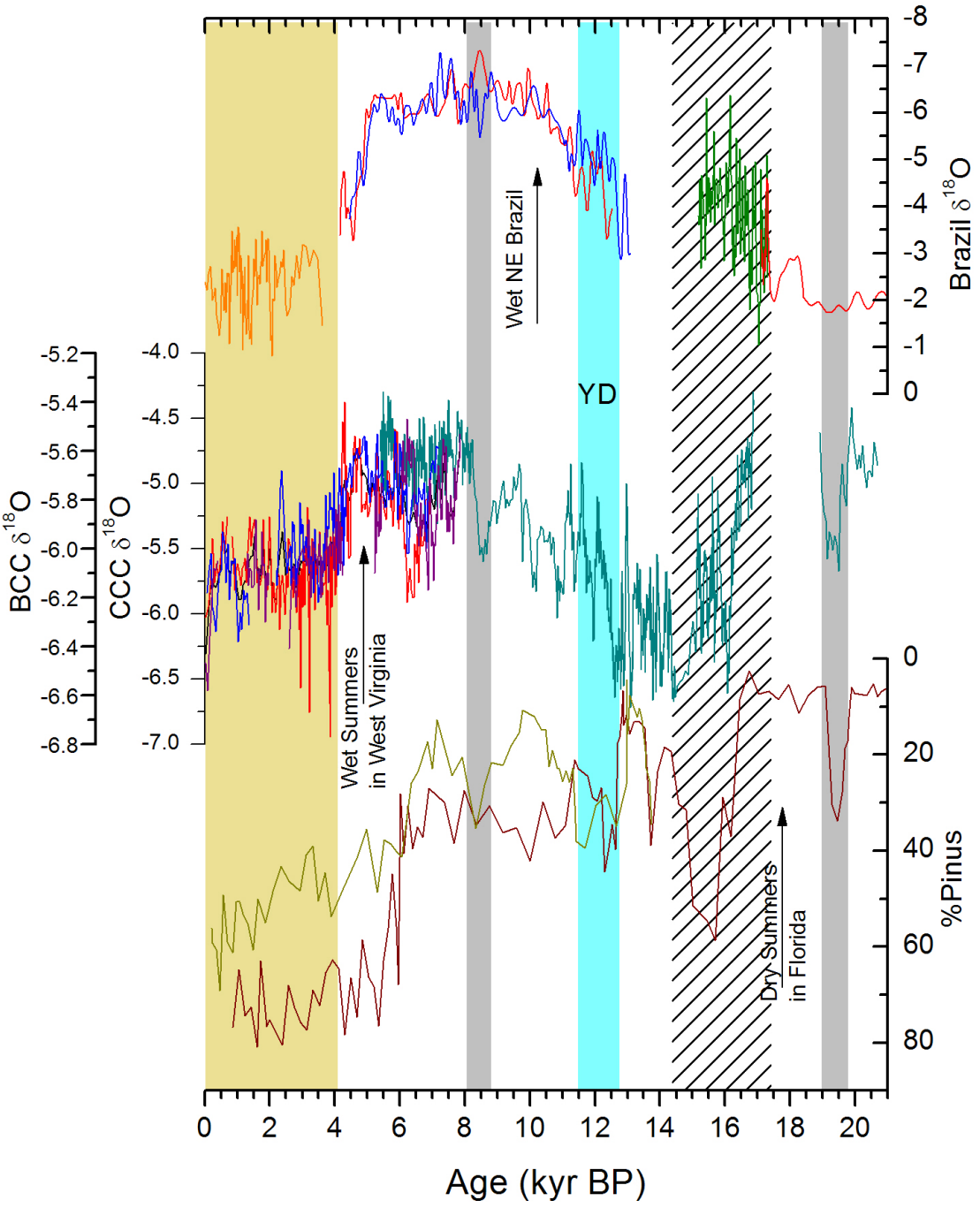

Figure 6. Comparison of records of precipitation change in the Americas. Top: $\delta^{18}O$ from Cruz et al., 2009. Samples RN1 and RN4 were smoothed using a fast Fourier transform in order to assist in comparison with CCC1. Middle: Ice volume corrected $\delta^{18}O$ from CCC1 is plotted in teal along with $\delta^{18}O$ from nearby BCC (Hardt et al., 2010). Bottom: %Pinus from lakes in Florida(Grimm et al., 2006; Watts, 1975), a proxy for changes in summer precipitation (Donders & de Boer et al., 2009).The interval following the mid-Holocene transition is highlighted in beige, when Brazil is dry, as are WV summers, while Florida summers are wet. This is consistent with an eastward shift in the position of the Bermuda High driven by El Niño-like conditions in the tropical Pacific. The YD is as marked. Hatching indicates the Mystery Interval and grey bars indicates other points of comparison between the records.

Figure 4-7 Potential relationships between CCC1 $\delta^{18}O$ and changes in thermohaline circulation.

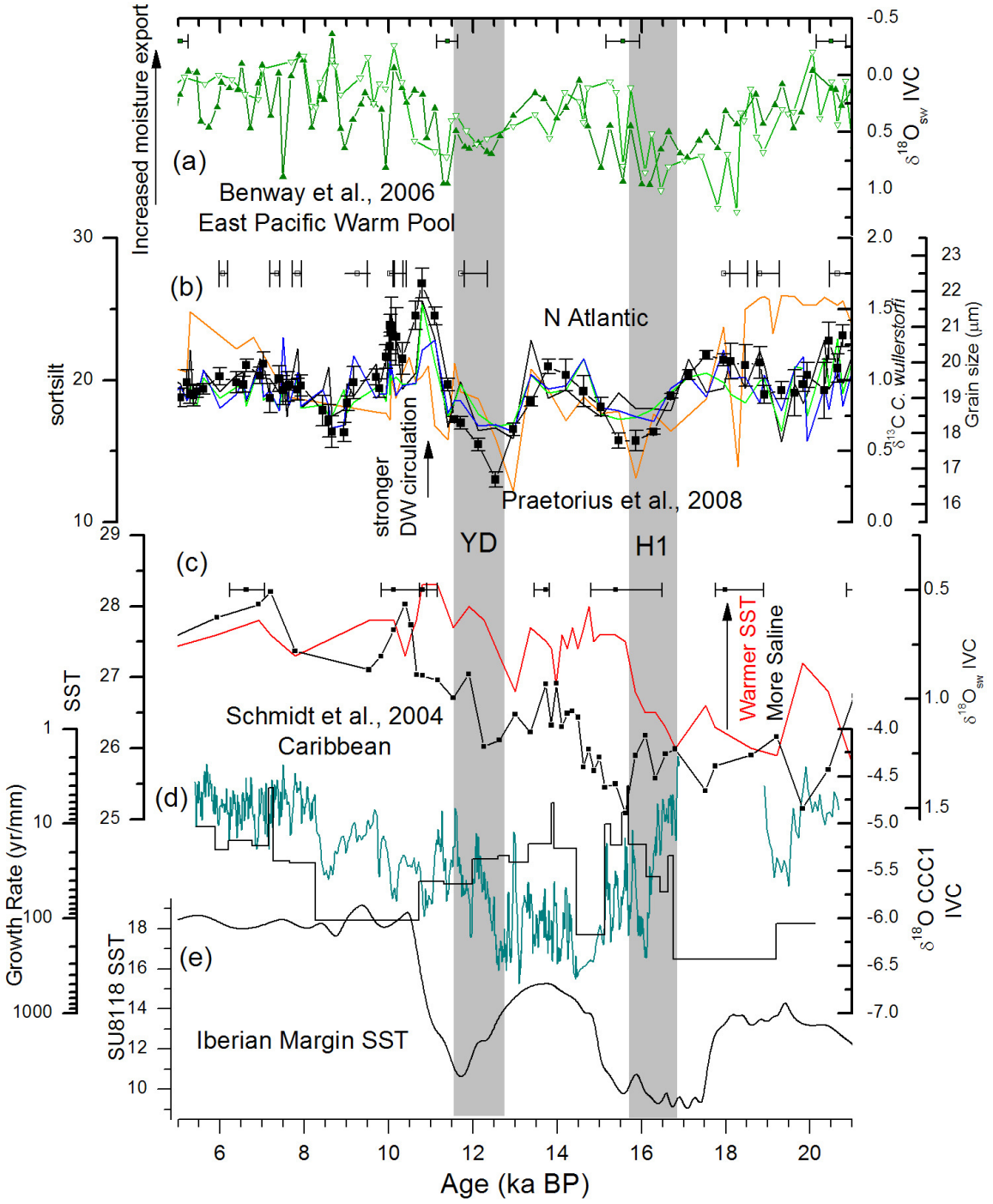

Figure 7. Comparison of CCC1 with marine records of circulation. (a) Salinity changes from the eastern Pacific reflected changes in moisture export from the Atlantic Basin(Benway et al., 2006). (b) Changes in mean grain size of sediments in the North Atlantic and $\delta^{13}C$ from *C. wullerstorfi*. Larger grain size indicates more vigorous deep water circulation and $\delta^{13}C$ is a measure of downwelling (Praetorius et al., 2008). (c) SST and salinity changes in the Caribbean (Schmidt et al., 2004). (d) Ice volume corrected $\delta^{18}O$ and growth rate (yr/mm) from sample CCC1 (this study). (e) SSTs from the core SU81-18 on the Iberian margin (Bard, 2006). All records were corrected for ice volume following the methods described in the text. The Younger Dryas and H1 are as marked.

Figure 4-8 $\delta^{18}O$ of West Virginia speleothems at glacial terminations compared to China.

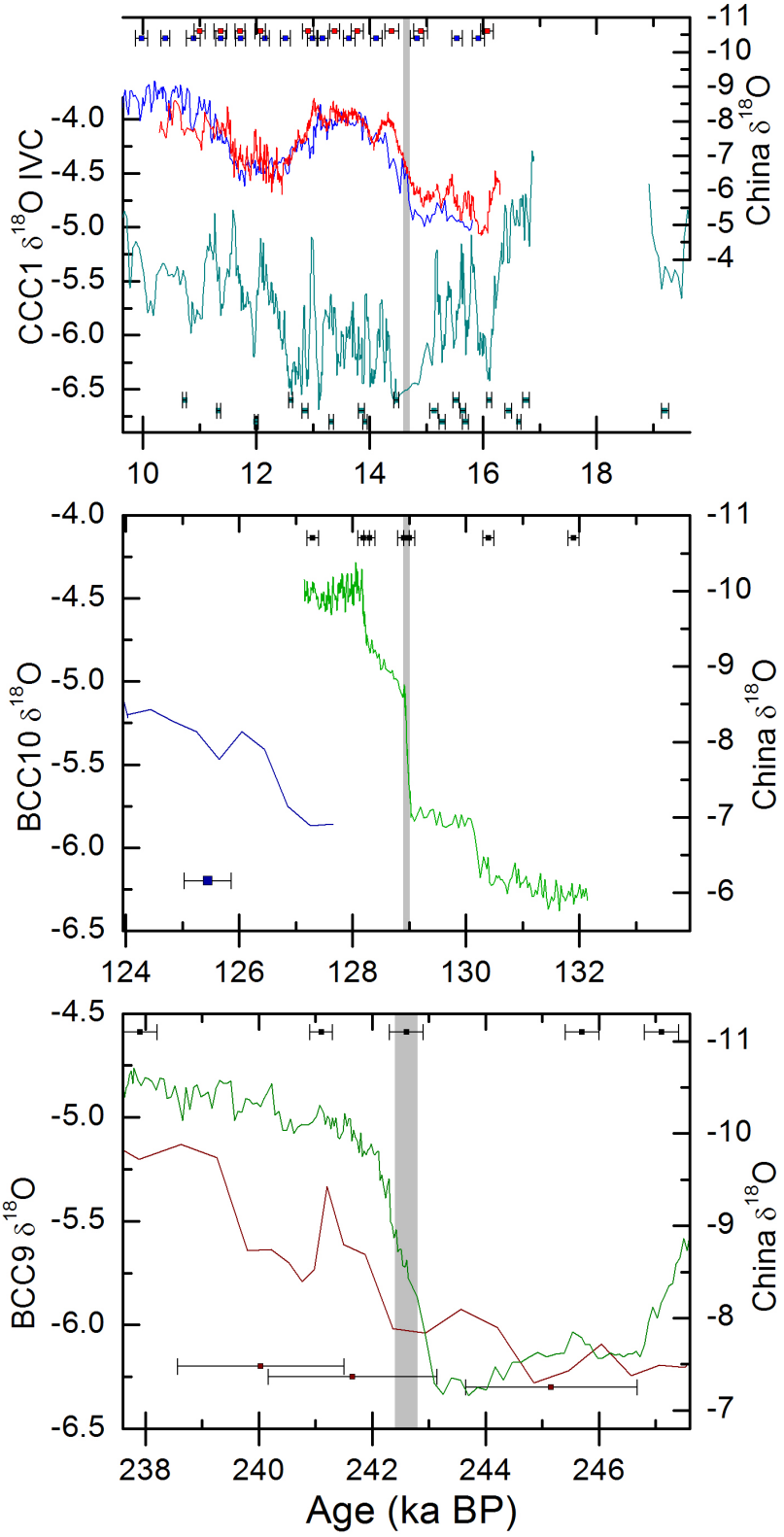

Figure 8. West Virginia stalagmite records near Terminations I (top), II (middle), and III (bottom) plotted on the left axis (this study, Chapter 3). Records of the ASM from Chinese caves are included for comparison (Cheng et al., 2009; Dykoski et al., 2005; Wang et al., 2001). Grey bars indicate the timing of the Termination events based on the results from Chinese caves.

Chapter 5: Conclusion

Challenges of Mid-latitudes

The primary challenge in working on mid-latitude stalagmites is determining the primary controls on isotopic variability. This problem is compounded by the limited amplitude of variability in the record in $\delta^{18}O$ and the difficulties in constraining the behavior of $\delta^{13}C$. For oxygen, temperature must be considered as a significant factor due to the potential for large temperature changes over glacial-interglacial cycles. Fortunately, the mass of oxygen in the precipitating solution limits the number of processes that can impact the record. Carbon is much more challenging in this regard as dissolved carbon (primarily as bicarbonate) represents a very small fraction of the total solution and the small mass means that several factors require consideration.

The interpretation of the oxygen record can be achieved by analysis of the isotopic behavior of modern precipitation. Regional data indicate that temperature may not substantially determine $\delta^{18}O$ of speleothem calcite for samples from West Virginia. This determination is corroborated by the $\delta^{18}O$ record from Culverson Creek Cave, which shows enriched values at 20 ka, a result that is inconsistent with a temperature control (Chapter 4).

The carbon record requires an alternate approach. By evaluating the variability in trace metals from the speleothems and comparing that to $\delta^{13}C$, it is possible to establish a working hypothesis. Those results are consistent with prior precipitation of calcite in the vadose zone above the cave as determining $\delta^{13}C$. The consequence of this process is to drive $\delta^{13}C$ to enriched values during periods of aridity or drought.

The oxygen record

As modern precipitation does not show a significant relationship with the amount of precipitation, the most likely control on $\delta^{18}O$ is seasonality. By altering the balance of annual precipitation between summer and winter, mean annual $\delta^{18}O$ becomes more enriched (more summer) or more depleted (more winter). Such changes would impact species composition, lake levels, and groundwater recharge (Shuman and Donnelly, 2006). Results from three stalagmites that grew during the Holocene show enriched values at 6 ka, consistent with model results showing an increase in summer precipitation at that time (Braconnot et al., 2007; COHMAP Members, 1988; Diffenbaugh et al., 2006; Harrison et al., 2003).

Over orbital time-scales, $\delta^{18}O$ varies on precessional scales, similar to the behavior of ice sheets and the Asian summer monsoon. As $\delta^{18}O$ most likely represents changes in the summer and winter seasons, such behavior may not be surprising. The phasing of this variability, however, is substantially lagged behind summer (June 21). Such a phase-lag is unlikely to arise from a direct response to summer or winter insolation change, as that would require time constants of up to 7000 years. The more likely scenario is a response to variability that is a seasonal-lagged response during the summer months to conditions during spring. This has been observed in modeling result of the North Atlantic as strong meridional sea surface temperature (SST) gradients produced a state similar to the North Atlantic Oscillation (NAO) (Hall et al., 2005). Variability in the El Niño-Southern Oscillation, due to phase-locking between insolation change in the annual cycle and cloud effects, produce La Niña (El Niño) -like conditions when Buckeye Creek Cave (BCC) $\delta^{18}O$ is enriched (depleted). SSTs in the Gulf of Mexico may also be a factor, as warmer SSTs in the northeast Gulf produce an increase in summer rainfall in the eastern

United States (Wang et al., 2010) and seasonal warming peaks in September. However, because Gulf SSTs begin to warm in the spring, changes in the duration of the warm season, which is controlled by obliquity, would matter more than seasonal effects on precessional scales. As BCC $\delta^{18}O$ does not exhibit any clear variability with obliquity (41 kyr cycle), it is considered less likely as a major control.

Sample CCC1 from Culverson Creek Cave (CCC), which grew over the last glacial termination, supports this conclusion as the $\delta^{18}O$ record exhibits variability that is consistent with changes in the Bermuda High (BH) strength and position. Pollen records from Florida lakes show variability in %Pinus, which is strongly correlated with summer precipitation, that is antiphased with the record from CCC1. When the BH extends over Florida, summers there become dry, either due to expansion of the BH, as occurs when the pressure cell is enhanced and circulation is stronger, or a westward shift in position. Either situation is likely to increase summer precipitation in WV, as recorded by speleothems $\delta^{18}O$.

Speleothems from northeast Brazil provide an additional perspective that is useful for distinguishing between changes in strength and changes in position. When the BH is strong, precipitation in NE Brazil is decreased (Namias, 1972). El Niño (La Niña) events also produce dry (wet) conditions in NE Brazil, while simultaneously shifting the BH eastward (westward) (Seager et al., 2005), resulting in wet (dry) summers in Florida and dry (wet) summers in WV. These three points of comparison make it possible to begin to distinguish two modes of variability in the BH.

Implicit in these scenarios is the behavior of the Gulf of Mexico. Warmer SSTs in the northern GOM produce increased summer precipitation in the eastern US (Wang et al., 2010). A stronger BH could produce warmer GOM SSTs by strengthening the NE

trade winds and enhancing Ekman transport of warm tropical water through the Yucatan strait. This provides the possibility that WV summer precipitation and GOM SSTs are responses to a common forcing in the BH. During glacial intervals, a melting ice sheet will also impact SSTs by adding cold, isotopically light, meltwater via the Mississippi river (Flower et al., 2004; Oglesby et al., 1989).

While the BH provides an immediate control on seasonal precipitation patterns in WV, it is only a component of the Earth's internal climate variability. The BH is essentially an intermediary between the primary climate forcing and the response in WV seasonality. Processes that alter the character of the BH include the Asian Summer monsoon, the North American monsoon, ENSO, and changes in the land-sea temperature contrast between continental North America (and Europe) and the subtropical North Atlantic. Variability in the ASM is well documented by Chinese speleothems, and there is a clear phase offset with the results from BCC, suggesting that the ASM is not the primary control on orbital timescales. The NASM appears to respond similarly to the ASM, with stronger circulation associated with summer insolation maxima. ENSO variability, as determined by a transient model over the last 140 ka may explain the observed phasing at the precessional scale (Timmermann et al., 2007). Alternatively, a seasonally-lagged SST response to reduced spring insolation, similar to that shown by Hall et al., 2005 could produce a similar effect (Chapter 2).

Millennial events

On millennial scales, there is some degree of correspondence between the WV record and the ASM, although the response is muted and appears to be non-linear. These millennial events produce more precipitation in both northeast and southern Brazil, which

indicates that ENSO is not a likely control on short timescales (Wang et al., 2007). During these events, $\delta^{18}O$ shows a short term shift to depleted values, consistent with a decrease in summer precipitation. The $\delta^{13}C$ record, however, shows a much clearer manifestation of these events as they produce clear shifts to enriched values.

This enrichment of $\delta^{13}C$ was most likely caused by droughts that cause prior precipitation of calcite in the vadose zone (Fairchild et al., 2006a, 2006b). Trace metal data corroborate this interpretation as both Mg/Ca and Sr/Ca ratios show good correlation with $\delta^{13}C$, consistent with an aridity driven mechanism. Throughout the record, intervals of enriched $\delta^{13}C$ occur when $\delta^{18}O$ becomes more depleted. The signal is greater in $\delta^{13}C$, but is still apparent in $\delta^{18}O$, indicating that relative summer rainfall likely decreased when annual precipitation decreased.

Potential for future work

One broader consequence of the variability recorded in $\delta^{18}O$ is the potential effect on moisture export from the Atlantic basin. This could be a useful contribution as the processes governing moisture export remains poorly understood, yet have clear implications for global climate. When more fresh water is removed from the Atlantic basin, the residual ocean becomes more saline, which will impact thermohaline circulation.

Benefits of this study

Recent work on ice cores and tropical speleothems has greatly improved our understanding of these regions on orbital and millennial time scales. A lack of high resolution, well-dated records has prevented similar progress in the mid-latitudes. The

results from BCC and CCC provide a useful advance in the paleoclimate of temperate regions.

Bibliography

Adams, D.K., Comrie, A.C., 1997. The North American monsoon. Bulletin of the American Meteorological Society, 78(10), 2197-2213.

Amundson, R., Chadwick, O., Kendall, C., Wang, Y., DeNiro, M., 1996. Isotopic evidence for shifts in atmospheric circulation patterns during the late Quaternary in mid-North America. Geology, 24(1), 23-26.

Andersen, K.K., Azuma, N., Barnola, J.M., Bigler, M., Biscaye, P., Caillon, N., Chappellaz, J., Clausen, H.B., Dahl-Jensen, D., Fischer, H., 2004. High-resolution record of Northern Hemisphere climate extending into the last interglacial period. Nature, 431(7005), 147-151.

Arz, H., Lamy, F., Pätzold, J., 2006. A pronounced dry event recorded around 4.2 ka in brine sediments from the northern Red Sea. Quaternary Research, 66(3), 432-441.

Arz, H., Nowaczyk, N., Pätzold, J., Lamy, F., Ganopolski, A., 2007. Dominant Northern Hemisphere climate control over millennial-scale glacial sea-level variability. Quaternary Science Reviews, 26(3-4), 312-321.

Baker, A., Barnes, W., Smart, P., 1997. Variations in the Discharge and Organic Matter Content of Stalagmite Drip Waters in Lower Cave, Bristol. Hydrological Processes, 11, 1541-1555.

Bard, E., 2006. Age, alkenone data and sea surface temperature records of sediment core SU81-18.

Bard, E., Rostek, F., Turon, J.L., Gendreau, S., 2000. Hydrological impact of Heinrich events in the subtropical northeast Atlantic. Science, 289(5483), 1321.

Bartlein, P.J., Anderson, K.H., Anderson, P.M., Edwards, M.E., Mock, C.J., Thompson, R.S., Webb, R.S., Webb III, T., Whitlock, C., 1998. Paleoclimate simulations for North America over the past 21,000 years: features of the simulated climate and comparisons with paleoenvironmental data. Quaternary Science Reviews, 17(6), 549-586.

Benedict, J.B., Benedict, R.J., Lee, C.M., Staley, D.M., 2008. Spruce trees from a melting ice patch: evidence for Holocene climatic change in the Colorado Rocky Mountains, USA. The Holocene, 18(7), 1067.

Benway, H.M., Mix, A.C., Haley, B.A., Klinkhammer, G.P., 2006. Eastern Pacific Warm Pool paleosalinity and climate variability: 0–30 kyr.

Bjerknes, J., 1964. Atlantic air-sea interaction. Advances in Geophysics, 10(1), 82.

Blaauw, M., Methods and code for [`]classical' age-modelling of radiocarbon sequences. Quaternary Geochronology, In Press, Corrected Proof. Available at: http://www.sciencedirect.com/science/article/B83WJ-4YB5MCX-1/2/7649547e6fd4cfbd5eedb2eafa6a7303.

Blackman, R., Tukey, J., 1959. The measurement of power spectra, from the point of view of communications engineering, Dover Publications, New York.

Booth, R.K., Jackson, S.T., Forman, S.L., Kutzbach, J.E., Bettis III, E.A., Kreigs, J., Wright, D.K., 2005. A severe centennial-scale drought in midcontinental North America 4200 years ago and apparent global linkages. The Holocene, 15(3), 321.

Bowen, G.J., 2009. WaterIsotopes.org. Gridded maps of the isotopic composition of meteoric precipitation. Available at: http://www.waterisotopes.org/ [Accessed July 24, 2009].
Bowen, G.J., Wassenaar, L.I., Hobson, K.A., 2005. Global application of stable hydrogen and oxygen isotopes to wildlife forensics. Oecologia, 143(3), 337-348.
Bowen, G.J., Wilkinson, B., 2002. Spatial distribution of d¹8O in meteoric precipitation. Geology, 30(4), 315-318.
Braconnot, P., Otto-Bliesner, B., Harrison, S., Joussaume, S., Peterchmitt, J.Y., Abe-Ouchi, A., Crucifix, M., Driesschaert, E., Fichefet, T., Hewitt, C.D., 2007. Results of PMIP2 coupled simulations of the Mid-Holocene and Last Glacial Maximum–Part 1: experiments and large-scale features. Climate of the Past, 3(2), 261-277.
Broecker, W., 1963. A preliminary evaluation of uranium series inequilibrium as a tool for absolute age measurements on marine carbonates. Journal of Geophysical Research, 68, 2817-2834.
Broecker, W.S., McGee, D., Adams, K.D., Cheng, H., Edwards, R.L., Oviatt, C.G., Quade, J., 2009. A Great Basin-wide dry episode during the first half of the Mystery Interval? Quaternary Science Reviews, 28(25-26), 2557-2563.
Bromwich, D.H., Toracinta, E.R., Oglesby, R.J., Fastook, J.L., Hughes, T.J., 2005. LGM Summer Climate on the Southern Margin of the Laurentide Ice Sheet: Wet or Dry?*. Journal of Climate, 18(16), 3317-3338.
Bush, M.B., Correa-metrio, A.Y., Hodell, D.A., Brenner, M., Anselmetti, F.S., Ariztegui, D., Mueller, A.D., Curtis, J.H., Grzesik, D.A., Burton, C., 2009. Re-evaluation of climate change in lowland Central America during the Last Glacial Maximum using new sediment cores from Lake Petén Itzá, Guatemala. Past Climate Variability in South America and Surrounding Regions, 113-128.
Calov, R., Ganopolski, A., Petoukhov, V., Claussen, M., Greve, R., 2002. Large-scale instabilities of the Laurentide ice sheet simulated in a fully coupled climate-system model. Geophysical Research Letters, 29(24), 69-1.
Cardwell, D.H., Erwin, R.B., Woodward, H.P., Lotz, C.W., 1968. Geologic Map of West Virginia. scale 1: 250,000.
Chang, F.C., Smith, E.A., 2001. Hydrological and dynamical characteristics of summertime droughts over US Great Plains. Journal of Climate, 14(10), 2296-2316.
Chang, F.C., Smith, E.A., 2001. Hydrological and dynamical characteristics of summertime droughts over US Great Plains. Journal of Climate, 14(10), 2296-2316.
Cheng, H., Edwards, R., Hoff, J., Gallup, C., Richards, D., Asmerom, Y., 2000. The half-lives of uranium-234 and thorium-230. Chemical Geology, 169, 17-33.
Cheng, H., Edwards, R., Wang, Y., Kong, X., Ming, Y., Kelly, M., Wang, X., Gallup, C., Liu, W., 2006. A penultimate glacial monsoon record from Hulu Cave and two-phase glacial terminations. Geology, 34(3), 217-220.
Cheng, H., Edwards, R.L., Broecker, W.S., Denton, G.H., Kong, X., Wang, Y., Zhang, R., Wang, X., 2009. Ice Age Terminations. Science, 326(5950), 248-252.
Chiang, J., Biasutti, M., Battisti, D., 2003. Sensitivity of the Atlantic Intertropical Convergene Zone to Last Glacial Maximum boundary conditions. Paleoceanography, 18(4), 18-1-18-18.

Clark, P.U., Mix, A.C., 2002. Ice sheets and sea level of the Last Glacial Maximum. Quaternary Science Reviews, 21(1-3), 1-7.
COHMAP Members, 1988. Climatic changes of the last 18,000 years: observations and model simulations. Science, 241, 1043-1052.
Conroy, J.L., Overpeck, J.T., Cole, J.E., Shanahan, T.M., Steinitz-Kannan, M., 2008. Holocene changes in eastern tropical Pacific climate inferred from a Galapagos lake sediment record. Quaternary Science Reviews, 27(11-12), 1166-1180.
Cruz, F.W., Burns, S.J., Karmann, I., Sharp, W.D., Vuille, M., Cardoso, A.O., Ferrari, J.A., Dias, P.L.S., Viana, O., 2005. Insolation-driven changes in atmospheric circulation over the past 116,000 years in subtropical Brazil. Nature, 434(7029), 63-66.
Cruz, F.W., Vuille, M., Burns, S.J., Wang, X., Cheng, H., Werner, M., Edwards, R.L., Karmann, I., Auler, A.S., Nguyen, H., 2009. Orbitally driven east–west antiphasing of South American precipitation. Nature Geoscience, 2(3), 210-214.
Cuffey, K.M., Clow, G.D., Alley, R.B., Stuiver, M., Waddington, E.D., Saltus, R.W., 1995. Large Arctic Temperature Change at the Wisconsin-Holocene Glacial Transition. Science, 270(5235), 455-458.
Curtis, J.H., Hodell, D.A., Brenner, M., 1996. Climate variability on the Yucatan Peninsula (Mexico) during the past 3500 years, and implications for Maya cultural evolution. Quaternary Research, 46(1), 37–47.
Cutler, K., Adkins, J., Gallup, C., Cutler, P., Burr, G., Bloom, A., Edwards, R.L., Taylor, F., Cheng, H., 2003. Rapid sea-level fall and deep-ocean temperature change since the last interglacial period. Earth and Planetary Science Letters, 206(3-4), 253-271.
Czaja, A., Frankignoul, C., 1999. Influence of the North Atlantic SST on the atmospheric circulation. Geophysical Research Letters, 26(19), 2969-2972.
Dansgaard, W., 1964. Stable Isotopes in Precipitation. Tellus, 16, 436-468.
Dasher, G.R., Balfour, W.M., 1994. The Caves and Karst of the Buckeye Creek Basin, Greenbrier County, West Virginia. West Virginia Speleological Survey Bulletin, 12.
Davis, R.E., 1976. Predictability of sea surface temperature and sea level pressure anomalies over the North Pacific Ocean. J. Phys. Oceanogr, 6(3), 249–266.
Davis, R.E., Hayden, B.P., Gay, D.A., Phillips, W.L., Jones, G.V., 1997. The North Atlantic subtropical anticyclone. Journal of Climate, 10(4), 728-744.
Denton, G., Alley, R., Comer, G., Broecker, W., 2005. The role of seasonality in abrupt climate change. Quaternary Science Reviews, 24, 1159-1182.
Denton, G.H., Broecker, W.S., Alley, R.B., 2006. The mystery interval 17.5 to 14.5 kyrs ago. Pages News, 14(20), 14–16.
Denton, G.H., Broecker, W.S., Alley, R.B., 2006. The mystery interval 17.5 to 14.5 kyrs ago. Pages News, 14(20), 14–16.
Diffenbaugh, N.S., Ashfaq, M., Shuman, B., Williams, J.W., Bartlein, P.J., 2006. Summer aridity in the United States: Response to mid-Holocene changes in insolation and sea surface temperature. Geophysical Research Letters, 33(22), 151-168.
Donders, T.H., de Boer, H.J., Finsinger, W., Grimm, E.C., Dekker, S.C., Reichart, G.J., Wagner-Cremer, F., 2009. Impact of the Atlantic Warm Pool on precipitation and temperature in Florida during North Atlantic cold spells. Climate Dynamics, 1-10.

Dong, B., Sutton, R.T., 2005. Mechanism of Interdecadal Thermohaline Circulation Variability in a Coupled Ocean-Atmosphere GCM. Journal of Climate, 18, 1117-1135.

Dorale, J., Edwards, R.L., Ito, E., Gonzalez, L., 1998. Climate and Vegetation History of the Midcontinent from 75 to 25 ka: A Speleothem Record from Crevice Cave, Missouri, USA. Science, 282, 1871-1874.

Dykoski, C., Edwards, R.L., Cheng, H., Yuan, D., Cai, Y., Zhang, M., Lin, Y., An, Z., Revenaugh, J., 2005. A high resolution, absolute-dated Holocene and deglacial Asian monsoon record from Dongge Cave, China. Earth and Planetary Science Letters, 233, 71-86.

Edwards, R.L., Chen, J., Wasserburg, G., 1987. ^{238}U-^{234}U-^{230}Th-^{232}Th systematics and the precise measurement of time over the past 500,000 years. Earth and Planetary Science Letters, 81(2-3), 175-192.

Edwards, R.L., Cutler, K., Cheng, H., Gallup, C., 2003. Geochemical Evidence for Quaternary Sea-level Changes, in: Treatise on Geochemistry. Pergamon, Oxford, pp. 343-364. Available at: http://www.sciencedirect.com/science/article/B782S-4CJV6M2-5W/2/2c0d046f131b6315bfcab6e3d8313a9b.

Edwards, T.W.D., Wolfe, B.B., MacDonald, G.M., 1996. Influence of Changing Atmospheric Circulation on Precipitation d^{1}8O-Temperature Relations in Canada during the Holocene. Quaternary Research, 46(3), 211-218.

Fairchild, I., Borsato, A., Tooth, A., Frisia, S., Hawkesworth, C., Huang, Y., McDermott, F., Spiro, B., 2000. Controls on trace element (Sr-Mg) compositions of carbonate cave waters: implications for speleothem climatic records. Chemical Geology, 166, 255-269.

Fairchild, I., Smith, C., Baker, A., Fuller, L., Spotl, C., Mattey, D., McDermott, F., E.I.M.F., 2006a. Modification and preservation of environmental signals in speleothems. Earth-Science Reviews, 75, 105-153.

Fairchild, I., Tooth, A., Tuckwell, G., Baker, A., 2006b. Modelling of dripwater hydrology and hydrogeochemistry in a weakly karstified aquifer (Bath, UK): Implications for climate change studies. Journal of Hydrology, 321(1-4), 213-231.

Flower, B.P., Hastings, D.W., Hill, H.W., Quinn, T.M., 2004. Phasing of deglacial warming and Laurentide Ice Sheet meltwater in the Gulf of Mexico. Geology, 32(7), 597.

Folland, C.K., Knight, J., Linderholm, H.W., Fereday, D., Ineson, S., Hurrell, J.W., 2009. The Summer North Atlantic Oscillation: Past, Present, and Future. Journal of Climate, 22(5), 1082-1103.

Grimm, E.C., Watts, W.A., Jacobson Jr, G.L., Hansen, B., Almquist, H.R., Dieffenbacher-Krall, A.C., 2006. Evidence for warm wet Heinrich events in Florida. Quaternary Science Reviews, 25(17-18), 2197-2211.

Hall, A., Clement, A., Thompson, D.W.J., Broccoli, A., Jackson, C., 2005. The Importance of Atmospheric Dynamics in the Northern Hemisphere Wintertime Climate Response to Changes in the Earth's Orbit. Journal of Climate, 18(9), 1315-1325.

Hardt, B., Rowe, H.D., Springer, G.S., Cheng, H., Edwards, R.L., 2010. The seasonality of east central North American precipitation based on three coeval Holocene

speleothems from southern West Virginia. Earth and Planetary Science Letters, 295(3-4), 342-348.
Hardt, B., Rowe, H.D., Springer, G.S., Edwards, R.L., Cheng, H., Precession-scale variability in eastern North American seasonal precipitation and potential links to Atlantic ITCZ migration and thermohaline circulation.
Harrison, S.P., Kutzbach, J.E., Liu, Z., Bartlein, P.J., Otto-Bliesner, B., Muhs, D., Prentice, I.C., Thompson, R.S., 2003. Mid-Holocene climates of the Americas: a dynamical response to changed seasonality. Climate Dynamics, 20(7), 663-688.
Haug, G.H., Gunther, D., Peterson, L.C., Sigman, D.M., Hughen, K.A., Aeschlimann, B., 2003. Climate and the collapse of Maya civilization. Science, 299, 1731–1735.
Haug, G.H., Hughen, K.A., Sigman, D.M., Peterson, L.C., Rohl, U., 2001. Southward Migration of the Intertropical Convergence Zone Through the Holocene. Science, 293(5533), 1304.
Hays, J.D., Imbrie, J., Shackleton, N.J., 1976. Variations in the Earth's orbit: pacemaker of the ice ages.
Henderson, K.G., Vega, A.J., 1996. Regional precipitation variability in the southern United States. Physical Geography, 17(2), 93-112.
Hendy, C., 1971. The isotopic geochemistry of speleothems: 1. The calculation of the effects of different modes of formation on the isotopic composition of speleothems and their applicability as paleoclimatic indicators. Geochimica et Cosmochimica Acta, 35(8), 801-824.
Hendy, C.H., Wilson, A.T., 1968. Palaeoclimatic data from speleothems. Nature, 219(5149), 48-51.
Higgins, R.W., Yao, Y., Wang, X.L., 1997. Influence of the North American monsoon system on the US summer precipitation regime. Journal of Climate, 10(10), 2600-2622.
Hill, H.W., Flower, B.P., Quinn, T.M., Hollander, D.J., Guilderson, T.P., 2006. Laurentide Ice Sheet meltwater and abrupt climate change during the last glaciation. Paleoceanography, 21(1), 1-A1006.
Hodell, D.A., Brenner, M., Curtis, J.H., 2005a. Terminal Classic drought in the northern Maya lowlands inferred from multiple sediment cores in Lake Chichancanab (Mexico). Quaternary Science Reviews, 24(12-13), 1413–1427.
Hodell, D.A., Brenner, M., Curtis, J.H., 2007. Climate and cultural history of the Northeastern Yucatan Peninsula, Quintana Roo, Mexico. Climatic Change, 83(1), 215–240.
Hodell, D.A., Brenner, M., Curtis, J.H., Guilderson, T., 2001. Solar forcing of drought frequency in the Maya lowlands. Science, 292(5520), 1367–1370.
Hodell, D.A., Brenner, M., Curtis, J.H., Medina-González, R., Ildefonso-Chan Can, E., Albornaz-Pat, A., Guilderson, T.P., 2005b. Climate change on the Yucatan peninsula during the Little Ice Age. Quaternary Research, 63(2), 109–121.
Holzhauser, H., Magny, M., Zumbuuhl, H.J., 2005. Glacier and lake-level variations in west-central Europe over the last 3500 years. The Holocene, 15(6), 789.
Huang, Y., Fairchild, I., 2001. Partitioning of Sr2+ and Mg2+ into calcite under karst-analogue experimental conditions. Geochimica et Cosmochimica Acta, 65(1), 47-62.

Huybers, P., 2006. Early Pleistocene glacial cycles and the integrated summer insolation forcing. Science, 313(5786), 508.
IAEA/WMO, 2006. Global Network of Isotopes in Precipitation, International Atomic Energy Agency, Vienna. Available at: http://isohis.iaea.org.
Jouzel, J., Koster, R.D., Suozzo, R.J., Russell, G.L., 1994. Stable water isotope behavior during the last glacial maximum: A general circulation model analysis. Journal of Geophysical Research, 99D(12), 25791-25801.
Jouzel, J., Russell, G.L., Suozzo, R.J., Koster, R.D., White, J.W.C., Broecker, W.S., 1987. Simulations of the HDO and H218O atmospheric cycles using the NASA/GISS general circulation model: the seasonal cycle for present-day conditions. Journal Geophysical Research, 92D, 14739-14760.
Keim, B., 1997. Preliminary Analysis of the Temporal Patterns of Heavy Rainfall across the Southeastern United States. Professional Geographer, 49(1), 94-104.
Kelly, M., Edwards, R.L., Cheng, H., Yuan, D., Cai, Y., Zhang, M., Lin, Y., An, Z., 2006. High resolution characterization of the Asian Monsoon between 146,000 and 99,000 years B.P. from Dongge Cave, China and global correlation of events surrounding Termination II. Palaeogeography, Palaeoclimatology, Palaeoecology, 236, 20-38.
Kim, S., O'Neil, J., 1997. Equilibrium and nonequilibrium oxygen isotope effects in synthetic carbonates. Geochimica et Cosmochimica Acta, 61, 3461-3475.
Kirby, M.E., Mullins, H.T., Patterson, W.P., Burnett, A.W., 2001. Lacustrine isotopic evidence for multidecadal natural climate variability related to the circumpolar vortex over the northeast United States during the past millennium. Geology, 29(9), 807-810.
Kneller, M., Peteet, D., 1993. Late-Quaternary Climate in the Ridge and Valley of Virginia, USA: Changes in Vegetation and Depositional Environment. Quaternary Science Reviews, 12, 613-628.
Kneller, M., Peteet, D., 1999. Late-glacial to early Holocene climate changes from a central Appalachian pollen and macrofossil record. Quaternary Research, 51(2), 133-147.
Kushnir, Y., Robinson, W.A., Bladé, I., Hall, N.M.J., Peng, S., Sutton, R., 2002. Atmospheric GCM Response to Extratropical SST Anomalies: Synthesis and Evaluation*. Journal of Climate, 15, 2233-2256.
Lachniet, M.S., 2009. Climatic and environmental controls on speleothem oxygen-isotope values. Quaternary Science Reviews, 28(5-6), 412-432.
Laskar, J., Robutel, P., Joutel, F., Gastineau, M., Correia, A., Levrard, B., 2004. A long-term numerical solution for the insolation quantities of the Earth. Astronomy & Astrophysics, 428(1), 261-85.
Lau, K.M., Zhou, J., 2003. Anomalies of the South American summer monsoon associated with the 1997-99 El Nino-Southern Oscillation. International Journal of Climatology, 23(5), 529-539.
Leduc, G., Vidal, L., Tachikawa, K., Rostek, F., Sonzogni, C., Beaufort, L., Bard, E., 2007. Moisture transport across Central America as a positive feedback on abrupt climatic changes. Nature, 445, 908-911.

Li, W., Lundberg, J., Dickin, A., Ford, D., Schwarcz, H., McNutt, R., Williams, D., 1989. High-precision mass-spectrometric uranium-series dating of cave deposits and implications for palaeoclimate studies. Nature, 339(6225TY - JOUR 10.1038/339534a0), 534-536.
Lowell, T.V., Hayward, R.K., Denton, G.H., 1999. Role of climate oscillations in determining ice-margin position: Hypothesis, examples, and implications. Geological Society of America Special Papers, 337, 193.
Marchant, R., Hooghiemstra, H., 2004. Rapid environmental change in African and South American tropics around 4000 years before present: A review. Earth-Science Reviews, 66(3-4), 217-260.
Marshall, S.J., Koutnik, M.R., 2006. Ice sheet action versus reaction: Distinguishing between Heinrich events and Dansgaard-Oeschger cycles in the North Atlantic. Paleoceanography, 21(2), 1-A2021.
Martinson, D.G., Pisias, N.G., Hays, J.D., Imbrie, J., Moore, T.C., 1987. Age dating and the orbital theory of the ice ages: Development of a high-resolution 0 to 300,000-year chronostratigraphy* 1. Quaternary Research, 27(1), 1-29.
Mo, K.C., Schemm, J.E., 2008. Droughts and Persistent Wet Spells over the United States and Mexico. Journal of Climate, 21, 980-994.
Muñoz, E., Busalacchi, A.J., Nigam, S., Ruiz-Barradas, A., 2008. Winter and summer structure of the Caribbean low-level jet. Journal of Climate, 21, 1260-1276.
Namias, J., 1972. Influence of northern hemisphere general circulation on drought in northeast Brazil1. Tellus, 24(4), 336–343.
Nürnberg, D., Ziegler, M., Karas, C., Tiedemann, R., Schmidt, M.W., 2008. Interacting Loop Current variability and Mississippi River discharge over the past 400 kyr. Earth and Planetary Science Letters, 272(1-2), 278-289.
Oglesby, R.J., Maasch, K.A., Saltzman, B., 1989. Glacial meltwater cooling of the Gulf of Mexico: GCM implications for Holocene and present-day climates. Climate dynamics, 3(3), 115-133.
Pahnke, K., Sachs, J.P., Keigwin, L., Timmermann, A., Xie, S., 2007. Eastern tropical Pacific hydrologic changes during the past 27,000 years from D/H ratios in alkenones. Paleoceanography, 22(4), PA4214.
Paillard, D., Labeyrie, L., Yiou, P., 1996. Macintosh program performs time-series analysis. Eos Trans. AGU, 77(39), 379.
Parrish, J.T., Peterson, F., 1988. Wind directions predicted from global circulation models and wind directions determined from eolian sandstones of the western United States--a comparison. Sedimentary Geology, 56(1-4), 261-282.
Partin, J.W., Cobb, K.M., Adkins, J.F., Clark, B., Fernandez, D.P., 2007. Millennial-scale trends in west Pacific warm pool hydrology since the Last Glacial Maximum. Nature, 449(7161), 452-455.
Peixóto, J., Oort, A., 1983. The atmospheric branch of the hydrological cycle and climate, in: Variations in the global water budget. Reidel, pp. 5-65.
Praetorius, S.K., McManus, J.F., Oppo, D.W., Curry, W.B., 2008. Episodic reductions in bottom-water currents since the last ice age. Nature Geoscience, 1(7), 449-452.
Prokopenko, A.A., Hinnov, L.A., Williams, D.F., Kuzmin, M.I., 2006. Orbital forcing of continental climate during the Pleistocene: a complete astronomically tuned climatic

record from Lake Baikal, SE Siberia. Quaternary Science Reviews, 25(23-24), 3431-3457.
Reimer, P.J., Baillie, M.G.L., Bard, E., Bayliss, A., Beck, J.W., Bertrand, C.J.H., Blackwell, P.G., Buck, C.E., Burr, G.S., Cutler, K.B., 2004. IntCal04 terrestrial radiocarbon age calibration, 0–26 cal kyr BP.
Rodwell, M.J., Hoskins, B.J., 2001. Subtropical anticyclones and summer monsoons. Journal of Climate, 14(15), 3192-3211.
Rohli, R.V., Henderson, K.G., 1998. Upper-level steering flow and continental anticyclones on the central Gulf Coast of the United States. International Journal of Climatology, 18(9).
Rozanski, K., Araguas-Araguas, L., Gonfiantini, R., 1993. Isotopic Patterns in Modern Global Precipitation, in: Climate Change in Continental Isotopic Records. Geophysical Monograph. American Geophysical Union, pp. 1-36.
Schmidt, G.A., LeGrande, A.N., Hoffmann, G., 2007. Water isotope expressions of intrinsic and forced variability in a coupled ocean-atmosphere model. Journal of Geophysical Research-Atmospheres, 112(D10), D10103.
Schmidt, M.W., Spero, H.J., Lea, D.W., 2004. Links between salinity variation in the Caribbean and North Atlantic thermohaline circulation. Nature, 428(6979), 160-163.
Schmittner, A., Appenzeller, C., Stocker, T.F., 2000. Enhanced Atlantic freshwater export during El Niño. Geophysical Research Letters, 27(8), 1163-1166.
Seager, R., Kushnir, Y., Herweijer, C., Naik, N., Velez, J., 2005. Modeling of Tropical Forcing of Persistent Droughts and Pluvials over Western North America: 1856–2000*. Journal of Climate, 18, 4065–4088.
Shackleton, N.J., Imbrie, J., Hall, M.A., 1983. Oxygen and carbon isotope record of East Pacific core V19-30: implications for the formation of deep water in the late Pleistocene North Atlantic. Earth and Planetary Science Letters, 65(2), 233-244.
Shen, C., Dorale, J., Thomas, R., Moran, S., Weinstein, S., Edmonds, H., Edwards, R., Cheng, H., 2002. Uranium and thorium isotopic and concentration measurements by magnetic sector inductively coupled plasma mass spectrometry. Chemical Geology, 185(3-4), 165-178.
Shuman, B., Bartlein, P., Logar, N., Newby, P., Webb, T., 2002. Parallel climate and vegetation responses to the early Holocene collapse of the Laurentide Ice Sheet. Quaternary Science Reviews, 21(16-17), 1793-1805.
Shuman, B., Bravo, J., Kaye, J., Lynch, J.A., Newby, P., Webb, T., 2001. Late Quaternary water-level variations and vegetation history at Crooked Pond, southeastern Massachusetts. Quaternary Research, 56(3), 401-410.
Shuman, B., Donnelly, J.P., 2006. The influence of seasonal precipitation and temperature regimes on lake levels in the northeastern United States during the Holocene. Quaternary Research, 65(1), 44-56.
Shuman, B., Newby, P., Huang, Y., Webb III, T., 2004. Evidence for the Close Climatic Control of New England Vegetation History. Ecology, 85(5), 1297-1310.
Siddall, M., Meischner, D., Schmelzer, I., Smeed, D., Rohling, E., Almogi-Labin, A., Hemleben, C., 2003. Sea-level fluctuations during the last glacial cycle. Nature, 423(6942), 853-858.

Springer, G.S., Rowe, H.D., Hardt, B., Edwards, R.L., Cheng, H., 2008. Solar forcing of Holocene droughts in a stalagmite record from West Virginia in east-central North America. Geophysical Research Letters, 35(17), L17703.
Springer, G.S., Rowe, H.D., Hardt, B., Edwards, R.L., Cheng, H., Changes in aridity in West Virginia driven by north Atlantic climate and ice sheets.
Staubwasser, M., Sirocko, F., Grootes, P.M., Segl, M., 2003. Climate change at the 4.2 ka BP termination of the Indus valley civilization and Holocene south Asian monsoon variability. Geophysical Research Letters, 30(8), 1425.
Svensson, A., Andersen, K.K., Bigler, M., Clausen, H.B., Dahl-Jensen, D., Davies, S.M., Johnsen, S.J., Muscheler, R., Parrenin, F., Rasmussen, S.O., 2008. A 60 000 year Greenland stratigraphic ice core chronology. Climate of the Past, 4(1), 47-57.
Tarasov, L., Peltier, W.R., 2005. Arctic freshwater forcing of the Younger Dryas cold reversal. Nature, 435(7042), 662-665.
Timmermann, A., Lorenz, S.J., An, S.I., Clement, A., Xie, S.P., 2007. The effect of orbital forcing on the mean climate and variability of the tropical Pacific. Journal of Climate, 20(16), 4147-4159.
Vachon, R.W., White, J.W.C., Gutmann, E., Welker, J.M., 2007. Amount-weighted annual isotopic (δ18O) values are affected by the seasonality of precipitation: A sensitivity study. Geophysical Research Letters, 34(21), L21707.
Vetter, L., Spero, H.J., Eggins, S.M., Flower, B.P., Williams, C.C., 2009. Reconstructing Laurentide Ice Sheet Meltwater Geochemistry Using Combined Stable Isotope And Laser Ablation Trace Element Analyses, in: AGU Fall Meeting Abstracts. p. 1328.
Wan, X., Chang, P., Saravanan, R., Zhang, R., Schmidt, M.W., 2009. On the interpretation of Caribbean paleo-temperature reconstructions during the Younger Dryas. Geophys. Res. Lett, 36, L02701.
Wang, C., 2005. ENSO, Atlantic climate variability, and the Walker and Hadley circulations. The Hadley Circulation: Present, Past, and Future, 173-202.
Wang, C., Enfield, D.B., Lee, S., Landsea, C.W., 2006. Influences of the Atlantic Warm Pool on Western Hemisphere Summer Rainfall and Atlantic Hurricanes. Journal of Climate, 19(12), 3011-3028.
Wang, C., Lee, S., Enfield, D.B., 2007. Impact of the Atlantic warm pool on the summer climate of the Western Hemisphere. Journal of Climate, 20(20), 5021-5040.
Wang, H., Schubert, S., Suarez, M., Koster, R., 2010. The physical mechanisms by which the leading patterns of SST variability impact US precipitation. Journal of Climate, 23(7), 1815-1836.
Wang, X., Auler, A., Edwards, R.L., Cheng, H., Cristalli, P., Smart, P., Richards, D., Shen, C., 2004. Wet periods in northeastern Brazil over the past 210 kyr linked to distant climate anomalies. Nature, 432, 740-743.
Wang, X., Auler, A.S., Edwards, R.L., Cheng, H., Ito, E., Wang, Y., Kong, X., Solheid, M., 2007. Millennial-scale precipitation changes in southern Brazil over the past 90,000 years. Geophysical Research Letters, 34(23), L23701.
Wang, Y., Cheng, H., Edwards, R.L., An, Z., Wu, J., Shen, C., Dorale, J., 2001. A high-resolution absolute-dated Late Pleistocene monsoon record from Hulu Cave, China. Science, 294, 2345-2348.

Wang, Y., Cheng, H., Edwards, R.L., Kong, X., Shao, X., Chen, S., Wu, J., Jiang, X., Wang, X., An, Z., 2008. Millennial-and orbital-scale changes in the East Asian monsoon over the past 224,000 years. Nature, 451(7182), 1090-1093.

Watts, W., 1979. Late Quaternary vegetation of central Appalachia and the New Jersey coastal plain. Ecological Monographs, 49, 427-469.

Watts, W.A., 1975. A late Quaternary record of vegetation from Lake Annie, south-central Florida. Geology, 3(6), 344.

Weaver, S.J., Schubert, S., Wang, H., 2009. Warm season variations in the low-level circulation and precipitation over the central United States in observations, AMIP simulations, and idealized SST experiments. Journal of Climate, 22, 5401-5420.

Welker, J.M., White, J., Vachon, R.W., Esposito, D., Larson, R., 2002. High resolution spatial patterns of the isotopic characteristics of precipitation across the U.S. during El Nino and La Nina phases. EOS Transactions, 83(47).

Werner, M., Mikolajewicz, U., Heimann, M., Hoffmann, G., 2000. Borehole versus isotope temperatures on Greenland: seasonality does matter. Geophysical Research Letters, 27(5), 723-726.

White, W., 2004. Paleoclimate Records from Speleothems in Limestone Caves, in: Sasowsky, I., Mylroie, J. (Eds.), Studies of Cave Sediments: Physical and Chemical Records of Paleoclimate. Kluwer Academic/Plenum Publishers, New York, pp. 135-175.

Willard, D.A., Bernhardt, C.E., Korejwo, D.A., Meyers, S.R., 2005. Impact of millennial-scale Holocene climate variability on eastern North American terrestrial ecosystems: pollen-based climatic reconstruction. Global and Planetary Change, 47(1), 17-35.

Williams, D.F., 1984. Correlations of Pleistocene Marine Sediments of the Gulf of Mexico and Other Basins Using Oxygen Isotope Stratigraphy, in: Healy-Williams, N. (Ed.), Principles of Pleistocene Stratigraphy applied to the Gulf of Mexico. International Human Resources Development Corp., Boston, pp. 65-118.

Xie, S., Xu, H., Kessler, W.S., Nonaka, M., 2005. Air–Sea Interaction over the Eastern Pacific Warm Pool: Gap Winds, Thermocline Dome, and Atmospheric Convection*. Journal of Climate, 18(1), 5-20.

Yurtsever, Y., 1975. Worldwide survey of stable isotopes in precipitation. Report, Section on Isotopic Hydrology, International Atomic Energy Agency. Vienna.

Zhang, P., Cheng, H., Edwards, R.L., Chen, F., Wang, Y., Yang, X., Liu, J., Tan, M., Wang, X., Liu, J., An, C., Dai, Z., Zhou, J., Zhang, D., Jia, J., Jin, L., Johnson, K.R., 2008. A Test of Climate, Sun, and Culture Relationships from an 1810-Year Chinese Cave Record. Science, 322(5903), 940-942.

Ziegler, M., Nurnberg, D., Karas, C., Tiedemann, R., Lourens, L.J., 2008. Persistent summer expansion of the Atlantic Warm Pool during glacial abrupt cold events. Nature Geosci, 1(9), 601-605.

Appendix 1: Supplemental Materials for Chapter 2

Figure S2-1 Images of samples BCC2, 4, and 6.

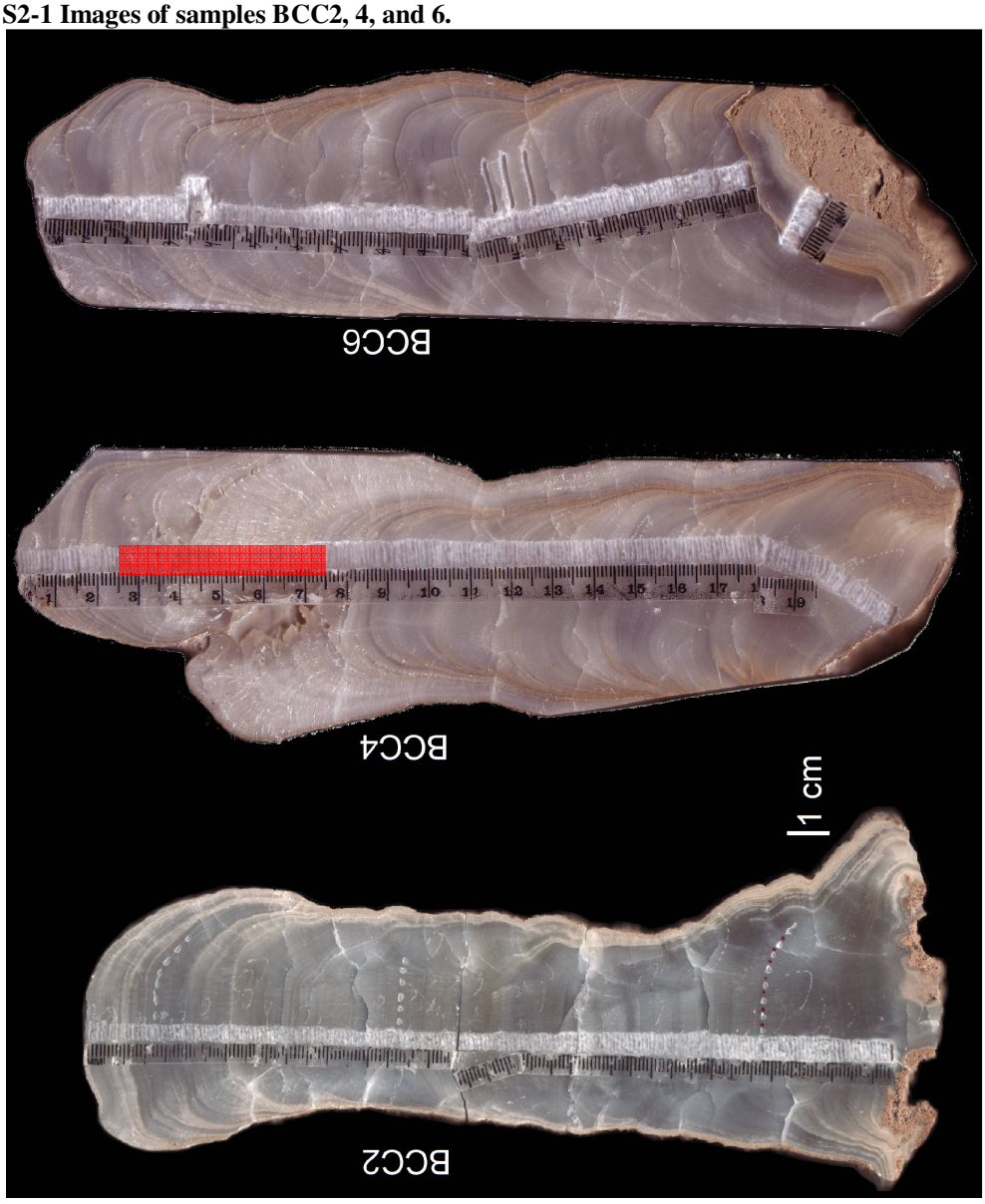

Figure S1. Images of samples (left to right) BCC-2, BCC-4, BCC-6. The shaded interval in BCC-4 was excluded from analysis. 1 cm scale bar included for each sample.

Figure S2-2 Age/Depth Plot for samples BCC2, 4, and 6.

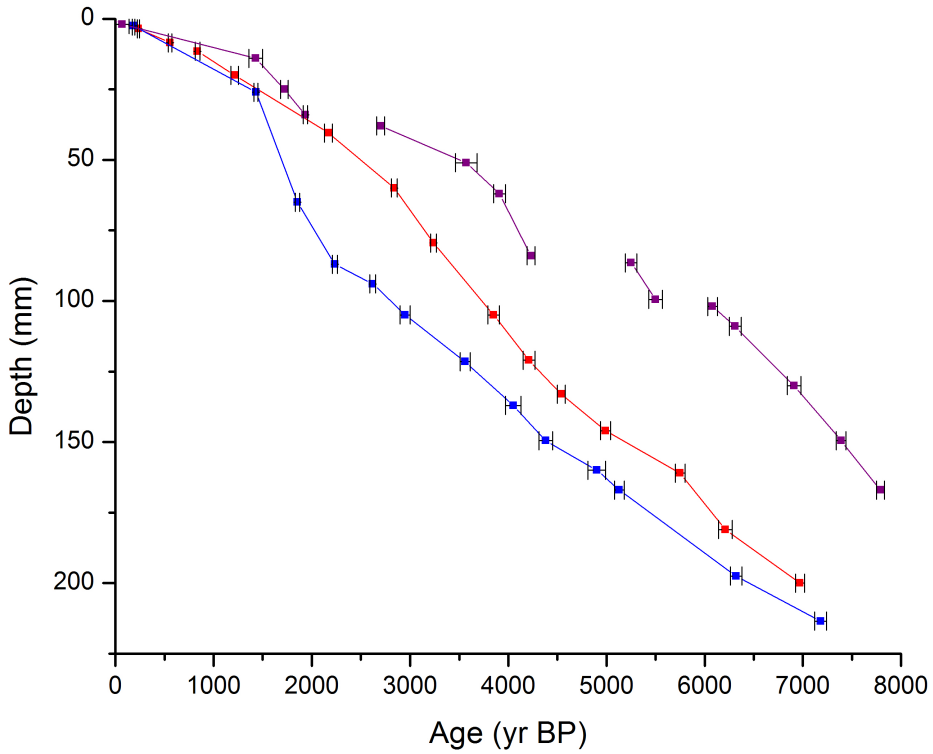

Figure S2. Age v. Depth plot for the three samples presented in the text. BCC-2 is in red, BCC-4 in blue, and BCC-6 in purple. Line breaks indicate apparent hiatuses. Age error bars are included. Assumed depth error is 1 mm.

Figure S2-3 Power Spectra, Coherency, and Phase relationship between SNAO and WV summer precipitation.

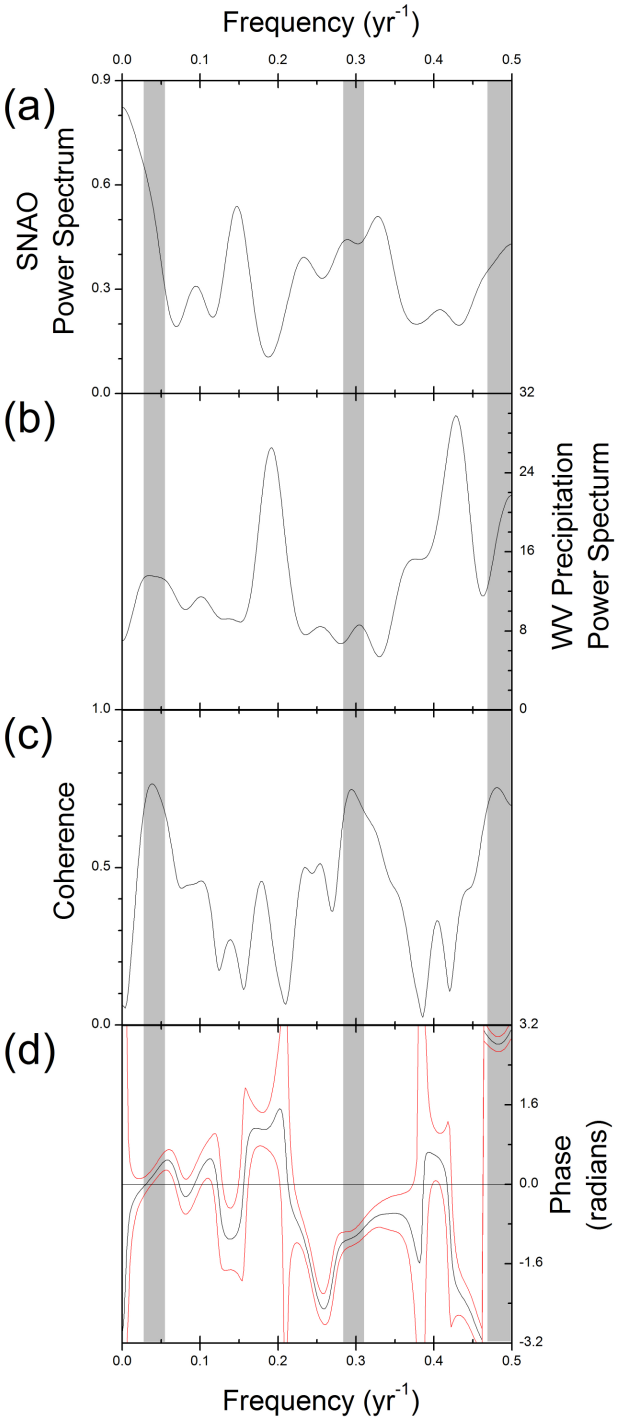

Figure S3. Time series analysis of the Summer North Atlantic Oscillation (SNAO) (Folland et al., 2009) and West Virginia Precipitation (see Section 3 for locations) from 1902-2007. (a) Power spectrum of the SNAO. (b) Power Spectrum of West Virginia Precipitation. (c) Coherence between the two records. (d) Phasing between the two records, with red lines indicating the error envelope about the mean phase value. Areas with grey shading indicate frequencies of significant coherence ($p \leq 0.01$).

Table S2-1 U/Th data table and 230Th ages for samples BCC2, 4, and 6.

Table S1. Uranium and thorium isotopic compositions and ^{230}Th ages by ICP-MS. Sample ID indicates sample name followed by drilling depth in mm. Reported error is 2σ error. Decay constant values are from Cheng et al., 2000. Age corrections were calculated using an average crustal ^{230}Th/^{232}Th atomic ratio of (4.4 ± 2.2) x 10^{-6}. ^{230}Th ages are indicated in bold.

Sample *ID*	^{238}U *ppb*	^{232}Th *ppt*	δ^{234}U *measured*	[^{230}Th/^{238}U] *Activity*	Age (yr BP) *uncorrected*	Age (yr BP) corrected	$\delta^{234}U_{initial}$ *corrected*
BCC2-3.5	535.1±0.8	438±20	1531±3	0.00686±0.00024	241±10	**232±11**	1532±3
BCC2-8.5	582.7±1.1	671.8±2.2	1522±4	0.0145±0.0004	570±17	**557±19**	1524±4
BCC2-11.5	505.4±0.9	275.1±1.0	1527±4	0.0207±0.0005	841±24	**835±24**	1531±4
BCC2-20	507.1±1.0	2121±8	1556±4	0.0307±0.0008	1260±40	**1214±40**	1561±4
BCC2-40.5	504.3±1.1	643±4	1611±5	0.0532±0.0010	2180±40	**2170±40**	1621±5
BCC2-60	721.9±1.8	559.4±2.3	1583±5	0.0680±0.0007	2850±30	**2840±30**	1596±5
BCC2-79.5	686.0±1.7	438.5±1.9	1596±5	0.0776±0.0008	3250±30	**3240±30**	1611±5
BCC2-105	707.1±1.8	238.9±2.2	1583±5	0.0911±0.0013	3850±60	**3850±60**	1600±5
BCC2-121	685.3±2.0	92.3±2.3	1608±6	0.1004±0.0012	4210±50	**4210±60**	1628±6
BCC2-130	772.5±1.8	92±3	1600±5	0.1075±0.0009	4530±40	**4540±40**	1621±5
BCC2-146	726.5±2.5	113.0±2.2	1610±7	0.1185±0.0012	4990±50	**4990±50**	1633±7
BCC2-161	680.0±2.1	1278±5	1627±6	0.1371±0.0012	5760±50	**5750±50**	1654±6
BCC2-181	784.7±2.5	2150±8	1614±7	0.1473±0.0014	6240±60	**6210±70**	1643±7
BCC2-200	810±1	1700±20	1559.5±2.5	0.1608±0.0010	6980±40	**6970±45**	1590.8±2.5
BCC4-2.5	535±1	991±19	1560.9±2.9	0.00609±0.00018	205±8	**184±13**	1562.0±2.9
BCC4-26	747.4±1.9	75.6±0.4	1564.7±2.7	0.0348±0.0005	1432±20	**1431±20**	1571.3±2.7
BCC4-63	910±40	94±4	1592.4±2.2	0.0451±0.0005	1854±21	**1853±21**	1601.0±2.2
BCC4-87	778.1±1.4	894±3	1525.5±2.5	0.0529±0.0006	2247±26	**2235±27**	1535.5±2.5
BCC4-90	740±29	352±14	1531±3	0.0615±0.0007	2620±30	**2620±30**	1542±3
BCC4-105	630.7±1.2	1025±6	1571±3	0.0704±0.0010	2960±40	**2950±50**	1585±3
BCC4-121	716±29	2500±100	1559±4	0.0847±0.0008	3600±40	**3560±50**	1575±4
BCC4-137	698.3±1.2	1034±5	1594±3	0.0965±0.0017	4060±70	**4050±80**	1613±3
BCC4-149.5	774.4±1.2	95.7±1.4	1623.3±2.5	0.1049±0.0016	4380±70	**4380±70**	1643.8±2.5
BCC4-160	682.0±1.0	1570±9	1612.9±2.7	0.1171±0.0020	4920±90	**4900±90**	1635.6±2.7
BCC4-167	860±30	2370±90	1572.1±2.3	0.1206±0.0010	5160±40	**5130±50**	1595.3±2.4
BCC4-197.5	720.8±1.1	2513±7	1675.1±2.8	0.1534±0.0013	6350±60	**6320±60**	1705.5±2.9
BCC4-213.5	932±1	6811±27	1565.2±2.5	0.1674±0.0008	7270±40	**7180±60**	1597.6±2.6
BCC6-2	569±1	7278±22	1556.6±2.4	0.00624±0.00019	212±8	**70±70**	1557.1±2.4
BCC6-14	536.9±1.1	677±4	1569±3	0.0352±0.0015	1450±60	**1430±70**	1576±3
BCC6-25	628.1±1.4	160.6±1.4	1564±3	0.0416±0.0009	1720±40	**1720±40**	1572±3
BCC6-34	762.0±1.3	139.2±1.6	1547.7±2.5	0.0462±0.0005	1936±21	**1934±21**	1556.5±2.5
BCC6-38	614.2±1.5	1476±7	1583±4	0.0652±0.0009	2730±40	**2700±40**	1595±4

Sample *ID*	^{238}U *ppb*	^{232}Th *ppt*	δ^{234}U *measured*	[^{230}Th/^{238}U] *Activity*	**Age (yr BP)** *uncorrected*	**Age (yr BP)** **corrected**	$\delta^{234}U_{initial}$ *corrected*
BCC6-51	631±12	275.7±2.2	1510±30	0.0823±0.0021	3570±110	**3570±110**	1520±30
BCC6-62	647.0±1.1	117.5±1.5	1573±3	0.0922±0.0013	3910±60	**3910±60**	1591±3
BCC6-84	724.7±1.2	146.1±1.2	1597.4±2.8	0.1004±0.0009	4230±40	**4230±40**	1616.8±2.8
BCC6-86.5	783.3±1.4	46.4±1.6	1595±3	0.1238±0.0013	5250±60	**5250±60**	1619±3
BCC6-99.5	664.8±1.0	85.2±1.5	1630.1±2.9	0.1312±0.0015	5500±70	**5500±70**	1655.9±2.9
BCC6-102	612.8±1.0	157.3±1.4	1595.9±2.9	0.1428±0.0010	6080±50	**6080±50**	1624±3
BCC6-109	710.1±1.5	694±4	1623±4	0.1496±0.0014	6310±60	**6310±60**	1652±4
BCC6-130	928.1±2.0	160.8±2.7	1582±4	0.1607±0.0016	6910±70	**6910±70**	1614±4
BCC6-149.5	985.8±1.5	299.0±1.3	1534.5±2.7	0.1683±0.0010	7390±50	**7390±50**	1567.1±2.8
BCC6-167	1178±2	3897±20	1493.1±1.7	0.1748±0.0007	7830±30	**7790±40**	1526.7±1.8

Table S2-2 Isotopic data for samples BCC2, 4, and 6.

Table S2. $\delta^{18}O_c$ time series. Gaps indicate depositional hiatuses.

Composite Record		BCC-2			BCC-4			BCC-6		
Age (yr BP)	$\delta^{18}O$	Age (yr BP)	$\delta^{18}O$	$\delta^{13}C$	Age (yr BP)	$\delta^{18}O$	$\delta^{13}C$	Age (yr BP)	$\delta^{18}O$	$\delta^{13}C$
37	-6.43	37	-6.28	-5.35	78	-6.18	-5.07	-24	-6.47	-5.70
97	-6.32	102	-6.24	-4.92	131	-6.09	-4.89	36	-6.47	-5.77
157	-6.19	167	-6.15	-4.86	184	-6.02	-4.92	96	-6.58	-5.86
217	-6.12	232	-5.96	-4.81	237	-6.24	-5.10	156	-6.36	-5.35
277	-6.15	297	-6.14	-5.09	290	-6.27	-4.93	216	-6.20	-5.34
337	-6.16	362	-6.06	-4.91	343	-6.34	-4.89	276	-6.08	-5.43
397	-6.13	427	-6.12	-4.74	397	-6.18	-4.99	336	-6.09	-5.79
457	-6.10	492	-6.04	-4.77	450	-6.10	-5.27	395	-6.05	-5.36
517	-6.01	558	-5.89	-4.75	503	-6.09	-5.01			
577	-5.95	623	-6.02	-4.90	556	-5.93	-4.58	1290	-6.08	-5.04
637	-6.02	688	-5.87	-4.87	609	-5.98	-4.53	1316	-6.02	-4.73
697	-6.00				662	-6.14	-4.87	1343	-6.15	-5.22
757	-6.13	835	-5.95	-4.97	715	-5.98	-4.64	1369	-6.12	-5.16
818	-6.07	880	-6.04	-4.82	768	-6.21	-4.84	1395	-6.08	-4.99
878	-6.05	925	-6.17	-5.12	821	-6.05	-4.80	1421	-6.09	-5.22
938	-6.10	969	-6.09	-4.95	874	-6.06	-4.63	1447	-6.16	-5.06
998	-6.16	1014	-6.06	-5.02	927	-6.04	-4.75	1473	-6.16	-5.25
1058	-6.21	1058	-6.09	-5.28	980	-6.18	-5.02	1499	-6.15	-5.25
1118	-6.21	1103	-6.15	-5.45	1033	-6.38	-5.28	1525	-6.01	-4.99
1178	-6.15	1147	-6.08	-5.29	1086	-6.26	-5.38	1551	-5.94	-5.14
1238	-6.13	1192	-6.07	-5.22	1140	-6.33	-5.52	1577	-5.88	-5.09
1298	-6.13	1238	-6.04	-5.50	1193	-6.17	-5.54	1603	-6.08	-5.49
1358	-6.05	1284	-6.14	-5.33	1246	-6.21	-5.56	1629	-6.10	-5.73
1418	-6.03	1331	-6.01	-5.36	1299	-6.18	-5.50	1656	-6.25	-5.59
1478	-6.03	1378	-5.87	-5.27	1352	-6.31	-5.41	1682	-6.08	-5.00
1538	-5.95	1424	-5.99	-5.47				1708	-6.10	-5.20
1599	-6.04	1471	-5.92	-5.53	2209	-6.09	-5.25	1733	-6.11	-5.09
1659	-6.14	1518	-5.88	-5.25	2226	-6.15	-5.52	1756	-5.93	-5.32
1719	-6.10	1564	-5.95	-5.49	2262	-6.01	-4.91	1780	-6.03	-5.14
1779	-6.00	1611	-6.14	-5.45	2316	-5.75	-5.01	1804	-6.07	-5.59
1839	-6.09	1658	-6.11	-5.50	2371	-5.68	-5.54	1828	-6.06	-5.19
1899	-6.15	1704	-6.15	-5.64	2425	-5.86	-5.93	1851	-6.11	-5.09
1959	-6.05	1751	-6.11	-5.63	2479	-5.97	-6.02	1875	-6.30	-5.29
2019	-6.00	1798	-5.88	-5.66	2534	-6.10	-5.56	1899	-6.10	-5.34
2079	-6.20	1844	-6.12	-5.87	2588	-6.01	-5.33	1922	-6.10	-5.67
2139	-6.20	1891	-6.13	-5.65	2630	-5.99	-5.39	1946	-6.15	-5.81
2199	-6.21	1938	-6.17	-5.64	2660	-6.15	-5.49	1970	-6.10	-5.40
2259	-6.07	1984	-5.87	-5.96	2690	-5.89	-5.47			
2319	-6.00	2031	-6.04	-6.07	2720	-5.93	-5.42	2600	-6.41	-5.63
2380	-5.93	2078	-6.26	-6.38	2750	-5.90	-5.42	2667	-6.17	-5.93
2440	-6.04	2124	-6.14	-6.51	2781	-6.04	-5.64	2734	-6.07	-5.65
2500	-6.11	2171	-6.26	-6.24	2811	-6.15	-5.55	2801	-6.24	-5.47
2560	-6.07	2205	-6.23	-6.36	2841	-6.08	-5.67	2868	-6.10	-5.54
2620	-6.09	2240	-6.10	-6.35	2871	-6.05	-5.74	2935	-6.03	-5.33

Composite Record		BCC-2			BCC-4			BCC-6		
Age (yr BP)	$\delta^{18}O$	Age (yr BP)	$\delta^{18}O$	$\delta^{13}C$	Age (yr BP)	$\delta^{18}O$	$\delta^{13}C$	Age (yr BP)	$\delta^{18}O$	$\delta^{13}C$
2680	-6.09	2274	-6.11	-6.05	2901	-6.03	-5.76	3002	-6.00	-5.97
2740	-6.06	2308	-6.33	-6.18	2931	-5.81	-5.87	3069	-6.04	-6.11
2800	-6.16	2343	-6.15	-6.50	2965	-5.94	-6.14	3136	-6.07	-5.66
2860	-6.13	2377	-6.11	-6.54	3002	-5.90	-6.21	3202	-5.88	-5.57
2920	-6.07	2412	-6.14	-6.07	3040	-6.05	-5.91	3269	-6.20	-5.83
2980	-6.05	2446	-6.22	-6.23	3077	-5.99	-5.59	3336	-5.97	-5.82
3040	-6.06	2480	-6.27	-6.13	3114	-5.95	-5.32	3403	-6.02	-5.82
3100	-6.04	2515	-6.11	-6.17	3152	-6.04	-5.26	3470	-6.08	-6.08
3161	-6.00	2549	-6.16	-6.13	3189	-5.90	-5.27	3537	-5.94	-6.12
3221	-6.11	2584	-5.96	-5.89	3227	-6.10	-5.35	3586	-6.20	-6.54
3281	-6.08	2618	-5.98	-5.91	3264	-6.03	-5.36	3617	-6.07	-6.66
3341	-6.04	2652	-6.09	-6.11	3302	-6.05	-5.56	3648	-6.10	-5.76
3401	-6.05	2687	-6.08	-5.98	3339	-6.18	-5.55	3679	-6.02	-4.89
3461	-6.08	2721	-6.20	-6.13	3377	-5.92	-5.57	3709	-6.00	-5.19
3521	-6.05	2755	-6.13	-5.78	3414	-6.02	-5.49	3740	-5.92	-5.27
3581	-6.10	2790	-6.17	-5.79	3452	-6.07	-5.65	3771	-5.99	-5.49
3641	-6.10	2824	-6.26	-5.99	3489	-6.22	-5.59	3802	-6.14	-5.65
3701	-6.02	2852	-6.20	-6.17	3526	-6.16	-5.21	3833	-5.99	-5.54
3761	-6.05	2872	-6.19	-6.17	3564	-6.03	-5.24	3864	-5.97	-5.43
3821	-6.11	2893	-6.11	-6.20	3595	-6.18	-5.41	3895	-6.03	-5.21
3881	-6.03	2913	-6.33	-6.16	3626	-6.05	-5.33	3917	-5.98	-5.18
3942	-5.95	2934	-6.11	-6.43	3658	-5.98	-5.17	3932	-5.98	-5.14
4002	-5.98	2954	-6.57	-6.45	3689	-6.09	-5.19	3946	-5.93	-5.20
4062	-5.97	2975	-6.08	-5.89	3720	-5.78	-5.44	3960	-5.97	-5.14
4122	-5.91	2995	-6.15	-5.87	3752	-6.00	-5.17	3975	-6.08	-5.10
4182	-5.89	3016	-6.24	-6.28	3783	-5.91	-4.85	3989	-6.09	-5.35
4242	-5.77	3036	-6.02	-6.18	3814	-5.92	-4.93	4003	-6.01	-5.55
4302	-5.72	3057	-6.21	-6.00	3845	-5.77	-5.22	4018	-5.99	-5.28
4362	-5.76	3077	-6.23	-6.01	3877	-5.84	-5.38	4032	-5.90	-5.16
4422	-5.81	3098	-6.06	-5.98	3908	-5.83	-5.16	4046	-5.84	-5.41
4482	-5.78	3118	-5.97	-5.88	3939	-5.94	-5.06	4061	-5.88	-5.80
4542	-5.71	3139	-6.02	-5.90	3970	-5.69	-5.34	4075	-5.86	-5.85
4602	-5.61	3159	-5.83	-5.78	4002	-5.91	-5.61	4089	-6.00	-5.93
4662	-5.64	3180	-6.13	-5.72	4033	-5.92	-5.42	4104	-5.97	-5.96
4723	-5.61	3200	-6.28	-6.19	4062	-5.89	-5.45	4118	-6.06	-5.87
4783	-5.63	3221	-6.67	-6.34	4088	-6.11	-5.47	4132	-5.82	-5.69
4843	-5.70	3241	-6.09	-6.29	4114	-5.77	-5.10	4147	-5.97	-5.67
4903	-5.69	3265	-6.12	-6.20	4140	-5.67	-5.31	4161	-5.89	-5.63
4963	-5.71	3289	-6.05	-6.07	4167	-5.74	-5.28	4175	-6.09	-5.79
5023	-5.76	3312	-5.96	-6.07	4193	-5.78	-5.18	4190	-5.92	-5.99
5083	-5.79	3336	-6.07	-6.21	4219	-5.91	-5.56	4204	-6.05	-5.66
5143	-5.73	3360	-5.99	-6.33	4245	-5.75	-5.55	4218	-6.06	-5.94
5203	-5.76	3384	-6.25	-6.20	4272	-6.07	-5.55	4233	-6.11	-6.06
5263	-5.73	3407	-6.11	-5.89	4298	-5.83	-6.23			
5323	-5.72	3431	-6.06	-6.00	4324	-5.87	-6.13	5235	-6.10	-6.16
5383	-5.80	3455	-6.05	-5.90	4350	-5.72	-6.13	5254	-5.76	-5.37
5443	-5.75	3479	-6.14	-5.95	4376	-5.75	-6.17	5273	-6.02	-5.34

Composite Record		BCC-2			BCC-4			BCC-6		
Age (yr BP)	$\delta^{18}O$	Age (yr BP)	$\delta^{18}O$	$\delta^{13}C$	Age (yr BP)	$\delta^{18}O$	$\delta^{13}C$	Age (yr BP)	$\delta^{18}O$	$\delta^{13}C$
5504	-5.79	3502	-6.03	-6.17	4426	-5.69	-5.77	5291	-5.70	-5.57
5564	-5.83	3526	-5.93	-5.86	4476	-5.65	-5.68	5310	-5.91	-5.58
5624	-5.74	3550	-6.03	-5.53	4526	-5.75	-5.64	5329	-5.89	-5.78
5684	-5.75	3574	-6.03	-5.51	4576	-5.62	-5.79	5348	-5.95	-6.06
5744	-5.80	3597	-6.14	-5.48	4626	-5.63	-5.93	5366	-5.86	-6.17
5804	-5.75	3621	-6.19	-5.76	4676	-5.59	-5.85	5385	-5.93	-6.32
5864	-5.57	3645	-6.14	-5.93	4726	-5.63	-5.66	5404	-5.80	-5.64
5924	-5.75	3669	-6.15	-5.65	4776	-5.62	-5.62	5423	-5.92	-5.59
5984	-5.78	3692	-6.14	-5.68	4826	-5.61	-5.78	5441	-5.73	-5.83
6044	-5.70	3716	-5.99	-5.80	4876	-5.55	-5.86	5460	-5.76	-5.98
6104	-5.76	3740	-6.23	-5.82	4917	-5.54	-5.90	5479	-5.75	-6.17
6164	-5.83	3764	-6.31	-5.85	4950	-5.66	-5.94	5498	-5.75	-5.71
6224	-5.88	3787	-6.17	-6.00	4983	-5.56	-5.85			
6285	-5.90	3811	-6.31	-5.93	5016	-5.67	-5.77	6033	-5.68	-5.96
6345	-5.88	3835	-6.50	-6.11	5048	-5.73	-5.72	6065	-5.72	-5.52
6405	-5.85	3858	-6.77	-6.16	5081	-5.81	-5.51	6097	-5.56	-5.52
6465	-5.87	3881	-5.95	-5.81	5114	-5.69	-5.42	6129	-5.73	-5.71
6525	-5.91	3903	-6.24	-6.01	5150	-5.68	-5.41	6161	-5.70	-5.46
6585	-5.92	3926	-6.02	-5.98	5189	-5.73	-5.33	6193	-5.74	-5.86
6645	-5.88	3949	-5.98	-5.92	5228	-5.78	-5.53	6226	-5.47	-5.62
6705	-5.89	3972	-5.95	-5.72	5266	-5.61	-5.35	6258	-5.64	-5.65
6765	-5.87	3994	-6.03	-6.02	5305	-5.53	-5.34	6290	-5.55	-5.42
6825	-5.92	4017	-6.19	-6.30	5344	-5.71	-5.57	6320	-5.65	-5.68
6885	-5.85	4040	-6.16	-6.16	5383	-5.70	-5.73	6349	-5.67	-5.50
6945	-5.76	4063	-5.88	-6.17	5422	-5.69	-5.85	6378	-5.56	-5.52
7005	-5.81	4085	-6.11	-6.06	5461	-5.64	-5.81	6407	-5.59	-5.54
7066	-5.84	4108	-5.94	-6.33	5500	-5.78	-5.83	6435	-5.59	-5.48
7126	-5.74	4131	-5.92	-6.26	5538	-5.83	-5.71	6464	-5.84	-5.52
7186	-5.68	4154	-5.99	-6.16	5577	-5.83	-5.81	6493	-5.89	-5.59
7246	-5.80	4176	-5.91	-6.35	5597	-5.77	-5.73	6522	-5.82	-5.45
7306	-5.73	4199	-5.97	-6.62	5616	-5.72	-5.80	6550	-5.91	-5.35
7366	-5.61	4224	-5.61	-6.11	5655	-5.80	-5.69	6579	-5.99	-5.12
7426	-5.76	4251	-5.48	-5.76	5694	-5.76	-5.46	6608	-5.91	-5.11
7486	-5.88	4278	-5.65	-5.61	5733	-5.75	-5.48	6637	-5.81	-4.79
7546	-5.86	4305	-5.40	-6.16	5772	-5.80	-5.57	6665	-5.95	-4.88
7606	-5.87	4333	-5.76	-5.93	5810	-5.77	-5.45	6694	-5.92	-4.93
7666	-5.83	4360	-5.66	-5.90	5849	-5.52	-5.57	6723	-5.86	-5.31
7726	-5.75	4387	-5.97	-5.78	5888	-5.61	-5.50	6752	-5.90	-5.25
7786	-5.67	4414	-5.77	-5.53	5927	-5.88	-5.66	6780	-5.93	-5.10
7847	-5.57	4441	-6.04	-5.11	5966	-5.77	-5.85	6809	-6.01	-5.29
		4468	-6.03	-5.48	6005	-5.57	-5.77	6838	-6.05	-5.24
		4496	-5.74	-5.61	6044	-5.60	-5.72	6867	-6.17	-5.03
		4523	-5.75	-6.05	6083	-5.86	-5.62	6895	-5.81	-4.93
		4554	-5.77	-6.18	6121	-5.76	-5.74	6922	-5.71	-4.67
		4589	-5.59	-5.50	6160	-5.78	-5.78	6947	-5.73	-4.42
		4624	-5.54	-5.49	6199	-5.73	-5.65	6971	-5.99	-4.60
		4659	-5.77	-6.26	6219	-5.87	-5.69	6996	-5.93	-4.70

Composite Record		BCC-2			BCC-4			BCC-6		
Age (yr BP)	$\delta^{18}O$	Age (yr BP)	$\delta^{18}O$	$\delta^{13}C$	Age (yr BP)	$\delta^{18}O$	$\delta^{13}C$	Age (yr BP)	$\delta^{18}O$	$\delta^{13}C$
		4694	-5.59	-5.99	6238	-6.02	-5.66	7020	-5.97	-4.68
		4729	-5.62	-6.17	6277	-6.02	-5.60	7045	-6.13	-4.79
		4764	-5.55	-5.98	6316	-5.89	-5.69	7069	-5.98	-4.76
		4799	-5.70	-5.87	6370	-5.80	-5.64	7094	-5.99	-4.65
		4834	-5.85	-5.61	6424	-5.77	-5.54	7119	-5.86	-4.39
		4869	-5.82	-5.61	6479	-5.78	-5.55	7143	-5.89	-4.62
		4904	-5.82	-5.77	6533	-5.87	-5.64	7168	-5.73	-4.74
		4939	-5.84	-6.02	6587	-5.75	-5.50	7192	-5.66	-4.42
		4974	-5.77	-5.84	6641	-5.79	-5.36	7217	-5.74	-4.36
		5017	-5.87	-6.06	6696	-5.80	-5.15	7241	-5.75	-4.34
		5067	-5.85	-5.69	6750	-5.73	-5.10	7266	-5.88	-4.29
		5117	-5.79	-5.41	6804	-6.00	-5.27	7291	-5.88	-4.10
		5168	-5.75	-5.50	6859	-5.80	-5.46	7315	-5.62	-3.86
		5218	-5.77	-5.53	6913	-5.75	-5.45	7340	-5.55	-3.94
		5268	-5.68	-5.46	6967	-5.66	-5.22	7364	-5.68	-4.17
		5319	-5.58	-5.26	7021	-5.64	-4.91	7389	-5.62	-4.25
		5369	-5.86	-5.52	7076	-5.69	-4.75	7412	-5.58	-3.75
		5419	-5.79	-5.56	7130	-5.58	-4.75	7435	-5.88	-4.11
		5470	-5.79	-5.63	7184	-5.59	-4.54	7458	-5.93	-4.02
		5520	-5.84	-5.62				7481	-5.81	-4.27
		5570	-5.88	-5.56				7503	-5.89	-4.22
		5621	-5.68	-5.41				7526	-5.93	-4.16
		5671	-5.69	-5.25				7549	-5.85	-4.06
		5721	-5.83	-5.35				7572	-5.78	-3.84
		5758	-5.78	-5.45				7595	-5.88	-3.67
		5781	-5.91	-5.17				7618	-5.85	-3.75
		5804	-5.85	-5.55				7641	-5.98	-3.96
		5827	-5.57	-5.45				7664	-5.87	-4.07
		5850	-5.51	-5.78				7687	-5.67	-3.86
		5873	-5.55	-5.79				7710	-5.75	-3.77
		5896	-5.69	-5.75				7733	-5.80	-3.71
		5919	-5.52	-5.65				7756	-5.73	-3.55
		5943	-5.87	-5.67				7779	-5.64	-2.91
		5966	-5.92	-5.92				7802	-5.66	-2.68
		5989	-5.82	-5.79				7825	-5.63	-2.46
		6012	-5.88	-5.81				7848	-5.53	-2.08
		6035	-5.78	-5.76						
		6058	-5.70	-5.77						
		6081	-5.68	-5.73						
		6104	-5.84	-5.77						
		6127	-5.93	-5.78						
		6150	-6.00	-5.48						
		6173	-5.98	-5.47						
		6197	-6.09	-5.38						
		6228	-6.22	-5.39						
		6268	-6.14	-5.37						
		6308	-6.08	-5.33						

Composite Record		BCC-2			BCC-4			BCC-6		
Age (yr BP)	$\delta^{18}O$	Age (yr BP)	$\delta^{18}O$	$\delta^{13}C$	Age (yr BP)	$\delta^{18}O$	$\delta^{13}C$	Age (yr BP)	$\delta^{18}O$	$\delta^{13}C$
		6348	-6.17	-5.08						
		6387	-6.20	-5.14						
		6427	-6.20	-5.12						
		6467	-5.98	-5.21						
		6507	-6.06	-5.22						
		6547	-5.94	-5.08						
		6587	-6.14	-5.06						
		6627	-5.91	-5.14						
		6666	-5.99	-5.02						
		6706	-5.99	-4.88						
		6746	-5.95	-5.05						
		6786	-5.80	-5.01						
		6826	-5.80	-5.06						
		6866	-5.81	-5.02						
		6906	-5.86	-4.83						
		6945	-5.71	-4.61						

Appendix 2: Supplemental Materials for Chapter 3

Figure S3-1 Images of samples BCC9 and 10.

Supplemental Figure 1. Samples BCC9 (left) and BCC10 (right) after cutting along the growth axis and polishing.

Figure S3-2 Photo of samples BCC9 and 10 prior to collection.

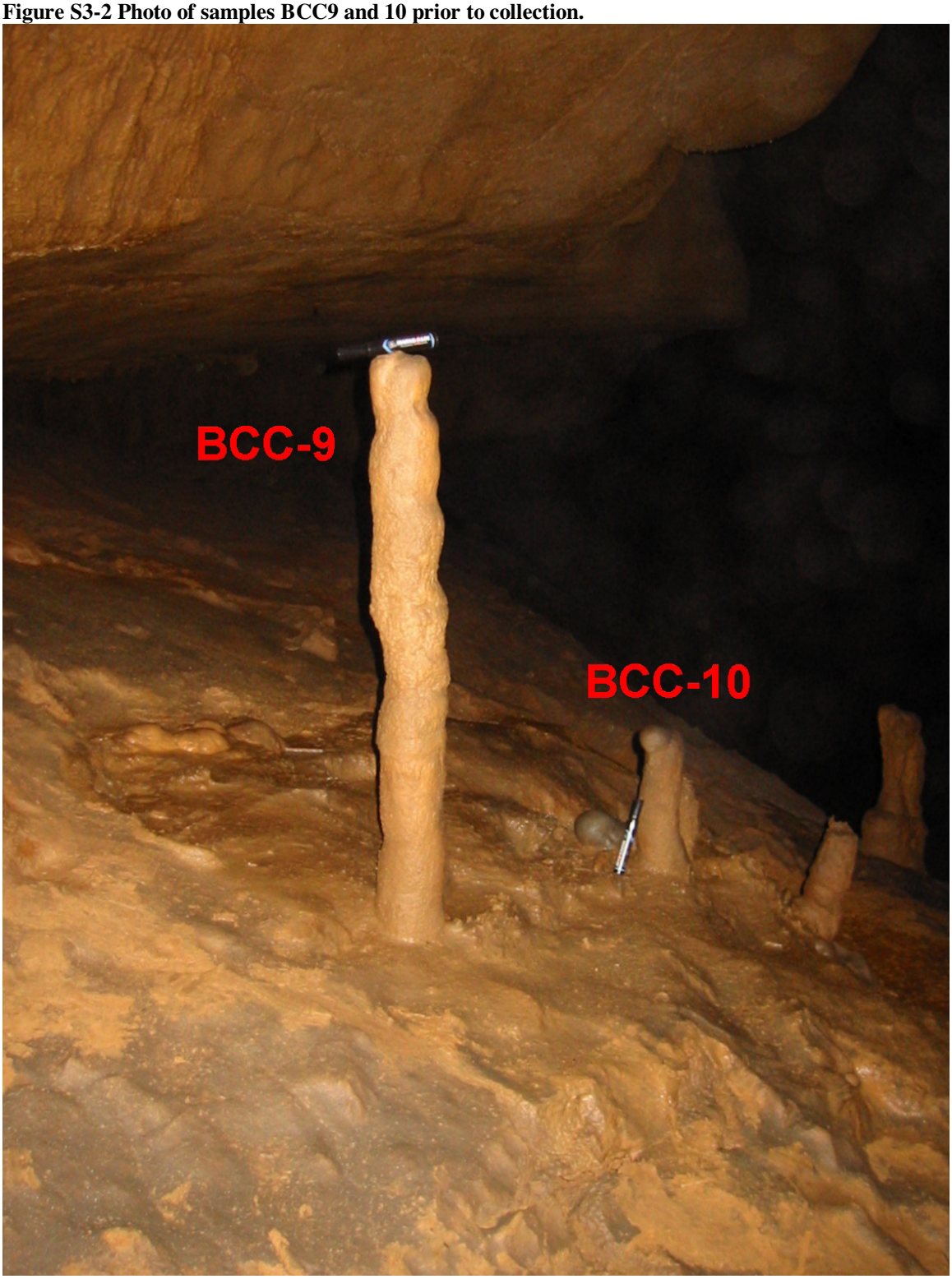

Supplemental Figure 2. BCC9 and BCC10 in situ (as labeled).

Table S3-1 U/Th data table and 230Th ages for sample BCC9.

Supplemental Table 1. ^{230}Th dating results for sample BCC9. Quoted errors are 2σ.

Depth (mm)	^{238}U (ppb)		^{232}Th (ppt)		^{230}Th / ^{232}Th (atomic x10^{-6})		δ^{234}U* (measured)		^{230}Th / ^{238}U (activity)		^{230}Th Age (yr BP) (uncorrected)		$\delta^{234}U_{Initial}$** (corrected)		^{230}Th Age (kyr BP)*** (corrected)	
9.5	2516.6	±0.6	1056	±2	52300	±110	685.28	±0.27	1.33130	±0.0005	144980	±110	1031.9	±0.5	144.97	±0.11
41	2029.0	±0.5	121	±2	429000	±9000	895.57	±0.24	1.55600	±0.0005	152560	±100	1377.7	±0.5	152.56	±0.10
69	1748.9	±1.7	888	±18	51300	±1000	894.7	±2.0	1.57870	±0.0023	157000	±600	1394.0	±4	157.0	±0.6
87.5	1725.5	±0.4	164	±2	276000	±4000	891.7	±0.3	1.59500	±0.0006	160720	±130	1403.6	±0.7	160.72	±0.13
109	1978.5	±0.5	72	±2	720000	±20000	859.57	±0.19	1.58720	±0.0013	165230	±280	1370.4	±1.1	165.23	±0.28
144	1550.0	±0.4	818	±2	50380	±120	839.23	±0.23	1.61170	±0.0005	174820	±120	1374.7	±0.6	174.81	±0.12
157.5	1588.5	±1.6	1360	±27	31000	±600	822.6	±2.0	1.61020	±0.0024	178300	±700	1361.0	±4	178.3	±0.7
181.75	1647.4	±1.7	171	±3	259000	±5000	817.2	±2.0	1.63010	±0.0024	184400	±800	1375.0	±5	184.4	±0.8
202	1702.9	±1.8	261	±5	176000	±4000	806.0	±2.0	1.63100	±0.0024	187500	±800	1368.0	±5	187.5	±0.8
228	1274.3	±0.4	2003	±2	17045	±19	778.5	±0.4	1.62500	±0.0003	193220	±140	1343.2	±0.9	193.20	±0.14
243.5	1113.36	±0.28	476	±2	62520	±260	752.78	±0.24	1.62030	±0.0015	199400	±400	1321.6	±1.7	199.4	±0.4
271.5	1048.7	±0.3	468	±2	59420	±240	716.27	±0.22	1.60980	±0.0011	207900	±400	1288.1	±1.4	207.9	±0.4
298	1117.9	±1.1	752	±15	39600	±800	692.9	±1.9	1.61510	±0.0022	218100	±1100	1282.0	±5	218.1	±1.1
301.25	1214.9	±1.4	219	±5	147000	±3000	663.4	±1.9	1.60470	±0.0024	226400	±1300	1257.0	±6	226.4	±1.3
308	1682.5	±1.7	3460	±70	12920	±260	663.4	±1.9	1.61210	±0.0023	229000	±1300	1266.0	±6	229.0	±1.3
320.5	1587.8	±1.7	1180	±24	35700	±700	638.5	±2.0	1.61080	±0.0024	240000	±1500	1257.0	±7	240.0	±1.5
325.5	1280.5	±1.4	2820	±60	11980	±240	624.0	±1.9	1.59820	±0.0024	241700	±1500	1234.0	±6	241.7	±1.5
334	1042.6	±1.2	673	±14	41470	±840	640.0	±1.90	1.62400	±0.0024	245160	±1500	1278.0	±7	245.2	±1.5
370	2050.6	±0.4	240	±3	223000	±2900	595.51	±0.24	1.58530	±0.0004	250900	±240	1209.1	±1.0	250.90	±0.24
387	3222.0	±0.6	76	±3	1110000	±50000	592.15	±0.20	1.58510	±0.0004	252740	±220	1208.6	±0.9	252.74	±0.22
416.75	3846.2	±0.7	95	±3	1060000	±40000	579.85	±0.24	1.57520	±0.0003	254950	±220	1190.8	±0.9	254.95	±0.22
470	3262.2	±0.5	220	±3	388000	±6000	583.58	±0.26	1.58520	±0.0004	257920	±250	1208.6	±1.0	257.92	±0.25
485	3242.6	±0.5	92	±3	920000	±30000	582.51	±0.22	1.58650	±0.0004	259270	±270	1211.0	±1.0	259.26	±0.27
525	2922.2	±0.5	178	±4	433000	±9000	585.21	±0.28	1.59490	±0.0010	262100	±500	1226.3	±2.0	262.1	±0.5
575	2769.5	±0.5	576	±4	126100	±800	575.29	±0.22	1.59050	±0.0012	266100	±700	1219.1	±2.4	266.1	±0.7
615	2618.9	±0.4	311	±3	223000	±1900	581.03	±0.22	1.60600	±0.0004	271100	±290	1248.9	±1.1	271.09	±0.29

Depth (mm)	^{238}U (ppb)		^{232}Th (ppt)		$^{230}Th / ^{232}Th$ (atomic x10^{-6})		$\delta^{234}U$* (measured)		$^{230}Th / ^{238}U$ (activity)		^{230}Th Age (yr BP) (uncorrected)		$\delta^{234}U_{Initial}$** (corrected)		^{230}Th Age (kyr BP)*** (corrected)	
644.75	2535.9	±0.5	201	±3	331000	±5000	561.93	±0.26	1.58880	±0.0005	274300	±400	1218.9	±1.4	274.3	±0.4
674.5	1529.3	±0.4	1794	±3	22310	±40	554.2	±0.3	1.58670	±0.0007	278800	±500	1217.3	±1.8	278.8	±0.5
709.5	1217.09	±0.25	1583	±2	19870	±30	526.49	±0.29	1.56720	±0.0009	288100	±700	1187.1	±2.3	288.0	±0.7
740	1791.6	±0.3	1046	±2	43970	±90	510.57	±0.24	1.55640	±0.0010	294200	±800	1171.5	±2.6	294.2	±0.8
765.75	892.5	±0.8	10200	±200	2190	±40	461.3	±1.7	1.51250	±0.0020	308000	±3000	1099.0	±9	308	±3
791.5	952.2	±1.1	111000	±2000	206	±4	395.3	±1.6	1.44840	±0.0025	326000	±3000	986.4	±10	324	±4

$\lambda_{230} = 9.17052 \times 10^{-6}\ y^{-1}$, $\lambda_{234} = 2.82206 \times 10^{-6}\ y^{-1}$, $\lambda_{238} = 1.55125 \times 10^{-10}\ y^{-1}$.
*$\delta^{234}U = ([^{234}U/^{238}U]activity - 1) \times 1000$. ** $\delta^{234}U_{initial}$ was calculated based on ^{230}Th age (T), i.e., $\delta^{234}Uinitial = \delta^{234}U_{measured} \times e^{\lambda 234 \times T}$.
Corrected ^{230}Th ages assume the initial $^{230}Th/^{232}Th$ atomic ratio of $4.4 \pm 2.2 \times 10^{-6}$. Those are the values for a material at secular equilibrium, with the bulk earth $^{232}Th/^{238}U$ value of 3.8. The errors are arbitrarily assumed to be 50%.
***B.P. stands for "Before Present" where the "Present" is defined as the year 1950 A.D

Table S3-2 U/Th data table and 230Th ages for sample BCC10.

Supplemental Table 2. ^{230}Th dating results for sample BCC10. Quoted errors are 2σ.

Depth (mm)	2nd transect depth	^{238}U (ppb)		^{232}Th (ppt)		^{230}Th / ^{232}Th (atomic x10^{-6})		δ^{234}U* (measured)		^{230}Th / ^{238}U (activity)		^{230}Th Age (yr BP) (uncorrected)		$\delta^{234}U_{Initial}$** (corrected)		^{230}Th Age (kyr BP)*** (corrected)	
1.25		1264.6	±1.4	2167	±40.0	7590	±150	1350.1	±2.8	0.7892	±0.0013	42780	±100	1523	±3.0	42.76	±0.10
12.5		1694.4	±2.1	282	±7	93600	±2400	1410.6	±2.4	0.9448	±0.0017	51450	±130	1631	±3	51.45	±0.13
24		1544.6	±2.0	357	±9	70600	±1700	1379.8	±2.5	0.9906	±0.0019	55430	±150	1614	±3.0	55.42	±0.15
31.5		1931.5	±2.4	190	±6	170000	±5000	1366.8	±2.2	1.0140	±0.0018	57470	±140	1608	±2.7	57.47	±0.14
41.25		2004.8	±2.4	468	±10.0	75000	±1600	1387.1	±2.2	1.0612	±0.0018	60180	±150	1644	±2.7	60.18	±0.15
50		2127.0	±2.3	268	±7.0	141000	±3000	1348.3	±1.8	1.0774	±0.0017	62680	±140	1609	±2.3	62.68	±0.14
58.25		2051.8	±2.4	509	±10.0	72300	±1500	1309.8	±2.7	1.0880	±0.0018	64860	±170	1573	±3.0	64.85	±0.17
68		1877.3	±2.0	128	±2.6	269000	±6000	1318.7	±2.4	1.1170	±0.0017	66810	±160	1593	±3.0	66.81	±0.16
75		1745.9	±1.9	137	±5.0	240000	±8000	1322.9	±1.9	1.1450	±0.0018	68800	±160	1607	±2.4	68.80	±0.16
82		1627.0	±1.9	190	±6.0	164000	±5000	1304.3	±2.2	1.1600	±0.0019	70790	±180	1593	±2.8	70.79	±0.18
91.25		1647.5	±1.9	449	±10.0	71200	±1600	1271.9	±1.9	1.1765	±0.0019	73530	±180	1565	±2.5	73.53	±0.18
103		1154.4	±1.4	712	±15.0	32300	±700	1232.5	±2.2	1.2093	±0.0021	78200	±220	1537	±2.8	78.20	±0.22
112.25		1265.0	±1.4	390	±9.0	66300	±1500	1218.3	±1.8	1.2390	±0.0020	81600	±210	1534	±2.5	81.60	±0.21
125.25		1360.4	±1.7	337	±8.0	85200	±2000	1172.3	±2.2	1.2800	±0.0023	88040	±260	1503	±3.0	88.04	±0.26
130.25		1123.7	±1.2	351	±7.0	67800	±1400	1140.7	±2.3	1.2830	±0.0019	90310	±240	1472	±3.0	90.31	±0.24
137.5		734.3	±0.8	1499	±30.0	10440	±210	1069.8	±2.1	1.2920	±0.0021	96140	±270	1403	±2.9	96.12	±0.27
142.75		977.8	±1.2	677	±14.0	31000	±700	1057.3	±2.3	1.3020	±0.0024	98100	±300	1395	±3.0	98.1	±0.3
146		864.0	±1.0	878	±18.0	21300	±400	1046.6	±1.8	1.3120	±0.0021	100020	±280	1388	±2.7	100.01	±0.28
158		937.7	±1.0	394	±9.0	52000	±1200	998.9	±1.7	1.3250	±0.0022	105500	±300	1346	±2.6	105.5	±0.3
171		684.6	±0.8	1474	±30.0	10510	±210	1009.2	±2.0	1.3732	±0.0023	110600	±300	1379	±3.0	110.6	±0.3
181.75		990.2	±1.2	488	±9.8	47200	±900	1009.8	±2.3	1.4092	±0.0023	115200	±400	1398	±4.0	115.2	±0.4
188.25		756.4	±0.8	895	±19.0	19500	±400	978.1	±1.8	1.4012	±0.0023	117300	±400	1362	±2.9	117.3	±0.4
195		853.2	±0.9	1389	±28.0	14270	±290	956.0	±2.2	1.4085	±0.0023	120600	±400	1344	±3.0	120.600	±400
201	1.0	928.1	±1.0	893	±18.0	24800	±500	985.2	±2.2	1.4456	±0.0024	122600	±400	1393	±4.0	122.600	±400
207.5	4.5	861.2	±1.0	1697	±30	12260	±250	984.5	±2.2	1.4649	±0.0023	125500	±400	1403	±4.0	125.400	±400

$\lambda_{230} = 9.17052 \times 10^{-6}\ y^{-1}$, $\lambda_{234} = 2.82206 \times 10^{-6}\ y^{-1}$, $\lambda_{238} = 1.55125 \times 10^{-10}\ y^{-1}$.
*$\delta^{234}U = ([^{234}U/^{238}U]activity - 1) \times 1000$. ** $\delta^{234}U_{initial}$ was calculated based on ^{230}Th age (T), i.e., $\delta^{234}Uinitial = \delta^{234}U_{measured} \times e^{\lambda 234 \times T}$.
Corrected ^{230}Th ages assume the initial $^{230}Th/^{232}Th$ atomic ratio of $4.4 \pm 2.2 \times 10^{-6}$. Those are the values for a material at secular equilibrium, with the bulk earth $^{232}Th/^{238}U$ value of 3.8. The errors are arbitrarily assumed to be 50%.
***B.P. stands for "Before Present" where the "Present" is defined as the year 1950 A.D

Table S3-3 Isotopic data for samples BCC9 and 10.

Supplemental Table 3. Stable Isotope Data by depth and Age.

BCC9				BCC10			
Depth (mm)	**Age (yr BP)**	**$\delta^{18}O$**	**$\delta^{13}C$**	**Depth (mm)**	**Age (yr BP)**	**$\delta^{18}O$**	**$\delta^{13}C$**
0.5	141557	-5.31	1.26	0.25	41604	-5.01	0.18
1.5	141973	-5.23	1.55	0.75	42188	-5.27	0.62
2.5	142379	-5.27	1.12	1.25	42755	-5.24	0.77
3.5	142776	-5.51	0.09	1.75	43303	-5.39	1.06
4.5	143164	-5.71	-0.26	2.25	43834	-5.02	0.37
5.5	143543	-5.77	-0.05	2.75	44347	-4.97	0.19
6.5	143913	-5.94	0.29	3.25	44844	-4.97	0.09
7.5	144274	-5.80	0.49	3.75	45324	-5.01	0.33
8.5	144627	-5.63	0.83	4.25	45788	-5.09	1.13
9.5	144972	-5.50	0.71	4.75	46237	-4.88	1.22
10.5	145309	-5.47	0.97	5.25	46670	-5.21	0.07
11.5	145637	-5.57	0.89	5.75	47088	-5.34	-0.74
12.5	145958	-5.53	0.49	6.25	47491	-5.30	-0.84
13.5	146272	-5.76	0.00	6.75	47880	-5.46	-0.96
14.5	146578	-5.79	-0.26	7.25	48255	-5.35	-0.95
15.5	146876	-5.67	-0.49	7.75	48617	-5.34	-1.01
16.5	147168	-5.79	-0.59	8.25	48965	-5.38	-1.06
17.5	147452	-5.88	-0.60	8.75	49301	-5.26	-1.06
18.5	147730	-5.80	-0.48	9.25	49624	-5.28	-0.99
19.5	148002	-5.72	-0.28	9.75	49936	-5.30	-0.98
20.5	148266	-5.55	0.17	10.25	50235	-5.44	-1.09
21.5	148525	-5.70	-0.64	10.75	50523	-5.22	-1.04
22.5	148778	-5.91	-0.99	11.25	50801	-5.30	-1.08
23.5	149024	-5.87	-1.12	11.75	51068	-5.32	-1.04
24.5	149265	-5.76	-1.04	12.25	51324	-5.26	-0.92
25.5	149500	-5.73	-0.91	12.75	51571	-5.30	-0.83
26.5	149730	-5.92	-1.12	13.25	51808	-5.20	-0.84
27.5	149955	-5.87	-1.15	13.75	52037	-5.09	-0.81
28.5	150175	-5.74	-1.18	14.25	52256	-5.32	-0.88
29.5	150389	-5.75	-0.94	14.75	52468	-5.28	-0.89
30.5	150599	-5.77	-0.90	15.25	52672	-5.50	-0.94
31.5	150805	-5.82	-0.96	15.75	52868	-5.58	-0.80
32.5	151006	-5.85	-1.20	16.25	53058	-5.53	-0.89
33.5	151203	-5.82	-1.06	16.75	53241	-5.45	-0.94
34.5	151395	-5.83	-1.16	17.25	53418	-5.58	-0.97
35.5	151584	-5.77	-1.02	17.75	53589	-5.81	-1.03
36.5	151770	-5.69	-0.92	18.25	53755	-5.71	-0.86
37.5	151951	-5.77	-1.03	18.75	53916	-5.84	-0.66
38.5	152129	-5.74	-1.03	19.25	54073	-5.83	-0.54
39.5	152304	-5.89	-1.02	19.75	54226	-5.99	-0.49
40.5	152477	-5.85	-1.13	20.25	54375	-5.33	-0.72
41.5	152646	-5.92	-1.34	20.75	54521	-5.81	-0.91

BCC9				BCC10			
Depth (mm)	**Age (yr BP)**	**$\delta^{18}O$**	**$\delta^{13}C$**	**Depth (mm)**	**Age (yr BP)**	**$\delta^{18}O$**	**$\delta^{13}C$**
42.5	152812	-5.95	-1.15	21.25	54665	-5.77	-0.85
43.5	152976	-5.81	-1.13	21.75	54806	-5.66	-0.88
44.5	153138	-5.75	-1.08	22.25	54945	-5.69	-0.92
45.5	153298	-5.78	-1.09	22.75	55083	-5.74	-1.04
46.5	153456	-6.05	-1.00	23.25	55219	-5.80	-1.14
47.5	153612	-5.92	-0.98	23.75	55355	-5.70	-1.06
48.5	153768	-5.85	-0.89	24.25	55491	-5.51	-0.84
49.5	153922	-5.91	-1.12	24.75	55627	-5.52	-0.68
50.5	154075	-5.94	-1.08	25.25	55763	-5.66	-0.51
51.5	154228	-6.06	-1.11	25.75	55898	-5.49	-0.50
52.5	154380	-5.99	-1.01	26.25	56034	-5.72	-0.41
53.5	154532	-6.02	-1.12	26.75	56170	-5.29	-0.24
54.5	154684	-6.09	-1.16	27.25	56306	-5.41	-0.28
55.5	154837	-6.12	-1.15	27.75	56442	-5.53	-0.40
56.5	154990	-6.16	-1.14	28.25	56578	-5.61	-1.32
57.5	155144	-6.03	-1.11	28.75	56714	-5.47	-1.53
58.5	155298	-6.20	-1.18	29.25	56851	-5.61	-1.62
59.5	155454	-6.17	-1.14	29.75	56987	-5.76	-1.67
60.5	155612	-6.09	-1.14	30.25	57124	-5.53	-1.61
61.5	155771	-6.19	-1.07	30.75	57260	-5.74	-1.66
62.5	155932	-6.15	-1.13	31.25	57397	-5.72	-1.76
63.5	156095	-6.07	-1.15	31.75	57534	-5.82	-1.67
64.5	156260	-6.38	-1.15	32.25	57671	-5.74	-1.67
65.5	156428	-6.29	-1.14	32.75	57809	-5.83	-1.71
66.5	156599	-6.30	-1.26	33.25	57946	-5.56	-1.57
67.5	156772	-6.39	-1.27	33.75	58084	-5.37	-1.63
68.5	156949	-6.41	-1.26	34.25	58222	-5.71	-1.72
69.5	157130	-6.41	-1.36	34.75	58360	-5.78	-1.59
70.5	157314	-6.30	-1.36	35.25	58498	-5.66	-1.55
71.5	157501	-6.53	-1.61	35.75	58637	-5.75	-1.57
72.5	157691	-6.39	-1.76	36.25	58776	-5.70	-1.51
73.5	157884	-6.35	-1.81	36.75	58915	-5.74	-1.57
74.5	158079	-6.27	-1.62	37.25	59054	-5.57	-1.53
75.5	158276	-6.20	-1.65	37.75	59193	-5.70	-1.29
76.5	158475	-6.13	-1.83	38.25	59333	-5.84	-1.40
77.5	158676	-6.16	-1.89	38.75	59473	-5.57	-1.41
78.5	158878	-6.21	-1.98	39.25	59614	-5.74	-1.33
79.5	159081	-6.16	-2.04	39.75	59754	-5.69	-1.20
80.5	159286	-6.13	-1.94	40.25	59895	-5.82	-1.20
81.5	159490	-6.29	-2.07	40.75	60036	-5.98	-1.17
82.5	159695	-6.13	-2.07	41.25	60178	-5.82	-1.22
83.5	159900	-6.21	-2.36	41.75	60319	-5.85	-1.29
84.5	160105	-6.13	-2.45	42.25	60461	-5.71	-1.39
85.5	160309	-6.27	-2.47	42.75	60604	-5.80	-1.52
86.5	160513	-6.25	-2.28	43.25	60746	-5.75	-1.43
87.5	160716	-6.11	-2.15	43.75	60889	-5.74	-1.25

BCC9				BCC10			
Depth (mm)	**Age (yr BP)**	**$\delta^{18}O$**	**$\delta^{13}C$**	**Depth (mm)**	**Age (yr BP)**	**$\delta^{18}O$**	**$\delta^{13}C$**
88.5	160917	-6.20	-1.96	44.25	61032	-5.55	-1.07
89.5	161118	-6.12	-2.10	44.75	61175	-5.79	-1.09
90.5	161317	-6.32	-2.08	45.25	61318	-5.72	-1.16
91.5	161517	-6.27	-2.22	45.75	61462	-5.69	-1.07
92.5	161716	-6.31	-2.18	46.25	61605	-5.63	-1.03
93.5	161915	-6.22	-2.45	46.75	61748	-5.78	-1.09
94.5	162115	-6.12	-2.67	47.25	61892	-5.55	-0.99
95.5	162315	-6.02	-2.42	47.75	62035	-5.59	-0.96
96.5	162516	-6.29	-2.47	48.25	62179	-5.63	-0.94
97.5	162718	-6.42	-2.36	48.75	62322	-5.60	-1.01
98.5	162922	-6.20	-2.52	49.25	62466	-5.57	-0.92
99.5	163128	-6.21	-2.61	49.75	62609	-5.53	-0.86
100.5	163336	-6.13	-2.66	50.25	62752	-5.57	-0.99
101.5	163546	-6.02	-2.71	50.75	62896	-5.59	-1.04
102.5	163758	-6.04	-2.49	51.25	63038	-5.72	-1.07
103.5	163974	-5.95	-2.31	51.75	63180	-5.69	-0.98
104.5	164192	-5.98	-2.53	52.25	63321	-5.59	-0.95
105.5	164414	-6.01	-2.46	52.75	63461	-5.86	-0.89
106.5	164640	-5.98	-2.39	53.25	63599	-5.79	-0.99
107.5	164869	-5.99	-2.30	53.75	63736	-5.84	-1.01
108.5	165103	-6.01	-2.17	54.25	63871	-5.89	-0.96
109.5	165341	-6.09	-2.26	54.75	64003	-5.62	-0.96
110.5	165584	-6.17	-2.24	55.25	64134	-5.68	-1.21
111.5	165831	-6.15	-2.44	55.75	64262	-5.84	-1.36
112.5	166082	-6.07	-2.48	56.25	64387	-5.64	-1.14
113.5	166338	-5.82	-2.42	56.75	64509	-5.54	-1.21
114.5	166596	-5.93	-2.42	57.25	64628	-5.69	-1.38
115.5	166858	-5.89	-2.51	57.75	64743	-5.89	-1.48
116.5	167123	-5.84	-2.42	58.25	64855	-5.67	-1.40
117.5	167392	-5.87	-2.42	58.75	64963	-5.73	-1.33
118.5	167663	-5.99	-2.68	59.25	65067	-5.68	-1.42
119.5	167936	-5.91	-2.85	59.75	65168	-5.76	-1.26
120.5	168212	-5.73	-2.59	60.25	65267	-5.87	-1.11
121.5	168490	-5.93	-2.56	60.75	65363	-5.77	-1.24
122.5	168770	-5.84	-2.59	61.25	65458	-5.69	-1.34
123.5	169051	-5.73	-2.81	61.75	65552	-5.35	-1.40
124.5	169334	-5.45	-2.23	62.25	65645	-5.39	-1.47
125.5	169618	-5.38	-1.61	62.75	65738	-5.59	-1.50
126.5	169902	-5.53	-2.09	63.25	65831	-5.64	-1.47
127.5	170188	-5.61	-2.46	63.75	65925	-5.58	-1.39
128.5	170474	-5.53	-2.32	64.25	66020	-5.53	-1.22
129.5	170761	-5.57	-2.36	64.75	66116	-5.61	-1.01
130.5	171047	-5.65	-2.30	65.25	66214	-5.49	-0.89
131.5	171334	-5.70	-2.04	65.75	66316	-5.66	-0.97
132.5	171620	-5.67	-1.96	66.25	66420	-5.41	-0.96
133.5	171905	-5.58	-1.97	66.75	66527	-5.44	-0.95

BCC9				BCC10			
Depth (mm)	**Age (yr BP)**	**$\delta^{18}O$**	**$\delta^{13}C$**	**Depth (mm)**	**Age (yr BP)**	**$\delta^{18}O$**	**$\delta^{13}C$**
134.5	172189	-5.63	-2.10	67.25	66639	-5.43	-1.00
135.5	172473	-5.67	-1.99	67.75	66754	-5.54	-1.03
136.5	172755	-5.76	-2.03	68.25	66875	-5.39	-1.04
137.5	173036	-5.81	-1.98	68.75	67001	-5.30	-1.00
138.5	173315	-5.71	-1.80	69.25	67130	-5.31	-1.03
139.5	173592	-5.87	-1.73	69.75	67264	-5.54	-1.11
140.5	173867	-5.92	-1.58	70.25	67402	-5.53	-1.14
141.5	174140	-5.94	-2.12	70.75	67542	-5.37	-1.14
142.5	174410	-5.83	-2.01	71.25	67686	-5.38	-1.21
143.5	174677	-5.41	-1.97	71.75	67831	-5.29	-1.27
144.5	174941	-5.60	-2.13	72.25	67978	-5.22	-1.20
145.5	175202	-5.93	-2.19	72.75	68127	-5.31	-1.26
146.5	175461	-5.91	-2.18	73.25	68276	-5.18	-1.44
147.5	175718	-5.93	-2.04	73.75	68426	-5.33	-1.52
148.5	175973	-6.04	-1.99	74.25	68576	-5.38	-1.75
149.5	176227	-6.03	-1.98	74.75	68726	-5.64	-1.77
150.5	176480	-5.99	-1.87	75.25	68874	-5.47	-1.64
151.5	176734	-6.14	-1.97	75.75	69022	-5.25	-1.74
152.5	176987	-6.21	-1.93	76.25	69169	-5.41	-1.86
153.5	177241	-6.25	-1.80	76.75	69314	-5.16	-1.78
154.5	177497	-6.17	-1.79	77.25	69459	-5.23	-1.94
155.5	177754	-6.14	-1.85	77.75	69602	-5.26	-2.07
156.5	178013	-6.13	-1.79	78.25	69745	-5.24	-2.08
157.5	178274	-6.21	-1.82	78.75	69887	-5.18	-1.96
158.5	178539	-6.16	-2.01	79.25	70028	-5.14	-1.79
159.5	178806	-6.20	-1.99	79.75	70169	-5.08	-1.90
160.5	179075	-6.21	-1.91	80.25	70308	-5.21	-2.11
161.5	179346	-6.08	-1.92	80.75	70447	-5.32	-2.18
162.5	179617	-6.17	-1.96	81.25	70585	-5.45	-2.36
163.5	179890	-6.17	-1.82	81.75	70722	-5.45	-2.26
164.5	180162	-6.17	-1.85	82.25	70859	-5.16	-2.24
165.5	180435	-6.46	-1.93	82.75	70996	-5.14	-2.50
166.5	180707	-6.41	-1.91	83.25	71132	-5.08	-2.55
167.5	180977	-6.44	-2.08	83.75	71268	-5.03	-2.70
168.5	181246	-6.36	-2.19	84.25	71405	-5.10	-2.67
169.5	181513	-6.62	-2.12	84.75	71542	-5.10	-2.63
170.5	181777	-6.44	-2.03	85.25	71681	-5.16	-2.69
171.5	182038	-6.70	-1.97	85.75	71820	-4.95	-2.47
172.5	182296	-6.55	-1.98	86.25	71962	-4.96	-2.29
173.5	182550	-6.57	-2.02	86.75	72105	-4.97	-2.28
174.5	182799	-6.63	-1.98	87.25	72251	-4.90	-2.20
175.5	183043	-6.52	-2.05	87.75	72399	-4.84	-2.21
176.5	183282	-6.68	-2.12	88.25	72550	-4.83	-2.27
177.5	183515	-6.68	-2.01	88.75	72704	-4.93	-2.34
178.5	183742	-6.70	-1.96	89.25	72861	-5.16	-2.60
179.5	183962	-6.67	-1.94	89.75	73022	-5.15	-2.97

BCC9				BCC10			
Depth (mm)	**Age (yr BP)**	**$\delta^{18}O$**	**$\delta^{13}C$**	**Depth (mm)**	**Age (yr BP)**	**$\delta^{18}O$**	**$\delta^{13}C$**
180.5	184175	-6.76	-1.72	90.25	73188	-5.08	-2.87
181.5	184381	-6.62	-1.94	90.75	73357	-5.19	-2.97
182.5	184578	-6.58	-1.75	91.25	73531	-5.36	-3.01
183.5	184767	-6.49	-1.78	91.75	73710	-5.46	-2.72
184.5	184949	-6.49	-1.86	92.25	73893	-5.16	-3.22
185.5	185124	-6.56	-2.05	92.75	74081	-5.17	-3.15
186.5	185293	-6.59	-1.92	93.25	74272	-4.99	-2.87
187.5	185456	-6.41	-1.82	93.75	74467	-4.98	-2.93
188.5	185614	-6.42	-1.88	94.25	74664	-4.87	-3.11
189.5	185767	-6.39	-1.95	94.75	74865	-4.95	-3.15
190.5	185916	-6.35	-1.87	95.25	75067	-5.06	-3.11
191.5	186061	-6.44	-1.77	95.75	75271	-4.99	-3.00
192.5	186203	-6.29	-1.87	96.25	75477	-5.06	-3.03
193.5	186342	-6.34	-1.86	96.75	75684	-4.97	-3.10
194.5	186479	-6.37	-1.79	97.25	75891	-5.03	-2.85
195.5	186615	-6.31	-1.71	97.75	76099	-5.13	-2.45
196.5	186749	-6.24	-1.74	98.25	76306	-4.93	-2.23
197.5	186883	-6.25	-1.76	98.75	76513	-5.17	-2.30
198.5	187017	-6.44	-1.70	99.25	76719	-4.96	-2.41
199.5	187151	-6.30	-1.65	99.75	76924	-5.26	-2.49
200.5	187286	-6.24	-1.65	100.25	77127	-5.15	-2.63
201.5	187422	-6.15	-1.74	100.75	77328	-5.17	-3.05
202.5	187561	-6.09	-1.70	101.25	77527	-5.21	-3.38
203.5	187702	-6.29	-1.72	101.75	77722	-5.05	-3.42
204.5	187846	-5.99	-1.68	102.25	77915	-4.91	-3.40
205.5	187993	-5.81	-1.44	102.75	78104	-5.18	-3.34
206.5	188144	-6.05	-1.63	103.25	78289	-5.36	-3.29
207.5	188300	-5.92	-1.74	103.75	78470	-5.12	-2.85
208.5	188460	-5.83	-1.72	104.25	78648	-5.08	-2.78
209.5	188626	-5.76	-1.73	104.75	78823	-5.06	-2.90
210.5	188797	-5.83	-1.40	105.25	78997	-5.25	-3.25
211.5	188974	-5.85	-1.32	105.75	79169	-5.27	-3.22
212.5	189158	-5.82	-1.26	106.25	79341	-5.30	-3.39
213.5	189350	-5.70	-1.30	106.75	79512	-5.38	-3.36
214.5	189548	-5.78	-1.27	107.25	79685	-5.28	-3.53
215.5	189755	-5.78	-1.54	107.75	79859	-5.38	-3.60
216.5	189970	-5.81	-2.03	108.25	80035	-5.34	-3.66
217.5	190193	-5.85	-2.20	108.75	80214	-5.22	-3.72
218.5	190427	-5.83	-2.23	109.25	80396	-5.42	-3.70
219.5	190670	-5.88	-2.46	109.75	80582	-5.26	-3.60
220.5	190923	-5.80	-2.68	110.25	80773	-5.20	-3.53
221.5	191187	-5.80	-2.42	110.75	80969	-5.37	-3.53
222.5	191462	-5.82	-2.38	111.25	81171	-5.23	-3.56
223.5	191749	-5.62	-2.51	111.75	81380	-5.56	-3.63
224.5	192048	-5.46	-1.69	112.25	81596	-5.67	-3.38
225.5	192359	-5.33	-1.36	112.75	81820	-5.43	-3.28

BCC9				BCC10			
Depth (mm)	**Age (yr BP)**	**$\delta^{18}O$**	**$\delta^{13}C$**	**Depth (mm)**	**Age (yr BP)**	**$\delta^{18}O$**	**$\delta^{13}C$**
226.5	192683	-5.36	-1.40	113.25	82051	-5.43	-3.50
227.5	193021	-5.22	-1.47	113.75	82289	-5.46	-3.70
228.5	193373	-5.20	-1.45	114.25	82533	-5.45	-3.66
229.5	193738	-5.14	-1.36	114.75	82782	-5.51	-3.57
230.5	194115	-5.22	-1.06	115.25	83036	-5.54	-3.62
231.5	194502	-5.19	-1.16	115.75	83294	-5.39	-3.77
232.5	194898	-5.34	-0.92	116.25	83555	-5.50	-3.95
233.5	195300	-5.37	-1.31	116.75	83818	-5.63	-4.01
234.5	195708	-5.71	-2.34	117.25	84084	-5.52	-3.88
235.5	196120	-5.78	-2.16	117.75	84350	-5.48	-3.78
236.5	196535	-5.67	-1.54	118.25	84618	-5.59	-3.82
237.5	196950	-5.48	-1.30	118.75	84885	-5.55	-3.46
238.5	197364	-5.46	-1.50	119.25	85151	-5.56	-3.57
239.5	197776	-5.54	-1.69	119.75	85416	-5.48	-3.61
240.5	198184	-5.50	-1.60	120.25	85679	-5.55	-3.51
241.5	198586	-5.61	-2.01	120.75	85938	-5.58	-3.37
242.5	198981	-5.89	-3.32	121.25	86195	-5.77	-3.24
243.5	199367	-5.91	-3.29	121.75	86447	-5.54	-3.15
244.5	199743	-5.80	-3.28	122.25	86694	-5.69	-3.17
245.5	200110	-5.85	-3.19	122.75	86936	-5.55	-3.09
246.5	200467	-5.87	-2.91	123.25	87171	-5.39	-2.92
247.5	200816	-5.57	-2.80	123.75	87400	-5.23	-2.81
248.5	201156	-5.51	-2.89	124.25	87621	-5.51	-2.86
249.5	201488	-5.27	-2.77	124.75	87834	-5.27	-2.94
250.5	201814	-5.58	-2.89	125.25	88038	-5.43	-3.11
251.5	202132	-5.74	-2.99	125.75	88233	-5.42	-2.97
252.5	202444	-5.87	-2.75	126.25	88423	-5.39	-3.15
253.5	202751	-5.70	-2.47	126.75	88613	-5.44	-3.16
254.5	203052	-5.75	-2.33	127.25	88806	-5.38	-3.46
255.5	203349	-6.05	-2.33	127.75	89008	-5.31	-3.41
256.5	203642	-5.76	-2.44	128.25	89224	-5.36	-3.34
257.5	203931	-6.01	-2.62	128.75	89457	-5.22	-3.31
258.5	204217	-6.15	-2.78	129.25	89712	-5.49	-3.58
259.5	204500	-6.14	-2.99	129.75	89994	-5.40	-3.72
260.5	204781	-6.05	-3.19	130.25	90307	-5.52	-3.68
261.5	205061	-5.93	-3.34	130.75	90654	-5.54	-3.53
262.5	205340	-6.01	-3.26	131.25	91032	-5.41	-3.25
263.5	205618	-6.07	-3.16	131.75	91435	-5.24	-2.98
264.5	205896	-5.98	-2.74	132.25	91858	-4.94	-2.23
265.5	206174	-5.75	-2.29	132.75	92294	-4.67	-1.60
266.5	206454	-5.82	-1.86	133.25	92740	-5.19	-1.71
267.5	206735	-5.77	-1.74	133.75	93189	-5.18	-2.01
268.5	207018	-5.80	-1.55	134.25	93636	-4.83	-2.01
269.5	207304	-5.86	-1.45	134.75	94076	-4.95	-2.16
270.5	207593	-5.75	-1.38	135.25	94503	-5.07	-2.09
271.5	207885	-5.68	-1.39	135.75	94912	-4.96	-1.89

BCC9				BCC10			
Depth (mm)	**Age (yr BP)**	**$\delta^{18}O$**	**$\delta^{13}C$**	**Depth (mm)**	**Age (yr BP)**	**$\delta^{18}O$**	**$\delta^{13}C$**
272.5	208182	-5.79	-1.55	136.25	95297	-4.97	-1.96
273.5	208482	-5.77	-1.61	136.75	95653	-4.82	-2.79
274.5	208788	-5.64	-1.66	137.25	95976	-4.56	-5.30
275.5	209098	-5.56	-1.70	137.75	96258	-4.36	-5.25
276.5	209414	-5.62	-1.90	138.25	96502	-4.54	-4.79
277.5	209736	-5.65	-2.11	138.75	96715	-4.55	-4.99
278.5	210064	-5.52	-2.31	139.25	96903	-4.60	-5.07
279.5	210397	-5.54	-2.24	139.75	97073	-4.48	-5.08
280.5	210738	-5.44	-2.21	140.25	97233	-4.69	-4.89
281.5	211085	-5.37	-2.09	140.75	97390	-4.64	-4.80
282.5	211440	-5.29	-1.98	141.25	97551	-4.78	-4.89
283.5	211802	-5.28	-1.85	141.75	97722	-4.65	-4.88
284.5	212172	-5.27	-1.78	142.25	97912	-4.62	-4.90
285.5	212550	-5.07	-1.64	142.75	98128	-4.41	-4.82
286.5	212937	-5.20	-1.71	143.25	98373	-4.50	-4.88
287.5	213332	-5.12	-1.67	143.75	98645	-4.74	-4.96
288.5	213737	-4.93	-1.72	144.25	98936	-4.52	-5.00
289.5	214151	-4.80	-1.67	144.75	99240	-4.51	-4.93
290.5	214574	-4.79	-1.77	145.25	99551	-4.66	-4.94
291.5	215008	-4.90	-1.87	145.75	99862	-4.52	-5.10
292.5	215452	-4.92	-1.80	146.25	100168	-4.73	-5.07
293.5	215907	-5.17	-1.82	146.75	100465	-4.40	-5.02
294.5	216372	-4.84	-1.93	147.25	100753	-4.65	-4.95
295.5	216849	-4.99	-1.88	147.75	101033	-4.75	-4.72
296.5	217338	-4.86	-1.78	148.25	101304	-4.70	-4.82
297.5	217838	-4.80	-1.56	148.75	101569	-4.81	-4.80
298.5	218351	-4.79	-1.03	149.25	101825	-4.76	-4.78
299.5	218876	-5.03	-0.58	149.75	102075	-4.78	-4.59
300.5	219414	-5.33	-0.73	150.25	102319	-4.84	-4.61
				150.75	102556	-4.78	-4.63
301.5	226382	-5.74	-1.14	151.25	102788	-4.95	-4.58
302.5	226385	-6.01	-1.45	151.75	103013	-4.98	-4.61
303.5	226554	-5.81	-1.45	152.25	103234	-5.01	-4.69
304.5	226877	-5.82	-1.56	152.75	103450	-4.87	-4.73
305.5	227338	-5.68	-1.45	153.25	103662	-5.08	-4.73
306.5	227923	-5.65	-1.12	153.75	103869	-5.06	-4.64
307.5	228618	-5.54	-0.89	154.25	104073	-5.21	-4.68
308.5	229409	-5.67	-0.87	154.75	104273	-5.24	-4.72
309.5	230279	-5.74	-0.96	155.25	104470	-5.21	-4.64
310.5	231212	-5.83	-0.95	155.75	104665	-5.18	-4.55
311.5	232189	-5.79	-0.94	156.25	104857	-5.18	-4.48
312.5	233192	-5.30	-0.80	156.75	105048	-5.32	-4.35
313.5	234203	-5.16	-0.86	157.25	105236	-5.25	-4.46
314.5	235206	-5.00	-1.21	157.75	105424	-5.34	-4.57
315.5	236181	-5.09	-1.57	158.25	105610	-5.11	-4.73
316.5	237111	-5.07	-1.65	158.75	105796	-5.39	-4.86

BCC9				BCC10			
Depth (mm)	**Age (yr BP)**	**$\delta^{18}O$**	**$\delta^{13}C$**	**Depth (mm)**	**Age (yr BP)**	**$\delta^{18}O$**	**$\delta^{13}C$**
317.5	237978	-5.20	-1.42	159.25	105982	-5.54	-4.98
318.5	238765	-5.13	-1.53	159.75	106167	-5.46	-5.15
319.5	239454	-5.19	-1.43	160.25	106352	-5.40	-5.29
320.5	240026	-5.64	-1.62	160.75	106536	-5.48	-5.22
321.5	240473	-5.64	-2.28	161.25	106721	-5.37	-5.13
322.5	240823	-5.70	-2.25	161.75	106907	-5.61	-5.05
323.5	241114	-5.79	-2.40	162.25	107092	-5.76	-5.22
324.5	241381	-5.73	-2.40	162.75	107279	-5.81	-5.32
325.5	241662	-5.33	-1.94	163.25	107466	-5.59	-5.34
326.5	241987	-5.61	-1.58	163.75	107654	-5.54	-5.31
327.5	242354	-5.66	-1.22	164.25	107843	-5.75	-5.23
328.5	242754	-6.02	-0.76	164.75	108033	-5.82	-5.27
329.5	243179	-6.04	-0.52	165.25	108224	-5.78	-5.08
330.5	243619	-5.93	-0.37	165.75	108418	-5.60	-4.98
331.5	244067	-6.01	-0.34	166.25	108612	-5.52	-4.90
332.5	244512	-6.28	-0.24	166.75	108809	-5.61	-5.00
333.5	244946	-6.22	-0.39	167.25	109008	-6.01	-4.91
334.5	245361	-6.09	-0.41	167.75	109209	-5.84	-4.76
335.5	245753	-6.25	-0.43	168.25	109412	-6.27	-4.43
336.5	246121	-6.19	-0.31	168.75	109617	-5.88	-4.29
337.5	246468	-6.21	-0.29	169.25	109826	-5.59	-3.73
338.5	246793	-6.07	-0.58	169.75	110037	-5.89	-3.63
339.5	247097	-6.14	-1.02	170.25	110251	-5.70	-4.62
340.5	247383	-6.13	-1.11	170.75	110468	-5.96	-5.34
341.5	247649	-6.10	-0.99	171.25	110688	-5.89	-5.21
342.5	247898	-5.99	-0.77	171.75	110911	-5.79	-3.86
343.5	248129	-6.24	-0.59	172.25	111137	-5.77	-4.44
344.5	248344	-5.97	-0.69	172.75	111365	-5.93	-4.57
345.5	248544	-6.02	-0.90	173.25	111594	-6.03	-4.56
346.5	248729	-6.08	-0.75	173.75	111824	-5.87	-4.62
347.5	248901	-6.06	-0.60	174.25	112054	-5.88	-4.80
348.5	249059	-6.18	-0.74	174.75	112284	-5.88	-4.81
349.5	249206	-6.20	-0.66	175.25	112514	-5.60	-4.85
350.5	249341	-5.94	-0.53	175.75	112741	-5.59	-4.78
351.5	249465	-5.93	-0.64	176.25	112967	-5.51	-4.71
352.5	249580	-5.97	-0.57	176.75	113191	-5.47	-4.78
353.5	249687	-5.87	-0.63	177.25	113411	-5.45	-4.73
354.5	249785	-5.99	-0.68	177.75	113628	-5.33	-4.63
355.5	249876	-6.05	-0.65	178.25	113841	-5.30	-5.12
356.5	249961	-6.04	-0.66	178.75	114049	-5.39	-5.78
357.5	250040	-6.03	-0.70	179.25	114252	-5.42	-5.20
358.5	250115	-6.06	-0.52	179.75	114449	-5.62	-4.87
359.5	250186	-5.83	-0.39	180.25	114640	-5.62	-4.74
360.5	250254	-6.01	-0.32	180.75	114823	-5.61	-4.58
361.5	250320	-5.75	-0.18	181.25	115000	-5.29	-3.51
362.5	250385	-5.83	-0.14	181.75	115168	-5.38	-3.95

BCC9				BCC10			
Depth (mm)	**Age (yr BP)**	**$\delta^{18}O$**	**$\delta^{13}C$**	**Depth (mm)**	**Age (yr BP)**	**$\delta^{18}O$**	**$\delta^{13}C$**
363.5	250449	-5.95	-0.34	182.25	115328	-4.91	-4.41
364.5	250513	-5.85	-0.21	182.75	115482	-5.29	-4.24
365.5	250579	-6.25	-0.04	183.25	115631	-5.21	-4.71
366.5	250646	-5.80	-0.30	183.75	115776	-5.62	-4.58
367.5	250717	-5.78	-0.51	184.25	115921	-5.28	-2.93
368.5	250791	-5.84	-0.49	184.75	116067	-5.16	-2.76
369.5	250869	-5.82	-0.57	185.25	116215	-5.11	-2.69
370.5	250953	-6.06	-0.60	185.75	116367	-5.17	-2.64
371.5	251043	-6.12	-0.68	186.25	116526	-5.00	-2.91
372.5	251137	-5.99	-0.45	186.75	116694	-5.05	-3.62
373.5	251236	-6.11	-0.21	187.25	116871	-5.03	-4.23
374.5	251338	-5.91	-0.28	187.75	117061	-5.11	-3.94
375.5	251445	-5.75	-0.53	188.25	117264	-4.89	-3.08
376.5	251554	-6.05	-0.60	188.75	117483	-4.74	-2.94
377.5	251665	-6.03	-0.66	189.25	117715	-4.67	-2.69
378.5	251778	-6.13	-0.80	189.75	117958	-4.74	-2.41
379.5	251893	-6.07	-0.94	190.25	118210	-4.77	-2.57
380.5	252009	-5.91	-0.83	190.75	118469	-4.74	-2.59
381.5	252125	-6.15	-0.86	191.25	118732	-4.83	-2.50
382.5	252241	-5.98	-0.81	191.75	118998	-4.84	-2.33
383.5	252356	-6.03	-0.77	192.25	119263	-4.99	-2.26
384.5	252470	-6.10	-0.72	192.75	119526	-4.61	-2.52
385.5	252582	-6.15	-0.64	193.25	119784	-4.79	-2.64
386.5	252692	-6.39	-0.71	193.75	120035	-4.61	-2.39
387.5	252799	-6.48	-0.74	194.25	120277	-4.68	-2.46
388.5	252903	-6.16	-0.69	194.75	120508	-4.61	-2.71
389.5	253005	-6.12	-0.83	195.25	120724	-4.61	-3.09
390.5	253103	-6.17	-1.27	195.75	120927	-4.39	-2.59
391.5	253199	-6.02	-1.29	196.25	121118	-4.63	-2.85
392.5	253293	-5.96	-1.15	196.75	121298	-4.54	-2.93
393.5	253383	-5.94	-1.01	197.25	121468	-4.67	-3.17
394.5	253471	-5.95	-0.97	197.75	121632	-4.78	-3.39
395.5	253557	-5.98	-1.19	198.25	121790	-4.72	-3.54
396.5	253641	-6.05	-1.23	198.75	121944	-4.79	-3.45
397.5	253722	-5.89	-0.89	199.25	122095	-4.67	-3.63
398.5	253801	-6.06	-0.70	199.75	122246	-4.71	-3.69
399.5	253878	-6.09	-0.68	200.25	122399	-4.88	-4.39
400.5	253952	-6.11	-0.80	200.75	122554	-4.98	-4.42
401.5	254025	-6.23	-0.85	201.25	122713	-4.94	-4.52
402.5	254096	-6.16	-0.71	201.75	122879	-4.89	-4.42
403.5	254165	-5.99	-0.83	202.25	123051	-4.81	-4.41
404.5	254232	-5.93	-0.94	202.75	123230	-4.81	-4.31
405.5	254298	-5.86	-0.98	203.25	123417	-4.88	-4.31
406.5	254362	-6.08	-0.83	203.75	123613	-5.15	-4.48
407.5	254425	-5.87	-0.78	204.25	123819	-4.92	-4.15
408.5	254486	-6.21	-0.84	204.75	124036	-5.22	-3.68

BCC9				BCC10			
Depth (mm)	**Age (yr BP)**	**$\delta^{18}O$**	**$\delta^{13}C$**	**Depth (mm)**	**Age (yr BP)**	**$\delta^{18}O$**	**$\delta^{13}C$**
409.5	254546	-6.04	-0.80	**Begin 2nd Transect***			
410.5	254604	-5.95	-0.79	0.25	122031	-4.74	-3.70
411.5	254661	-5.98	-0.75	0.75	122433	-4.74	-4.54
412.5	254717	-6.01	-0.74	1.25	122835	-5.07	-4.56
413.5	254773	-6.07	-0.63	1.75	123237	-4.83	-4.40
414.5	254827	-6.10	-0.49	2.25	123639	-4.85	-4.11
415.5	254880	-6.12	-0.50	2.75	124041	-5.20	-3.78
416.5	254932	-5.90	-0.78	3.25	124442	-5.17	-3.89
417.5	254984	-6.08	-0.51	3.75	124844	-5.24	-4.09
418.5	255034	-5.99	-0.66	4.25	125246	-5.30	-4.09
419.5	255085	-5.87	-0.75	4.75	125648	-5.47	-3.13
420.5	255134	-5.93	-0.63	5.25	126050	-5.30	-2.44
421.5	255183	-5.85	-0.75	5.75	126451	-5.41	-1.74
422.5	255232	-5.85	-0.86	6.25	126853	-5.75	-1.32
423.5	255280	-6.10	-0.74	6.75	127255	-5.87	-0.54
424.5	255327	-6.01	-0.79	7.25	127657	-5.86	-0.26
425.5	255375	-5.89	-0.73				
426.5	255422	-5.92	-0.77				
427.5	255468	-5.80	-0.78				
428.5	255515	-5.92	-0.86				
429.5	255561	-5.76	-0.71				
430.5	255608	-5.93	-0.82				
431.5	255654	-5.94	-0.92				
432.5	255700	-5.87	-0.98				
433.5	255747	-5.85	-1.02				
434.5	255793	-5.84	-0.78				
435.5	255840	-5.82	-0.87				
436.5	255886	-5.86	-0.90				
437.5	255934	-5.92	-0.97				
438.5	255981	-5.97	-1.00				
439.5	256029	-5.95	-0.86				
440.5	256077	-5.98	-1.06				
441.5	256125	-6.02	-0.92				
442.5	256174	-5.97	-0.91				
443.5	256224	-6.01	-0.96				
444.5	256274	-5.84	-0.96				
445.5	256325	-5.93	-1.13				
446.5	256377	-5.73	-1.06				
447.5	256429	-5.77	-0.89				
448.5	256483	-5.68	-0.82				
449.5	256537	-5.71	-0.81				
450.5	256592	-5.57	-0.85				
451.5	256648	-5.70	-0.87				
452.5	256705	-5.53	-0.70				
453.5	256763	-5.67	-0.74				
454.5	256822	-5.61	-0.82				

BCC9				BCC10			
Depth (mm)	Age (yr BP)	$\delta^{18}O$	$\delta^{13}C$	Depth (mm)	Age (yr BP)	$\delta^{18}O$	$\delta^{13}C$
455.5	256882	-5.65	-1.04				
456.5	256944	-5.65	-1.32				
457.5	257006	-5.63	-1.07				
458.5	257071	-5.75	-0.99				
459.5	257136	-5.85	-0.93				
460.5	257203	-5.73	-0.89				
461.5	257271	-5.66	-0.85				
462.5	257341	-5.77	-0.77				
463.5	257413	-5.72	-0.67				
464.5	257486	-5.59	-0.80				
465.5	257561	-5.88	-0.80				
466.5	257637	-5.66	-0.57				
467.5	257716	-5.66	-0.60				
468.5	257796	-5.48	-0.62				
469.5	257878	-5.72	-0.56				
470.5	257962	-5.60	-0.47				
471.5	258047	-5.52	-0.75				
472.5	258135	-5.66	-1.18				
473.5	258224	-5.62	-1.10				
474.5	258314	-5.80	-1.43				
475.5	258404	-5.58	-1.67				
476.5	258496	-5.73	-1.71				
477.5	258588	-5.70	-1.76				
478.5	258680	-5.67	-2.00				
479.5	258773	-5.83	-1.97				
480.5	258865	-5.82	-2.06				
481.5	258956	-5.81	-1.83				
482.5	259048	-5.91	-1.48				
483.5	259138	-5.41	-2.04				
484.5	259227	-5.74	-1.32				
485.5	259315	-5.38	-1.21				
486.5	259401	-5.35	-1.16				
487.5	259486	-5.26	-1.29				
488.5	259570	-5.49	-1.70				
489.5	259652	-5.33	-1.54				
490.5	259733	-5.29	-1.30				
491.5	259813	-5.64	-1.17				
492.5	259891	-5.43	-1.22				
493.5	259969	-5.45	-1.27				
494.5	260045	-5.42	-1.13				
495.5	260121	-5.46	-1.04				
496.5	260195	-5.75	-1.03				
497.5	260268	-5.59	-1.07				
498.5	260341	-5.67	-0.98				
499.5	260412	-5.31	-0.85				
500.5	260483	-5.37	-1.01				

BCC9				BCC10			
Depth (mm)	Age (yr BP)	$\delta^{18}O$	$\delta^{13}C$	Depth (mm)	Age (yr BP)	$\delta^{18}O$	$\delta^{13}C$
501.5	260553	-5.56	-0.89				
502.5	260622	-5.52	-1.32				
503.5	260690	-5.56	-1.44				
504.5	260758	-5.71	-1.21				
505.5	260825	-5.54	-1.23				
506.5	260892	-5.48	-1.58				
507.5	260957	-5.67	-1.33				
508.5	261023	-5.56	-1.16				
509.5	261087	-5.78	-1.57				
510.5	261152	-5.62	-1.75				
511.5	261216	-5.67	-1.39				
512.5	261279	-5.59	-1.50				
513.5	261343	-5.87	-1.59				
514.5	261406	-5.95	-1.55				
515.5	261468	-5.84	-1.56				
516.5	261531	-5.77	-1.38				
517.5	261593	-5.73	-1.43				
518.5	261655	-5.66	-1.53				
519.5	261717	-5.62	-1.77				
520.5	261779	-5.41	-2.07				
521.5	261841	-5.72	-2.06				
522.5	261904	-5.62	-2.33				
523.5	261966	-5.59	-1.93				
524.5	262028	-5.59	-1.40				
525.5	262090	-6.08	-1.27				
526.5	262153	-5.85	-1.39				
527.5	262216	-5.82	-1.08				
528.5	262279	-5.88	-1.00				
529.5	262342	-5.78	-0.56				
530.5	262406	-5.74	-0.60				
531.5	262470	-5.80	-0.82				
532.5	262535	-5.83	-0.87				
533.5	262599	-5.78	-1.06				
534.5	262665	-5.67	-1.02				
535.5	262730	-5.58	-1.13				
536.5	262797	-5.77	-0.85				
537.5	262863	-6.15	-0.93				
538.5	262931	-5.92	-1.30				
539.5	262999	-6.13	-1.03				
540.5	263068	-5.89	-0.63				
541.5	263137	-6.05	-1.91				
542.5	263207	-5.92	-2.19				
543.5	263278	-5.95	-2.28				
544.5	263349	-5.82	-2.44				
545.5	263421	-5.91	-2.32				
546.5	263494	-5.97	-2.07				

BCC9				BCC10			
Depth (mm)	Age (yr BP)	$\delta^{18}O$	$\delta^{13}C$	Depth (mm)	Age (yr BP)	$\delta^{18}O$	$\delta^{13}C$
547.5	263568	-5.99	-2.17				
548.5	263643	-5.91	-2.17				
549.5	263719	-5.84	-1.92				
550.5	263796	-6.03	-1.87				
551.5	263873	-5.95	-1.71				
552.5	263952	-5.95	-1.51				
553.5	264032	-5.91	-1.58				
554.5	264113	-5.93	-1.63				
555.5	264195	-6.06	-1.71				
556.5	264278	-6.10	-1.76				
557.5	264362	-5.75	-1.90				
558.5	264448	-5.84	-1.97				
559.5	264534	-5.80	-1.76				
560.5	264622	-5.81	-1.78				
561.5	264712	-5.62	-1.70				
562.5	264802	-5.85	-1.88				
563.5	264894	-5.80	-2.02				
564.5	264988	-5.90	-1.83				
565.5	265083	-5.88	-2.17				
566.5	265179	-5.95	-1.81				
567.5	265277	-5.86	-1.99				
568.5	265376	-5.91	-1.82				
569.5	265477	-6.05	-2.01				
570.5	265579	-5.79	-1.98				
571.5	265683	-5.88	-2.14				
572.5	265789	-5.98	-2.20				
573.5	265897	-5.96	-2.28				
574.5	266006	-6.14	-1.79				
575.5	266117	-5.95	-2.30				
576.5	266229	-5.77	-2.13				
577.5	266343	-5.78	-2.00				
578.5	266459	-5.63	-2.12				
579.5	266576	-5.84	-2.15				
580.5	266695	-5.75	-2.03				
581.5	266815	-5.87	-2.34				
582.5	266937	-5.87	-2.87				
583.5	267059	-5.87	-2.66				
584.5	267183	-5.70	-2.36				
585.5	267307	-5.86	-2.40				
586.5	267433	-5.93	-2.28				
587.5	267560	-5.89	-2.05				
588.5	267687	-5.92	-1.98				
589.5	267815	-5.80	-1.79				
590.5	267944	-5.65	-1.69				
591.5	268073	-5.83	-2.04				
592.5	268203	-5.87	-1.89				

BCC9				BCC10			
Depth (mm)	Age (yr BP)	$\delta^{18}O$	$\delta^{13}C$	Depth (mm)	Age (yr BP)	$\delta^{18}O$	$\delta^{13}C$
593.5	268333	-5.69	-2.09				
594.5	268464	-5.79	-1.87				
595.5	268595	-5.77	-2.09				
596.5	268726	-5.79	-2.22				
597.5	268857	-5.91	-2.31				
598.5	268988	-5.82	-2.32				
599.5	269119	-5.87	-2.26				
600.5	269250	-5.71	-2.01				
601.5	269381	-5.65	-2.14				
602.5	269512	-5.93	-2.02				
603.5	269642	-5.63	-2.10				
604.5	269772	-5.95	-1.98				
605.5	269901	-5.85	-2.37				
606.5	270030	-6.00	-2.93				
607.5	270158	-5.80	-2.36				
608.5	270286	-6.01	-2.08				
609.5	270413	-5.84	-1.92				
610.5	270538	-5.77	-2.06				
611.5	270663	-6.20	-2.09				
612.5	270787	-6.09	-2.21				
613.5	270910	-6.20	-2.23				
614.5	271032	-6.18	-2.39				
615.5	271152	-6.16	-2.54				
616.5	271271	-6.08	-2.57				
617.5	271389	-6.05	-2.59				
618.5	271506	-6.37	-2.59				
619.5	271621	-6.28	-2.75				
620.5	271736	-5.93	-2.60				
621.5	271849	-6.11	-2.53				
622.5	271962	-6.14	-2.43				
623.5	272074	-6.02	-2.43				
624.5	272185	-6.04	-2.20				
625.5	272295	-6.01	-2.27				
626.5	272405	-6.14	-2.35				
627.5	272513	-5.85	-2.38				
628.5	272622	-5.92	-2.50				
629.5	272729	-6.03	-2.37				
630.5	272837	-6.10	-2.45				
631.5	272943	-6.23	-2.42				
632.5	273050	-6.19	-2.33				
633.5	273156	-6.25	-2.24				
634.5	273262	-6.10	-2.48				
635.5	273368	-5.94	-2.61				
636.5	273473	-6.04	-2.59				
637.5	273579	-6.04	-2.56				
638.5	273684	-6.08	-2.69				

BCC9				BCC10			
Depth (mm)	Age (yr BP)	$\delta^{18}O$	$\delta^{13}C$	Depth (mm)	Age (yr BP)	$\delta^{18}O$	$\delta^{13}C$
639.5	273789	-6.09	-2.83				
640.5	273895	-6.30	-2.59				
641.5	274001	-6.10	-2.97				
642.5	274106	-5.98	-2.67				
643.5	274212	-5.80	-2.52				
644.5	274319	-5.91	-2.67				
645.5	274425	-6.09	-2.77				
646.5	274533	-5.92	-2.99				
647.5	274641	-5.93	-3.05				
648.5	274750	-5.70	-2.84				
649.5	274860	-5.85	-2.85				
650.5	274972	-5.73	-2.86				
651.5	275086	-6.00	-2.98				
652.5	275202	-5.80	-2.76				
653.5	275320	-5.76	-2.61				
654.5	275441	-5.64	-2.85				
655.5	275564	-5.69	-3.03				
656.5	275690	-6.04	-3.23				
657.5	275820	-5.66	-3.57				
658.5	275953	-5.39	-3.36				
659.5	276091	-5.72	-3.36				
660.5	276232	-5.62	-3.39				
661.5	276377	-6.04	-3.42				
662.5	276527	-5.67	-3.33				
663.5	276682	-5.81	-3.56				
664.5	276841	-6.03	-3.89				
665.5	277006	-5.68	-3.00				
666.5	277177	-5.60	-2.59				
667.5	277353	-5.82	-2.62				
668.5	277536	-5.75	-2.58				
669.5	277724	-5.80	-2.64				
670.5	277919	-5.76	-2.42				
671.5	278121	-5.58	-2.62				
672.5	278330	-5.70	-2.35				
673.5	278546	-5.75	-2.48				
674.5	278770	-6.02	-2.58				
675.5	279001	-6.12	-2.91				
676.5	279240	-5.90	-2.88				
677.5	279485	-5.91	-2.76				
678.5	279737	-6.15	-2.69				
679.5	279994	-5.84	-2.49				
680.5	280257	-5.58	-2.49				
681.5	280525	-5.57	-2.53				
682.5	280797	-5.63	-2.51				
683.5	281073	-5.33	-2.42				
684.5	281353	-5.55	-2.69				

BCC9				BCC10			
Depth (mm)	Age (yr BP)	$\delta^{18}O$	$\delta^{13}C$	Depth (mm)	Age (yr BP)	$\delta^{18}O$	$\delta^{13}C$
685.5	281635	-5.66	-2.76				
686.5	281920	-5.59	-2.80				
687.5	282206	-5.36	-2.97				
688.5	282495	-5.40	-2.97				
689.5	282784	-5.26	-2.79				
690.5	283073	-5.33	-2.56				
691.5	283363	-5.16	-2.75				
692.5	283652	-5.37	-2.82				
693.5	283941	-5.39	-2.62				
694.5	284228	-5.15	-2.85				
695.5	284513	-5.05	-2.82				
696.5	284795	-5.34	-2.91				
697.5	285075	-5.21	-3.03				
698.5	285351	-4.93	-3.08				
699.5	285624	-5.32	-3.09				
700.5	285892	-5.19	-3.00				
701.5	286155	-5.14	-3.43				
702.5	286413	-5.19	-3.57				
703.5	286666	-5.52	-3.54				
704.5	286912	-5.35	-3.60				
705.5	287151	-5.48	-4.03				
706.5	287383	-5.80	-3.70				
707.5	287607	-5.81	-3.75				
708.5	287823	-6.05	-3.49				
709.5	288031	-5.79	-3.52				
710.5	288229	-5.81	-3.62				
711.5	288419	-5.78	-3.79				
712.5	288602	-5.76	-3.43				
713.5	288779	-5.86	-3.33				
714.5	288950	-5.89	-3.20				
715.5	289116	-5.80	-3.12				
716.5	289278	-6.06	-3.06				
717.5	289438	-5.78	-2.81				
718.5	289596	-5.84	-2.74				
719.5	289753	-6.08	-2.96				
720.5	289909	-5.98	-2.81				
721.5	290067	-5.94	-2.84				
722.5	290226	-6.05	-2.45				
723.5	290388	-5.96	-2.51				
724.5	290553	-5.92	-2.63				
725.5	290723	-5.95	-2.79				
726.5	290898	-5.89	-2.78				
727.5	291080	-6.03	-2.61				
728.5	291268	-5.94	-2.76				
729.5	291465	-6.20	-2.43				
730.5	291670	-6.22	-1.96				

BCC9				BCC10			
Depth (mm)	Age (yr BP)	$\delta^{18}O$	$\delta^{13}C$	Depth (mm)	Age (yr BP)	$\delta^{18}O$	$\delta^{13}C$
731.5	291886	-6.29	-2.24				
732.5	292112	-6.00	-2.51				
733.5	292350	-5.94	-2.37				
734.5	292601	-6.15	-2.62				
735.5	292865	-6.16	-2.84				
736.5	293143	-5.96	-2.69				
737.5	293437	-6.02	-2.52				
738.5	293747	-6.15	-2.20				
739.5	294074	-6.13	-2.24				
740.5	294420	-5.84	-2.10				
741.5	294783	-5.78	-2.03				
742.5	295164	-6.00	-2.20				
743.5	295562	-5.69	-2.20				
744.5	295976	-5.86	-2.21				
745.5	296407	-5.74	-2.45				
746.5	296852	-6.01	-2.35				
747.5	297312	-5.83	-2.28				
748.5	297786	-5.85	-2.00				
749.5	298273	-5.97	-2.05				
750.5	298774	-6.01	-2.11				
751.5	299286	-5.82	-2.47				
752.5	299810	-5.77	-2.56				
753.5	300345	-5.75	-1.78				
754.5	300891	-5.47	-2.26				
755.5	301446	-5.39	-1.81				
756.5	302011	-5.37	-1.60				
757.5	302584	-5.17	-1.48				
758.5	303165	-5.46	-1.81				
759.5	303754	-5.28	-2.30				
760.5	304349	-5.15	-2.12				
761.5	304951	-4.98	-1.70				
762.5	305559	-5.30	-1.17				
763.5	306171	-5.01	-1.42				
764.5	306788	-5.06	-1.55				
765.5	307408	-4.82	-1.39				
766.5	308032	-4.85	-1.38				
767.5	308659	-4.98	-1.44				
768.5	309289	-5.16	-1.01				
769.5	309921	-5.14	-1.44				
770.5	310555	-5.34	-1.57				
771.5	311191	-5.52	-1.03				
772.5	311829	-5.78	-0.66				
773.5	312468	-5.63	-0.98				
774.5	313109	-5.49	-0.53				
775.5	313751	-5.65	-0.18				
776.5	314393	-5.57	-0.21				

BCC9				BCC10			
Depth (mm)	**Age (yr BP)**	**$\delta^{18}O$**	**$\delta^{13}C$**	**Depth (mm)**	**Age (yr BP)**	**$\delta^{18}O$**	**$\delta^{13}C$**
777.5	315036	-5.59	-0.65				
778.5	315679	-5.79	-0.81				
779.5	316322	-5.92	-0.98				
780.5	316965	-5.68	-1.21				
781.5	317608	-5.72	-1.55				
782.5	318250	-5.21	-1.24				
783.5	318891	-5.21	-1.61				
784.5	319531	-5.28	-1.72				
785.5	320170	-5.60	-1.60				
786.5	320807	-5.53	-1.72				
787.5	321442	-5.35	-1.89				
788.5	322075	-5.47	-1.74				
789.5	322706	-5.33	-1.66				
790.5	323334	-5.33	-1.78				
791.5	323959	-5.31	-1.63				
792.5	324582	-5.53	-1.61				
793.5	325201	-5.46	-1.55				
794.5	325816	-5.76	-1.50				
795.5	326428	-5.49	-1.52				
796.5	327036	-5.84	-1.78				
797.5	327640	-6.03	-2.05				
798.5	328239	-5.92	-1.87				
799.5	328833	-6.03	-2.05				

Appendix 3: Supplemental Materials for Chapter 4

Figure S4-1 Image of sample CCC1.
Supplemental Figure 1. Image of Sample CCC1 after it has been cut in along the growth axis, polished and drilled for stable isotopes.

Table S4-1 U/Th data table and 230Th ages for sample CCC1.

Supplemental Table 1. ^{230}Th dating results. Quoted errors are 2σ.

Sample Number	Distance (mm)	^{238}U (ppb)		^{232}Th (ppt)		^{230}Th / ^{232}Th (atomic x10-6)		δ^{234}U* (measured)		^{230}Th / ^{238}U (activity)		^{230}Th Age (yr BP) (uncorrected)		$\delta^{234}U_{Initial**}$ (corrected)		^{230}Th Age (yr BP)*** (corrected)	
CCC1-3	3	419.6	±1.0	367	±8	1540	±30	658.0	±3.0	0.0819	±0.0003	5448	±22	668	±3	**5432**	**±25**
CCC1-46.5	46.5	541.7	±1.2	305	±6	2670	±60	706.0	±3.0	0.0912	±0.0003	5907	±23	718	±3.0	**5898**	**±24**
CCC1-63	63	535.4	±1.0	172	±4	4950	±110	722.1	±2.9	0.0966	±0.0003	6214	±22	735	±3.0	**6208**	**±22**
CCC1-101	101	410.6	±0.6	376	±8	1910	±40	732.5	±2.8	0.1062	±0.0003	6808	±25	747	±3.0	**6793**	**±28**
CCC1-123	123	495.1	±0.7	244	±5.0	3750	±80	739.8	±2.5	0.1122	±0.0004	7175	±27	755	±2.5	**7167**	**±28**
CCC1-150	150.25	552.2	±0.8	250	±6.0	4170	±90	755.4	±2.4	0.1148	±0.0002	7280	±19	771	±2.0	**7272**	**±20**
CCC1-166	166	634.8	±1.0	336	±7.0	3750	±80	748.4	±2.4	0.1204	±0.0003	7682	±21	765	±2.0	**7674**	**±22**
CCC1-189B	189	463.5	±0.7	690	±14.0	1450	±30	764.4	±2.7	0.1308	±0.0003	8293	±24	783	±3.0	**8268**	**±29**
CCC1-189A	189	459.3	±0.6	595	±12.0	1680	±30	770.1	±2.0	0.1316	±0.0004	8320	±27	789	±2.0	**8300**	**±30**
CCC1-212.5	212.5	414.9	±0.6	382	±8.0	3060	±60	802.6	±2.8	0.1713	±0.0004	10750	±30	827	±3.0	**10730**	**±30**
CCC1-227	227	320.9	±0.4	271	±6.0	3590	±80	837.9	±2.7	0.1839	±0.0004	11350	±30	865	±2.8	**11340**	**±30**
CCC1-242.5	242.5	544.1	±0.6	356	±7.0	4860	±100	826.3	±1.9	0.1928	±0.0004	12010	±30	855	±2.0	**12000**	**±30**
CCC1-268	268	574.0	±0.7	69	±2.6	27300	±1000	805.2	±2.0	0.1996	±0.0004	12610	±30	835	±2.0	**12610**	**±30**
CCC1-280	280	459.9	±0.6	275	±6.0	5690	±120	829.7	±2.4	0.2062	±0.0007	12870	±50	861	±2.0	**12860**	**±50**
CCC1-298	298	589.3	±0.9	38	±0.9	54000	±1300	812.3	±2.4	0.2110	±0.0005	13320	±40	844	±2.0	**13320**	**±40**
CCC1-330.5	330.5	592.8	±1.0	132	±2.8	16100	±300	801.0	±2.7	0.2177	±0.0007	13860	±50	833	±3.0	**13850**	**±50**
CCC1-340.5	340.25	574.6	±0.7	101	±2.2	20100	±400	761.2	±2.1	0.2137	±0.0005	13920	±40	792	±2.0	**13920**	**±40**
CCC1-370.5	370.75	535.1	±0.7	47	±1.1	41000	±1000	771.6	±1.9	0.2229	±0.0006	14470	±40	804	±2.0	**14470**	**±40**
CCC1-375	375	537.0	±0.8	55	±1.4	36900	±900	741.0	±2.5	0.2285	±0.0010	15130	±70	773	±2.6	**15130**	**±70**
CCC1-389	389	641.9	±1.1	79	±1.7	32200	±700	813.9	±2.7	0.2403	±0.0006	15280	±50	850	±3.0	**15280**	**±50**
CCC1-404	404	664.6	±1.2	163	±3.0	16300	±300	809.1	±2.8	0.2433	±0.0007	15530	±50	845	±3.0	**15520**	**±50**
CCC1-420.5	420.5	764.0	±1.3	47	±1.1	65100	±1500	779.9	±2.5	0.2410	±0.0006	15640	±50	815	±2.7	**15640**	**±50**
CCC1-430.75	430.75	960.1	±1.8	21	±0.7	184000	±6000	764.9	±2.6	0.2396	±0.0007	15690	±50	800	±2.7	**15690**	**±50**
CCC1-455.75	455.75	760.1	±1.1	54	±1.3	59500	±1400	829.9	±2.2	0.2548	±0.0005	16110	±40	869	±2.3	**16110**	**±40**
CCC1-465	465	678.3	±1.1	62	±1.5	45300	±1100	783.2	±2.6	0.2531	±0.0008	16450	±60	821	±2.8	**16450**	**±60**
CCC1-468.5A	468.5	510.1	±0.7	505	±10.0	4340	±90	807.4	±2.4	0.2603	±0.0006	16700	±50	846	±2.5	**16690**	**±50**

Sample Number	Distance (mm)	^{238}U (ppb)		^{232}Th (ppt)		$^{230}Th / ^{232}Th$ (atomic x10-6)		$\delta^{234}U^*$ (measured)		$^{230}Th / ^{238}U$ (activity)		^{230}Th Age (yr BP) (uncorrected)		$\delta^{234}U_{Initial**}$ (corrected)		^{230}Th Age (yr BP)*** (corrected)	
CCC1-468.5B	468.5	510.0	±0.8	450	±9.0	4800	±100	805.9	±2.6	0.2584	±0.0006	16590	±50	845	±2.7	**16570**	**±50**
CCC1-474	473.75	493.8	±0.8	772	±16.0	2780	±60	823.9	±2.6	0.2638	±0.0007	16780	±50	864	±2.7	**16750**	**±50**
CCC1-483	482.75	414.1	±0.7	579	±12.0	3460	±70	787.1	±2.5	0.2932	±0.0007	19230	±60	831	±2.7	**19210**	**±60**
CCC1-491	490.75	290.2	±0.4	2570	±50.0	561	±11	755.1	±2.5	0.3021	±0.0008	20260	±70	799	±2.7	**20120**	**±120**

$\lambda_{230} = 9.17052 \times 10^{-6}\ y^{-1}$, $\lambda_{234} = 2.82206 \times 10^{-6}\ y^{-1}$, $\lambda_{238} = 1.55125 \times 10^{-10}\ y^{-1}$.
*$\delta^{234}U = ([^{234}U/^{238}U]activity - 1)x1000$. ** $\delta^{234}U_{initial}$ was calculated based on ^{230}Th age (T), i.e., $\delta^{234}Uinitial = \delta^{234}U_{measured} \times e^{\lambda 234 x T}$.
Corrected ^{230}Th ages assume the initial $^{230}Th/^{232}Th$ atomic ratio of $4.4\pm2.2 \times 10^{-6}$. Those are the values for a material at secular equilibrium, with the bulk earth $^{232}Th/^{238}U$ value of 3.8. The errors are arbitrarily assumed to be 50%.
***B.P. stands for "Before Present" where the "Present" is defined as the year 1950 A.D.

Table S4-2 Isotopic data for sample CCC1.

Supplemental Table 2. Stable Isotope Data by depth and age.

Sample Depth (mm)	Age (yr BP)	$\delta^{18}O$ (‰, VPDB)	$\delta^{13}C$ (‰, VPDB)
0.25	5403	-4.54	-3.93
0.75	5408	-4.63	-4.89
1.25	5414	-4.68	-5.02
1.75	5419	-4.70	-5.07
2.25	5424	-5.15	-5.33
2.75	5430	-4.86	-5.67
3.25	5435	-5.08	-5.76
3.75	5440	-4.95	-5.74
4.25	5446	-5.02	-5.88
4.75	5451	-4.77	-5.90
5.25	5457	-4.47	-4.91
5.75	5462	-4.58	-4.92
6.25	5467	-4.52	-5.15
6.75	5473	-4.80	-5.43
7.25	5478	-4.62	-5.71
7.75	5483	-4.90	-5.85
8.25	5489	-4.68	-5.87
8.75	5494	-4.25	-5.38
9.25	5499	-4.54	-5.45
9.75	5505	-4.87	-5.55
10.25	5510	-4.75	-5.22
10.75	5515	-4.42	-5.20
11.25	5521	-4.69	-5.22
11.75	5526	-4.81	-5.57
12.25	5531	-4.82	-5.44
12.75	5537	-4.94	-5.44
13.25	5542	-5.00	-5.79
13.75	5547	-4.82	-5.76
14.25	5553	-4.49	-5.42
14.75	5558	-4.62	-5.39
15.25	5563	-4.77	-5.54
15.75	5569	-5.04	-5.87
16.25	5574	-4.75	-5.40
16.75	5580	-4.54	-5.33
17.25	5585	-4.88	-5.67
17.75	5590	-5.05	-5.84
18.25	5596	-4.56	-5.66
18.75	5601	-4.56	-5.58
19.25	5606	-4.66	-5.72
19.75	5612	-4.60	-6.00
20.25	5617	-4.47	-6.01
20.75	5622	-4.47	-6.07
21.25	5628	-4.47	-6.20
21.75	5633	-4.40	-5.87
22.25	5638	-4.57	-6.03
22.75	5644	-4.42	-5.98

Sample Depth (mm)	Age (yr BP)	$\delta^{18}O$ (‰, VPDB)	$\delta^{13}C$ (‰, VPDB)
23.25	5649	-4.28	-5.68
23.75	5654	-4.72	-5.92
24.25	5660	-4.53	-6.67
24.75	5665	-4.53	-6.55
25.25	5670	-4.62	-6.55
25.75	5676	-4.31	-6.19
26.25	5681	-4.38	-6.07
26.75	5686	-4.32	-5.78
27.25	5692	-4.47	-5.68
27.75	5697	-4.34	-5.56
28.25	5703	-4.45	-5.61
28.75	5708	-4.44	-5.67
29.25	5713	-4.62	-5.85
29.75	5719	-4.31	-5.90
30.25	5724	-4.69	-6.15
30.75	5729	-4.68	-5.95
31.25	5735	-4.76	-5.85
31.75	5740	-4.46	-5.91
32.25	5745	-4.59	-5.96
32.75	5751	-4.45	-5.95
33.25	5756	-4.54	-6.03
33.75	5761	-4.53	-6.01
34.25	5767	-4.48	-5.79
34.75	5772	-4.62	-5.76
35.25	5777	-4.49	-5.67
35.75	5783	-4.45	-5.61
36.25	5788	-4.69	-5.63
36.75	5793	-4.57	-5.56
37.25	5799	-4.56	-5.53
37.75	5804	-4.52	-5.63
38.25	5809	-4.74	-5.96
38.75	5815	-4.72	-6.14
39.25	5820	-4.73	-6.48
39.75	5826	-4.76	-6.45
40.25	5831	-4.90	-6.41
40.75	5836	-4.82	-6.30
41.25	5842	-4.83	-6.21
41.75	5847	-4.88	-6.18
42.25	5852	-4.67	-6.03
42.75	5858	-4.67	-6.17
43.25	5863	-4.72	-6.19
43.75	5868	-4.61	-6.11
44.25	5874	-4.55	-6.15
44.75	5879	-4.91	-6.32
45.25	5884	-4.86	-6.32
45.75	5890	-4.80	-6.16
46.25	5895	-4.79	-6.38
46.75	5902	-4.93	-6.31
47.25	5912	-4.56	-6.06

Sample Depth (mm)	Age (yr BP)	$\delta^{18}O$ (‰, VPDB)	$\delta^{13}C$ (‰, VPDB)
47.75	5921	-4.74	-6.31
48.25	5931	-4.81	-6.39
48.75	5940	-4.86	-6.49
49.25	5950	-5.02	-6.30
49.75	5959	-4.91	-6.25
50.25	5968	-5.01	-6.10
50.75	5978	-4.93	-6.05
51.25	5987	-4.91	-6.00
51.75	5997	-4.81	-6.01
52.25	6006	-4.78	-6.15
52.75	6015	-4.78	-6.11
53.25	6025	-4.80	-6.23
53.75	6034	-4.69	-6.10
54.25	6044	-4.75	-6.21
54.75	6053	-4.83	-6.12
55.25	6062	-4.76	-6.22
55.75	6072	-4.78	-6.25
56.25	6081	-4.79	-6.09
56.75	6091	-4.70	-6.09
57.25	6100	-4.88	-6.17
57.75	6110	-4.82	-6.29
58.25	6119	-4.94	-6.14
58.75	6128	-4.64	-6.03
59.25	6138	-4.83	-6.09
59.75	6147	-4.55	-5.98
60.25	6157	-4.64	-5.95
60.75	6166	-4.78	-6.00
61.25	6175	-4.85	-6.16
61.75	6185	-4.86	-6.07
62.25	6194	-4.84	-6.11
62.75	6204	-5.13	-6.08
63.25	6212	-5.13	-6.16
63.75	6220	-5.14	-6.11
64.25	6228	-5.10	-6.23
64.75	6235	-4.82	-6.20
65.25	6243	-4.65	-6.15
65.75	6251	-4.70	-6.15
66.25	6258	-4.88	-6.00
66.75	6266	-4.82	-5.97
67.25	6274	-4.79	-6.17
67.75	6281	-4.94	-6.01
68.25	6289	-4.79	-6.01
68.75	6297	-4.91	-5.72
69.25	6305	-4.60	-5.66
69.75	6312	-4.56	-5.63
70.25	6320	-4.74	-5.66
70.75	6328	-4.72	-5.57
71.25	6335	-4.74	-5.54
71.75	6343	-4.75	-5.78

Sample Depth (mm)	Age (yr BP)	$\delta^{18}O$ (‰, VPDB)	$\delta^{13}C$ (‰, VPDB)
72.25	6351	-4.62	-5.83
72.75	6358	-4.63	-5.93
73.25	6366	-4.84	-5.99
73.75	6374	-4.80	-5.95
74.25	6381	-4.81	-5.87
74.75	6389	-5.11	-6.09
75.25	6397	-5.13	-6.09
75.75	6404	-4.60	-5.71
76.25	6412	-4.66	-5.72
76.75	6420	-4.94	-5.66
77.25	6428	-5.11	-5.94
77.75	6435	-4.59	-5.84
78.25	6443	-4.67	-5.69
78.75	6451	-4.90	-6.01
79.25	6458	-4.76	-5.82
79.75	6466	-4.93	-5.78
80.25	6474	-4.72	-5.71
80.75	6481	-4.94	-5.75
81.25	6489	-4.84	-5.73
81.75	6497	-4.93	-5.76
82.25	6504	-5.07	-5.65
82.75	6512	-4.71	-5.61
83.25	6520	-4.61	-5.42
83.75	6528	-4.61	-5.38
84.25	6535	-4.72	-5.19
84.75	6543	-4.58	-5.26
85.25	6551	-4.68	-5.38
85.75	6558	-4.75	-5.29
86.25	6566	-4.66	-5.55
86.75	6574	-4.85	-5.74
87.25	6581	-4.97	-5.74
87.75	6589	-4.86	-5.80
88.25	6597	-4.78	-5.62
88.75	6604	-4.63	-5.59
89.25	6612	-4.42	-5.45
89.75	6620	-4.61	-5.42
90.25	6628	-4.74	-5.39
90.75	6635	-4.57	-5.36
91.25	6643	-4.69	-5.34
91.75	6651	-4.63	-5.21
92.25	6658	-4.63	-5.26
92.75	6666	-4.88	-5.37
93.25	6674	-4.88	-5.48
93.75	6681	-4.81	-5.52
94.25	6689	-4.72	-5.45
94.75	6697	-4.63	-5.50
95.25	6704	-4.76	-5.57
95.75	6712	-4.67	-5.44
96.25	6720	-4.80	-5.57

Sample Depth (mm)	Age (yr BP)	$\delta^{18}O$ (‰, VPDB)	$\delta^{13}C$ (‰, VPDB)
96.75	6728	-4.53	-5.33
97.25	6735	-4.40	-5.45
97.75	6743	-4.52	-5.63
98.25	6751	-4.66	-5.47
98.75	6758	-4.48	-5.53
99.25	6766	-4.45	-5.41
99.75	6774	-5.24	-5.82
100.25	6781	-4.81	-5.68
100.75	6789	-4.86	-5.93
101.25	6797	-4.83	-5.83
101.75	6806	-4.89	-5.71
102.25	6814	-4.75	-5.71
102.75	6823	-4.98	-6.09
103.25	6831	-4.96	-6.04
103.75	6840	-5.14	-6.07
104.25	6848	-5.10	-6.17
104.75	6857	-5.17	-6.19
105.25	6865	-5.19	-6.18
105.75	6874	-4.93	-6.19
106.25	6882	-5.36	-6.21
106.75	6891	-5.02	-6.04
107.25	6899	-5.08	-6.16
107.75	6908	-4.96	-5.93
108.25	6916	-4.75	-5.83
108.75	6925	-4.54	-5.90
109.25	6933	-4.74	-5.76
109.75	6942	-4.79	-5.98
110.25	6950	-4.81	-5.97
110.75	6958	-4.73	-5.93
111.25	6967	-4.61	-5.80
111.75	6975	-4.59	-5.70
112.25	6984	-4.53	-5.74
112.75	6992	-4.57	-5.53
113.25	7001	-4.57	-5.40
113.75	7009	-4.60	-5.56
114.25	7018	-4.81	-5.58
114.75	7026	-4.83	-5.62
115.25	7035	-4.81	-5.53
115.75	7043	-4.91	-5.59
116.25	7052	-4.75	-5.54
116.75	7060	-4.92	-5.58
117.25	7069	-5.02	-5.64
117.75	7077	-4.63	-5.41
118.25	7086	-4.45	-5.45
118.75	7094	-4.48	-5.42
119.25	7103	-4.89	-5.88
119.75	7111	-4.94	-5.94
120.25	7120	-5.06	-6.25
120.75	7128	-5.04	-6.18

Sample Depth (mm)	Age (yr BP)	$\delta^{18}O$ (‰, VPDB)	$\delta^{13}C$ (‰, VPDB)
121.25	7137	-5.08	-6.19
121.75	7145	-4.98	-6.06
122.25	7154	-5.15	-6.13
122.75	7162	-5.21	-5.99
123.25	7168	-5.09	-6.15
123.75	7169	-5.09	-6.22
124.25	7171	-5.05	-6.17
124.75	7173	-5.00	-6.03
125.25	7175	-4.86	-5.99
125.75	7177	-4.75	-5.86
126.25	7179	-4.76	-5.76
126.75	7181	-4.80	-5.75
127.25	7183	-4.68	-5.57
127.75	7185	-4.81	-5.67
128.25	7187	-4.76	-5.60
128.75	7189	-4.92	-5.68
129.25	7191	-4.73	-5.62
129.75	7193	-4.77	-5.53
130.25	7195	-4.86	-5.58
130.75	7197	-4.83	-5.55
131.25	7199	-4.94	-5.45
131.75	7201	-4.88	-5.48
132.25	7202	-4.81	-5.36
132.75	7204	-4.71	-5.36
133.25	7206	-4.77	-5.45
133.75	7208	-4.69	-5.35
134.25	7210	-4.62	-5.46
134.75	7212	-4.57	-5.45
135.25	7214	-4.93	-5.36
135.75	7216	-4.81	-5.40
136.25	7218	-4.79	-5.30
136.75	7220	-4.77	-4.99
137.25	7222	-4.72	-4.93
137.75	7224	-4.74	-4.89
138.25	7226	-4.75	-4.79
138.75	7228	-4.73	-4.89
139.25	7230	-4.75	-5.00
139.75	7232	-4.81	-5.09
140.25	7234	-4.72	-5.01
140.75	7236	-4.42	-5.05
141.25	7237	-4.51	-5.10
141.75	7239	-4.47	-5.17
142.25	7241	-4.64	-5.21
142.75	7243	-4.70	-5.23
143.25	7245	-4.57	-5.23
143.75	7247	-4.79	-5.32
144.25	7249	-5.05	-5.55
144.75	7251	-5.02	-5.59
145.25	7253	-5.00	-5.59

Sample Depth (mm)	Age (yr BP)	$\delta^{18}O$ (‰, VPDB)	$\delta^{13}C$ (‰, VPDB)
145.75	7255	-4.97	-5.63
146.25	7257	-5.08	-5.75
146.75	7259	-4.89	-5.69
147.25	7261	-4.78	-5.78
147.75	7263	-4.73	-5.93
148.25	7265	-4.69	-5.71
148.75	7267	-4.88	-6.12
149.25	7269	-4.71	-6.14
149.75	7270	-4.70	-6.06
150.25	7272	-4.67	-6.36
150.75	7285	-4.59	-6.27
151.25	7298	-4.46	-6.19
151.75	7311	-4.69	-6.12
152.25	7323	-4.57	-6.03
152.75	7336	-4.58	-6.17
153.25	7349	-4.45	-6.14
153.75	7362	-4.42	-6.21
154.25	7374	-4.62	-6.23
154.75	7387	-4.56	-6.13
155.25	7400	-4.98	-6.11
155.75	7413	-4.70	-6.00
156.25	7425	-4.51	-5.54
156.75	7438	-4.64	-5.53
157.25	7451	-4.81	-5.63
157.75	7464	-4.74	-5.54
158.25	7476	-4.41	-5.44
158.75	7489	-4.33	-5.24
159.25	7502	-4.25	-5.21
159.75	7514	-4.43	-5.22
160.25	7527	-4.68	-5.14
160.75	7540	-4.55	-5.09
161.25	7553	-4.50	-4.94
161.75	7565	-4.57	-5.09
162.25	7578	-4.55	-5.22
162.75	7591	-4.67	-4.96
163.25	7604	-4.68	-5.36
163.75	7616	-4.63	-5.34
164.25	7629	-4.67	-5.40
164.75	7642	-4.66	-5.43
165.25	7655	-4.78	-5.59
165.75	7667	-4.99	-5.54
166.25	7680	-4.91	-5.53
166.75	7694	-4.98	-5.59
167.25	7707	-4.81	-5.61
167.75	7720	-4.74	-5.51
168.25	7733	-4.66	-5.28
168.75	7747	-4.52	-5.14
169.25	7760	-4.50	-4.88
169.75	7773	-4.33	-5.02

Sample Depth (mm)	Age (yr BP)	$\delta^{18}O$ (‰, VPDB)	$\delta^{13}C$ (‰, VPDB)
170.25	7786	-4.33	-4.89
170.75	7800	-4.46	-4.89
171.25	7813	-4.41	-4.87
171.75	7826	-4.56	-4.79
172.25	7839	-4.52	-5.15
172.75	7853	-4.45	-4.92
173.25	7866	-4.53	-5.01
173.75	7879	-4.48	-4.91
174.25	7892	-4.45	-5.00
174.75	7905	-4.38	-5.19
175.25	7919	-4.54	-5.31
175.75	7932	-4.88	-5.06
176.25	7945	-4.64	-5.15
176.75	7958	-4.56	-5.12
177.25	7972	-4.75	-5.27
177.75	7985	-4.60	-5.34
178.25	7998	-4.78	-5.26
178.75	8011	-4.71	-5.18
179.25	8025	-4.64	-5.04
179.75	8038	-4.65	-5.13
180.25	8051	-4.47	-5.06
180.75	8064	-4.51	-5.15
181.25	8078	-4.44	-5.36
181.75	8091	-4.66	-5.76
182.25	8104	-4.55	-5.75
182.75	8117	-4.68	-6.06
183.25	8131	-4.78	-5.87
183.75	8144	-4.86	-5.64
184.25	8157	-4.61	-5.10
184.75	8170	-4.69	-5.26
185.25	8184	-4.80	-4.95
185.75	8197	-4.55	-4.75
186.25	8210	-4.59	-4.61
186.75	8223	-4.61	-4.56
187.25	8237	-4.51	-4.74
187.75	8250	-4.55	-4.68
188.25	8263	-4.73	-4.77
188.75	8276	-4.82	-4.70
189.25	8309	-4.94	-5.09
189.75	8361	-4.97	-5.36
190.25	8413	-5.23	-5.71
190.75	8465	-5.38	-6.31
191.25	8518	-5.31	-6.20
191.75	8570	-5.42	-6.14
192.25	8622	-5.24	-5.91
192.75	8674	-5.35	-5.83
193.25	8726	-5.09	-5.70
193.75	8778	-5.12	-5.47
194.25	8831	-5.01	-5.36

Sample Depth (mm)	Age (yr BP)	$\delta^{18}O$ (‰, VPDB)	$\delta^{13}C$ (‰, VPDB)
194.75	8883	-4.92	-5.13
195.25	8935	-4.92	-5.14
195.75	8987	-5.08	-5.05
196.25	9039	-4.96	-5.00
196.75	9091	-4.89	-5.00
197.25	9144	-4.78	-4.93
197.75	9196	-4.73	-4.78
198.25	9248	-4.94	-4.83
198.75	9300	-4.86	-4.77
199.25	9352	-4.90	-4.96
199.75	9405	-4.86	-4.74
200.25	9457	-4.84	-4.70
200.75	9509	-4.67	-3.30
201.25	9561	-4.76	-3.46
201.75	9613	-4.72	-3.58
202.25	9665	-4.55	-3.39
202.75	9718	-4.61	-3.21
203.25	9770	-5.30	-3.66
203.75	9822	-4.88	-3.78
204.25	9874	-4.81	-3.80
204.75	9926	-4.87	-4.38
205.25	9978	-4.98	-4.59
205.75	10031	-5.18	-4.69
206.25	10083	-5.46	-5.05
206.75	10135	-5.33	-4.90
207.25	10187	-5.48	-4.72
207.75	10239	-5.08	-4.56
208.25	10291	-5.04	-3.86
208.75	10344	-4.96	-3.77
209.25	10396	-4.98	-3.68
209.75	10448	-5.07	-3.63
210.25	10500	-5.06	-3.88
210.75	10552	-5.07	-3.79
211.25	10604	-4.97	-3.76
211.75	10657	-5.15	-3.82
212.25	10709	-5.00	-3.97
212.75	10745	-5.07	-4.09
213.25	10766	-5.19	-4.11
213.75	10787	-5.24	-4.33
214.25	10807	-5.41	-4.51
214.75	10828	-5.46	-4.62
215.25	10849	-5.61	-4.68
215.75	10870	-5.20	-4.53
216.25	10890	-5.39	-4.53
216.75	10911	-5.47	-4.61
217.25	10932	-5.41	-4.59
217.75	10952	-5.32	-4.42
218.25	10973	-5.37	-4.57
218.75	10994	-5.37	-4.57

Sample Depth (mm)	Age (yr BP)	$\delta^{18}O$ (‰, VPDB)	$\delta^{13}C$ (‰, VPDB)
219.25	11015	-5.41	-4.52
219.75	11035	-5.41	-4.91
220.25	11056	-5.19	-4.39
220.75	11077	-5.07	-4.34
221.25	11098	-4.85	-4.00
221.75	11118	-4.84	-3.97
222.25	11139	-4.72	-3.71
222.75	11160	-4.81	-3.71
223.25	11180	-4.60	-3.67
223.75	11201	-4.78	-4.03
224.25	11222	-4.78	-4.47
224.75	11243	-4.88	-4.97
225.25	11263	-4.40	-3.86
225.75	11284	-4.78	-3.84
226.25	11305	-5.06	-4.08
226.75	11326	-5.04	-4.14
227.25	11347	-4.92	-4.23
227.75	11368	-5.38	-4.47
228.25	11389	-5.25	-4.71
228.75	11411	-5.31	-5.36
229.25	11432	-5.13	-5.38
229.75	11454	-5.04	-5.40
230.25	11475	-4.98	-5.29
230.75	11496	-4.91	-5.28
231.25	11518	-5.02	-5.47
231.75	11539	-4.77	-5.18
232.25	11561	-4.80	-5.04
232.75	11582	-4.37	-4.71
233.25	11603	-4.42	-4.62
233.75	11625	-4.53	-4.57
234.25	11646	-5.00	-4.69
234.75	11668	-4.87	-4.76
235.25	11689	-5.08	-4.79
235.75	11710	-4.93	-4.70
236.25	11732	-5.36	-4.85
236.75	11753	-5.06	-4.78
237.25	11775	-5.29	-4.61
237.75	11796	-5.22	-4.36
238.25	11817	-5.27	-4.09
238.75	11839	-5.10	-4.20
239.25	11860	-5.23	-4.12
239.75	11882	-5.19	-4.28
240.25	11903	-5.27	-4.23
240.75	11924	-5.37	-4.54
241.25	11946	-5.72	-5.00
241.75	11967	-5.71	-5.51
242.25	11989	-5.33	-5.36
242.75	12005	-5.14	-5.31
243.25	12017	-5.08	-5.27

Sample Depth (mm)	Age (yr BP)	$\delta^{18}O$ (‰, VPDB)	$\delta^{13}C$ (‰, VPDB)
243.75	12029	-5.13	-5.63
244.25	12041	-5.06	-5.14
244.75	12053	-4.86	-4.55
245.25	12065	-4.74	-4.51
245.75	12077	-4.59	-4.56
246.25	12089	-4.74	-4.76
246.75	12101	-5.02	-4.97
247.25	12113	-4.76	-4.35
247.75	12125	-4.63	-4.25
248.25	12137	-5.10	-4.81
248.75	12148	-4.99	-5.13
249.25	12160	-4.94	-5.31
249.75	12172	-4.83	-4.99
250.25	12184	-4.92	-4.92
250.75	12196	-5.06	-5.06
251.25	12208	-5.12	-4.99
251.75	12220	-5.21	-4.77
252.25	12232	-5.19	-4.80
252.75	12244	-5.17	-4.56
253.25	12256	-5.00	-4.13
253.75	12268	-4.99	-4.12
254.25	12280	-5.18	-4.02
254.75	12291	-5.03	-3.90
255.25	12303	-5.28	-3.87
255.75	12315	-5.27	-3.84
256.25	12327	-5.23	-4.24
256.75	12339	-5.08	-4.18
257.25	12351	-5.16	-4.26
257.75	12363	-5.21	-4.81
258.25	12375	-5.31	-4.80
258.75	12387	-5.44	-4.90
259.25	12399	-5.23	-4.75
259.75	12411	-5.41	-4.92
260.25	12423	-5.49	-4.95
260.75	12435	-5.52	-5.17
261.25	12446	-5.49	-5.25
261.75	12458	-5.61	-5.21
262.25	12470	-5.53	-5.10
262.75	12482	-5.36	-4.96
263.25	12494	-5.19	-4.30
263.75	12506	-5.52	-4.69
264.25	12518	-5.66	-4.53
264.75	12530	-5.60	-4.13
265.25	12542	-5.81	-4.85
265.75	12554	-5.71	-5.00
266.25	12566	-5.93	-4.79
266.75	12578	-5.96	-4.69
267.25	12590	-5.87	-4.79
267.75	12601	-5.82	-4.58

Sample Depth (mm)	Age (yr BP)	$\delta^{18}O$ (‰, VPDB)	$\delta^{13}C$ (‰, VPDB)
268.25	12613	-6.09	-4.26
268.75	12623	-5.79	-3.96
269.25	12633	-5.77	-3.92
269.75	12644	-5.82	-3.83
270.25	12654	-5.69	-3.87
270.75	12664	-5.69	-4.46
271.25	12675	-5.78	-4.50
271.75	12685	-5.97	-4.45
272.25	12695	-5.72	-4.42
272.75	12706	-5.77	-4.62
273.25	12716	-5.81	-4.62
273.75	12726	-5.77	-4.69
274.25	12737	-5.87	-4.99
274.75	12747	-5.55	-4.97
275.25	12757	-5.73	-4.66
275.75	12768	-5.68	-4.47
276.25	12778	-5.80	-4.85
276.75	12789	-6.02	-4.92
277.25	12799	-5.98	-5.26
277.75	12809	-5.88	-4.96
278.25	12820	-5.56	-4.14
278.75	12830	-5.19	-3.80
279.25	12840	-5.11	-3.77
279.75	12851	-5.27	-4.12
280.25	12862	-5.54	-5.02
280.75	12875	-5.78	-5.24
281.25	12888	-5.97	-5.38
281.75	12901	-5.74	-5.39
282.25	12914	-5.87	-5.41
282.75	12927	-5.57	-5.15
283.25	12940	-5.26	-4.37
283.75	12952	-4.83	-4.00
284.25	12965	-4.86	-3.56
284.75	12978	-4.42	-3.37
285.25	12991	-4.59	-3.82
285.75	13004	-4.66	-4.36
286.25	13017	-5.05	-4.87
286.75	13030	-5.26	-4.93
287.25	13043	-5.26	-5.08
287.75	13056	-5.62	-5.31
288.25	13068	-5.66	-5.17
288.75	13081	-5.74	-5.24
289.25	13094	-6.13	-5.16
289.75	13107	-5.86	-4.78
290.25	13120	-6.04	-5.41
290.75	13133	-5.93	-5.49
291.25	13146	-5.70	-5.06
291.75	13159	-5.83	-4.69
292.25	13171	-5.35	-3.63

Sample Depth (mm)	Age (yr BP)	$\delta^{18}O$ (‰, VPDB)	$\delta^{13}C$ (‰, VPDB)
292.75	13184	-5.26	-3.69
293.25	13197	-5.30	-4.26
293.75	13210	-5.17	-3.93
294.25	13223	-5.17	-3.94
294.75	13236	-5.20	-3.91
295.25	13249	-5.24	-3.65
295.75	13262	-5.24	-3.73
296.25	13275	-5.29	-3.87
296.75	13287	-5.35	-4.04
297.25	13300	-5.01	-4.12
297.75	13313	-5.02	-4.09
298.25	13324	-5.13	-4.17
298.75	13332	-5.25	-4.30
299.25	13340	-5.48	-4.51
299.75	13348	-5.38	-4.92
300.25	13357	-5.13	-4.01
300.75	13365	-5.16	-3.69
301.25	13373	-5.21	-3.97
301.75	13381	-5.16	-3.98
302.25	13390	-5.05	-3.94
302.75	13398	-5.39	-4.40
303.25	13406	-5.30	-4.63
303.75	13414	-5.70	-4.64
304.25	13422	-5.82	-4.91
304.75	13431	-5.65	-5.04
305.25	13439	-5.56	-4.62
305.75	13447	-5.55	-4.72
306.25	13455	-5.64	-4.79
306.75	13464	-5.66	-4.87
307.25	13472	-5.58	-4.94
307.75	13480	-5.70	-4.83
308.25	13488	-5.62	-5.05
308.75	13497	-5.34	-4.87
309.25	13505	-5.36	-4.87
309.75	13513	-5.40	-4.99
310.25	13521	-5.41	-4.76
310.75	13529	-5.37	-4.63
311.25	13538	-5.58	-4.88
311.75	13546	-5.83	-4.82
312.25	13554	-5.56	-4.89
312.75	13562	-5.51	-4.92
313.25	13571	-5.40	-5.10
313.75	13579	-5.50	-5.29
314.25	13587	-5.28	-4.52
314.75	13595	-5.42	-4.31
315.25	13604	-5.21	-4.35
315.75	13612	-5.44	-4.69
316.25	13620	-5.35	-4.76
316.75	13628	-5.24	-4.86

Sample Depth (mm)	Age (yr BP)	$\delta^{18}O$ (‰, VPDB)	$\delta^{13}C$ (‰, VPDB)
317.25	13636	-5.31	-4.93
317.75	13645	-5.41	-4.91
318.25	13653	-5.30	-4.44
318.75	13661	-5.27	-4.31
319.25	13669	-5.20	-4.62
319.75	13678	-5.15	-4.37
320.25	13686	-5.12	-4.41
320.75	13694	-5.56	-4.27
321.25	13702	-5.00	-4.09
321.75	13710	-5.10	-4.24
322.25	13719	-5.37	-4.50
322.75	13727	-5.28	-4.63
323.25	13735	-5.67	-4.70
323.75	13743	-5.56	-4.43
324.25	13752	-5.55	-4.45
324.75	13760	-5.66	-4.21
325.25	13768	-5.47	-3.95
325.75	13776	-5.64	-3.87
326.25	13785	-6.01	-3.70
326.75	13793	-5.14	-3.56
327.25	13801	-5.25	-3.75
327.75	13809	-5.48	-4.44
328.25	13817	-5.64	-4.45
328.75	13826	-5.53	-4.75
329.25	13834	-5.58	-4.81
329.75	13842	-5.56	-4.82
330.25	13850	-5.53	-5.00
330.75	13856	-5.62	-4.93
331.25	13859	-5.33	-4.57
331.75	13862	-5.36	-4.49
332.25	13866	-5.74	-4.20
332.75	13869	-5.53	-4.25
333.25	13872	-5.76	-4.41
333.75	13875	-5.79	-4.70
334.25	13878	-5.82	-4.76
334.75	13882	-5.79	-4.81
335.25	13885	-5.80	-4.96
335.75	13888	-5.76	-4.87
336.25	13891	-5.94	-4.90
336.75	13894	-5.73	-4.95
337.25	13897	-5.71	-4.96
337.75	13901	-5.69	-4.89
338.25	13904	-5.63	-4.61
338.75	13907	-5.36	-4.04
339.25	13910	-5.38	-4.18
339.75	13913	-5.04	-4.54
340.25	13917	-4.87	-4.24
340.75	13926	-5.06	-4.72
341.25	13935	-4.93	-4.77

Sample Depth (mm)	Age (yr BP)	$\delta^{18}O$ (‰, VPDB)	$\delta^{13}C$ (‰, VPDB)
341.75	13944	-5.17	-4.77
342.25	13953	-5.26	-4.86
342.75	13962	-5.17	-4.50
343.25	13971	-5.17	-4.59
343.75	13980	-5.38	-4.54
344.25	13989	-5.28	-4.54
344.75	13998	-5.47	-4.61
345.25	14007	-5.88	-4.99
345.75	14016	-5.66	-4.94
346.25	14025	-5.77	-4.53
346.75	14034	-5.76	-4.40
347.25	14043	-5.61	-4.20
347.75	14052	-5.76	-4.42
348.25	14061	-5.89	-4.72
348.75	14070	-5.67	-4.54
349.25	14079	-5.64	-4.80
349.75	14088	-5.71	-4.56
350.25	14097	-5.75	-4.73
350.75	14105	-5.55	-4.89
351.25	14114	-5.54	-5.32
351.75	14123	-5.57	-5.40
352.25	14132	-5.42	-5.36
352.75	14141	-5.24	-4.85
353.25	14150	-5.26	-4.65
353.75	14159	-5.36	-4.67
354.25	14168	-5.41	-4.63
354.75	14177	-5.45	-4.80
355.25	14186	-4.99	-4.20
355.75	14195	-5.01	-4.19
356.25	14204	-4.99	-4.27
356.75	14213	-4.98	-4.03
357.25	14222	-5.07	-4.29
357.75	14231	-5.29	-4.54
358.25	14240	-5.53	-4.99
358.75	14249	-5.58	-5.06
359.25	14258	-5.76	-5.06
359.75	14267	-5.52	-4.88
360.25	14276	-5.64	-4.85
360.75	14285	-5.51	-4.68
361.25	14294	-5.11	-4.31
361.75	14303	-5.46	-4.61
362.25	14312	-5.36	-4.43
362.75	14321	-5.19	-3.90
363.25	14330	-5.32	-4.22
363.75	14339	-5.26	-4.49
364.25	14348	-5.45	-4.81
364.75	14357	-5.61	-4.99
365.25	14366	-5.63	-5.15
365.75	14375	-5.81	-5.10

Sample Depth (mm)	Age (yr BP)	$\delta^{18}O$ (‰, VPDB)	$\delta^{13}C$ (‰, VPDB)
366.25	14384	-5.73	-5.07
366.75	14393	-5.94	-5.30
367.25	14402	-5.87	-5.36
367.75	14411	-5.90	-5.24
368.25	14420	-5.86	-5.19
368.75	14429	-5.96	-5.27
369.25	14438	-5.92	-5.36
369.75	14447	-5.69	-5.41
370.25	14456	-5.70	-5.35
370.75	14465	-5.92	-5.38
371.25	14544	-5.82	-5.32
371.75	14623	-5.79	-5.29
372.25	14701	-5.76	-5.10
372.75	14780	-5.70	-5.16
373.25	14858	-5.72	-5.05
373.75	14937	-5.48	-4.63
374.25	15015	-5.30	-4.20
374.75	15094	-5.52	-4.14
375.25	15136	-5.22	-3.47
375.75	15141	-5.26	-3.69
376.25	15146	-4.78	-3.07
376.75	15151	-4.87	-2.91
377.25	15156	-4.50	-2.61
377.75	15161	-4.66	-2.62
378.25	15167	-4.48	-2.37
378.75	15172	-4.42	-2.56
379.25	15177	-4.30	-2.62
379.75	15182	-4.57	-2.78
380.25	15187	-4.70	-3.32
380.75	15192	-4.94	-3.50
381.25	15197	-5.02	-4.04
381.75	15202	-4.81	-4.06
382.25	15208	-4.92	-3.65
382.75	15213	-4.96	-3.59
383.25	15218	-5.09	-3.77
383.75	15223	-4.95	-3.76
384.25	15228	-4.99	-3.95
384.75	15233	-4.67	-3.87
385.25	15238	-4.85	-3.95
385.75	15243	-4.85	-4.23
386.25	15249	-4.98	-3.92
386.75	15254	-5.34	-3.85
387.25	15259	-5.01	-4.60
387.75	15264	-5.30	-4.77
388.25	15269	-5.49	-4.88
388.75	15274	-5.51	-5.05
389.25	15281	-5.31	-4.98
389.75	15289	-5.31	-5.23
390.25	15297	-5.45	-5.03

Sample Depth (mm)	Age (yr BP)	$\delta^{18}O$ (‰, VPDB)	$\delta^{13}C$ (‰, VPDB)
390.75	15305	-5.11	-4.98
391.25	15314	-5.23	-5.21
391.75	15322	-5.28	-5.44
392.25	15330	-5.37	-5.36
392.75	15338	-5.10	-5.34
393.25	15346	-4.87	-5.24
393.75	15355	-4.90	-5.35
394.25	15363	-4.77	-5.54
394.75	15371	-4.87	-5.52
395.25	15379	-4.68	-5.23
395.75	15387	-4.68	-5.31
396.25	15396	-4.83	-5.17
396.75	15404	-4.69	-4.54
397.25	15412	-4.75	-4.16
397.75	15420	-4.83	-4.27
398.25	15428	-4.71	-4.78
398.75	15437	-4.79	-5.07
399.25	15445	-5.02	-5.33
399.75	15453	-4.96	-5.38
400.25	15461	-5.26	-5.75
400.75	15469	-5.08	-6.04
401.25	15478	-5.32	-5.92
401.75	15486	-5.07	-5.88
402.25	15494	-5.34	-6.18
402.75	15502	-5.22	-6.29
403.25	15510	-5.18	-6.29
403.75	15519	-5.20	-6.22
404.25	15524	-5.07	-6.15
404.75	15528	-4.89	-5.84
405.25	15532	-5.04	-5.99
405.75	15535	-5.16	-6.32
406.25	15539	-5.02	-6.24
406.75	15543	-5.08	-6.00
407.25	15546	-4.95	-6.07
407.75	15550	-4.97	-6.12
408.25	15554	-4.93	-5.98
408.75	15557	-4.83	-5.89
409.25	15561	-5.06	-5.86
409.75	15565	-4.70	-5.56
410.25	15568	-4.79	-5.56
410.75	15572	-4.82	-5.56
411.25	15575	-4.91	-5.58
411.75	15579	-4.95	-5.39
412.25	15583	-5.05	-5.50
412.75	15586	-4.79	-5.68
413.25	15590	-4.93	-5.45
413.75	15594	-4.72	-4.86
414.25	15597	-4.67	-5.02
414.75	15601	-4.64	-4.80

Sample Depth (mm)	Age (yr BP)	$\delta^{18}O$ (‰, VPDB)	$\delta^{13}C$ (‰, VPDB)
415.25	15605	-4.34	-4.05
415.75	15608	-4.10	-3.72
416.25	15612	-4.38	-4.04
416.75	15616	-4.43	-4.20
417.25	15619	-4.68	-4.38
417.75	15623	-4.81	-4.51
418.25	15626	-4.90	-4.46
418.75	15630	-4.92	-4.58
419.25	15634	-4.80	-4.71
419.75	15637	-5.03	-4.99
420.25	15641	-4.95	-4.57
420.75	15645	-4.95	-4.25
421.25	15647	-4.39	-3.91
421.75	15649	-4.70	-4.30
422.25	15651	-4.89	-4.88
422.75	15653	-4.71	-4.76
423.25	15655	-4.61	-4.37
423.75	15658	-4.59	-4.48
424.25	15660	-4.57	-4.30
424.75	15662	-4.88	-4.35
425.25	15664	-4.63	-4.35
425.75	15666	-4.83	-4.56
426.25	15668	-4.83	-5.03
426.75	15670	-4.83	-5.16
427.25	15672	-4.95	-5.48
427.75	15674	-4.87	-5.78
428.25	15676	-4.91	-5.89
428.75	15678	-4.99	-5.95
429.25	15681	-5.02	-5.97
429.75	15683	-5.07	-5.77
430.25	15685	-5.01	-5.89
430.75	15686	-5.53	-5.83
431.25	15694	-5.38	-5.87
431.75	15703	-4.98	-6.01
432.25	15711	-5.07	-6.02
432.75	15720	-5.19	-6.08
433.25	15728	-5.00	-5.95
433.75	15737	-5.06	-5.88
434.25	15745	-5.11	-5.91
434.75	15754	-4.99	-5.94
435.25	15762	-4.98	-5.74
435.75	15771	-4.58	-5.30
436.25	15779	-4.52	-4.78
436.75	15788	-4.20	-3.99
437.25	15796	-4.30	-3.70
437.75	15805	-4.47	-3.67
438.25	15813	-4.60	-3.66
438.75	15822	-4.48	-3.59
439.25	15830	-4.51	-3.53

Sample Depth (mm)	Age (yr BP)	$\delta^{18}O$ (‰, VPDB)	$\delta^{13}C$ (‰, VPDB)
439.75	15839	-4.52	-3.47
440.25	15847	-4.51	-3.52
440.75	15856	-4.82	-3.60
441.25	15864	-4.83	-3.84
441.75	15873	-4.84	-4.29
442.25	15881	-5.00	-4.39
442.75	15890	-4.92	-4.37
443.25	15898	-5.05	-4.37
443.75	15907	-5.25	-4.60
444.25	15915	-5.36	-4.55
444.75	15924	-5.21	-4.57
445.25	15932	-5.39	-4.74
445.75	15941	-5.21	-4.81
446.25	15949	-5.10	-4.68
446.75	15958	-5.18	-4.57
447.25	15966	-5.25	-4.94
447.75	15975	-5.16	-5.12
448.25	15983	-5.36	-5.15
448.75	15992	-5.11	-5.07
449.25	16000	-5.22	-5.13
449.75	16009	-5.37	-5.20
450.25	16017	-5.18	-5.34
450.75	16026	-5.05	-5.12
451.25	16034	-5.29	-4.95
451.75	16043	-5.26	-5.15
452.25	16051	-5.35	-5.20
452.75	16060	-5.43	-5.07
453.25	16068	-5.50	-4.88
453.75	16077	-5.46	-4.98
454.25	16085	-5.75	-5.13
454.75	16094	-5.45	-5.24
455.25	16102	-5.46	-5.35
455.75	16111	-5.61	-5.48
456.25	16129	-5.45	-5.38
456.75	16147	-5.09	-5.26
457.25	16166	-5.18	-5.43
457.75	16184	-5.04	-5.43
458.25	16202	-4.49	-5.07
458.75	16220	-4.92	-5.14
459.25	16239	-4.81	-5.04
459.75	16257	-4.68	-4.94
460.25	16275	-4.64	-4.63
460.75	16294	-4.47	-4.10
461.25	16312	-4.43	-3.19
461.75	16330	-4.29	-2.88
462.25	16348	-4.59	-3.32
462.75	16367	-4.16	-3.68
463.25	16385	-3.92	-3.78
463.75	16403	-4.01	-3.70

Sample Depth (mm)	Age (yr BP)	$\delta^{18}O$ (‰, VPDB)	$\delta^{13}C$ (‰, VPDB)
464.25	16422	-4.27	-3.73
464.75	16440	-4.51	-3.85
465.25	16462	-4.44	-4.16
465.75	16489	-3.95	-3.76
466.25	16515	-3.88	-3.67
466.75	16542	-4.11	-3.78
467.25	16568	-4.14	-3.60
467.75	16594	-3.99	-3.77
468.25	16621	-4.12	-3.34
468.75	16640	-4.17	-2.62
469.25	16651	-3.90	-2.79
469.75	16663	-3.86	-2.70
470.25	16674	-3.94	-3.56
470.75	16686	-4.02	-3.83
471.25	16697	-3.79	-4.09
471.75	16709	-3.97	-4.51
472.25	16720	-4.42	-5.01
472.75	16732	-4.07	-4.53
473.25	16743	-3.87	-3.76
473.75	16755	-3.82	-3.51
474.25	16766	-3.97	-3.55
474.75	16778	-4.02	-3.25
475.25	16789	-4.09	-3.08
475.75	16801	-4.10	-3.26
476.25	16812	-4.33	-3.72
476.75	16824	-4.33	-3.24
477.25	16835	-3.78	-1.98
477.75	16847	-3.76	-1.23
478.25	16858	-3.53	-0.90
478.75	16870	-3.43	-0.76
479.25	16881	-3.54	-0.67
479.75	16893	-3.49	-0.48
480.25	18922	-3.69	-0.66
480.75	18979	-4.15	-0.75
481.25	19036	-4.29	-0.82
481.75	19093	-4.35	-1.01
482.25	19150	-4.64	-0.94
482.75	19207	-4.42	-1.13
483.25	19264	-4.48	-1.82
483.75	19321	-4.56	-1.60
484.25	19378	-4.44	-1.85
484.75	19435	-4.50	-1.68
485.25	19492	-4.70	-1.33
485.75	19550	-4.11	-1.02
486.25	19607	-3.87	-0.66
486.75	19664	-4.11	-0.72
487.25	19721	-4.18	-0.64
487.75	19778	-3.85	-0.72

Sample Depth (mm)	Age (yr BP)	$\delta^{18}O$ (‰, VPDB)	$\delta^{13}C$ (‰, VPDB)
488.25	19835	-3.65	-0.75
488.75	19892	-3.42	-0.48
489.25	19949	-3.66	-0.65
489.75	20006	-3.78	-0.70
490.25	20063	-3.90	-0.88
490.75	20120	-3.79	-0.76
491.25	20177	-3.89	-0.56
491.75	20234	-3.71	-0.48
492.25	20291	-3.92	-0.51
492.75	20348	-4.03	-0.45
493.25	20405	-3.91	-0.42
493.75	20463	-3.90	-0.48
494.25	20520	-3.95	-0.48
494.75	20577	-3.68	-0.42
495.25	20634	-3.75	-0.51
495.75	20691	-3.86	-0.49